Optimal Rejection of Nonstationary Narrowband Disturbances for Flexible Systems

by

Sean P. Kenny

B.S., Mechanical Engineering
Old Dominion University, 1988
M.S., Mechanical Engineering and Mechanics
Old Dominion University, 1990

Submitted to the Department of Aeronautics and Astronautics
in partial fulfillment for the degree of

Doctor of Philosophy

at the

MASSACHUSETTS INSTITUTE OF TECHNOLOGY

February 2002

Signature of Author .....
Department of Aeronautics and Astronautics
January 25, 2002

Certified by .....
Associate Professor David W. Miller
Thesis Committee Chairman

Certified by .....
Dr. Peiman Maghami
Thesis Committee Member

Certified by .....
Dr. Jer-Nan Juang
Thesis Committee Member

Certified by .....
Associate Professor Anuradha Annaswamy
Thesis Committee Member

Certified by .....
Dr. Marthinus van Schoor
Thesis Committee Member

Accepted by .....
Professor Wallace E. Vander Velde
Chair, Committee on Graduate Students

Optimal Rejection of Nonstationary Narrowband Disturbances for Flexible Systems

by

SEAN P. KENNY

Submitted to the Department of Aeronautics and Astronautics
on February 1, 2002 in Partial Fulfillment of the
Requirements for the Degree of Doctorate of Philosophy

ABSTRACT

Optimal performance and optimal allocation of resources, such as pointing accuracy and onboard fuel utilization, are of primary concern in the design and operation of precision pointing spacecraft. Ironically, internal spacecraft instruments and reaction control actuators often act as sources of narrowband disturbances and impede the optimal performance of these precision systems. The fundamental objective of this work is the development of an active control methodology capable of rejecting disturbances with narrowband nonstationary spectral distributions with particular focus on spacecraft reaction wheel induced disturbances.

A closed-form symbolically parameterized optimal feed-forward disturbance rejection methodology for flexible systems has been developed. The methodology combines disturbance modeling for narrowband disturbances together with quasi-stationary optimal control to yield a parameterized feed-forward control architecture. In the case of the reaction wheel disturbance rejection problem, the symbolic optimal control gains are parameterized in terms of wheel spin rate, enabling continuous and analytically exact gain adjustments as a function of the measurable scheduling parameter. The methodology was shown to be compatible with loop-shaping control design methods such as frequency-weighted optimal control. This quasi-stationary disturbance rejection methodology has been generalized and applied to the nonstationary reaction wheel imbalance problem. The nonstationary formulation involves expanding the reaction wheel's angular states in terms of a general series representation. Bessel functions and their properties are employed to define an equivalent finite-dimensional quasi-stationary disturbance signal. The effectiveness of the methodology has been experimentally demonstrated on a highly compliant system with non-collocated sensors and actuators. Experimental results show peak performance yielding nearly a 40 dB improvement over conventional broadband control with improved performance across a wide range of frequencies.

Thesis Supervisor:
Prof. David Miller
Dept. of Aeronautics and Astronautics

ACKNOWLEDGMENTS

I would like to thank my advisor Prof. David W. Miller for his guidance and support throughout this research. His expertise in space telescope systems has provided invaluable insights to this research effort. Committee member Dr. Peiman Maghami is deserving of particular acknowledgement. His unending patience and support throughout all phases of this endeavor have been imperative to the success of this research. I am profoundly grateful.

The guidance and technical support from the members of the Guidance and Control Branch of NASA Langley has not gone unnoticed. In particular, I would like to express my sincere thanks to the following people: Dr. Daniel Giesy, Mr. David Cox, Mr. Kevin Dutton, and Dr. Daniel Moerder.

I would also like to thank my parents, Edward and Mary Kenny, for the support they have given me over these many years. Finally, to my wife, Jan, for her love, support and patience. When all seemed dark you were there to help find the light.

Chapter 1

INTRODUCTION

Narrowband disturbances are present in many engineering systems. Examples of such disturbances exist in the following systems: turboprop aircraft, magnetic disk drives, precision pointing spacecraft, automobiles (engine vibration), and HVAC systems (ventilation noise). In most cases, these disturbances result from rotating machinery generating the undesired periodic components. The disturbances in the above mentioned systems impede their desired performances, thus rejection of these disturbances is imperative for optimal performance. Optimal performance and optimal allocation of resources, such as onboard fuel, pointing budget, etc., are of primary concern in the design and operation of precision pointing spacecraft and serve to motivate this work. Specifically, the motivation for this work is the optimal rejection of narrowband disturbances for precision pointing spacecraft. Sources of disturbances on precision spacecraft are many, but in particular, the following are common sources of narrowband noise:

- Cryogenic coolers
- Solar array drives
- Scanning instruments
- Reaction wheels
- Control moment gyros

The spectral distributions of these disturbance sources can be separated into those that are essentially stationary and those that are nonstationary. This work addresses the general

case of disturbance sources with nonstationary spectral distributions and in particular focuses on reaction wheel induced disturbances. Reaction wheel imbalances are a classic example of nonstationary disturbances due to the fact that they change wheel speeds to control spacecraft attitude and therefore change the frequencies at which the imbalances and other imperfections introduce vibrations. Reaction wheels play a critical role in spacecraft attitude and pointing control. In fact, many precision pointing spacecraft missions utilize reaction wheels as the primary control effector while operating in the science data-collecting mode. Reaction wheel manufacturers invest a great deal of engineering resources to minimize the forces and moments produced by rotating imbalances, bearings, lubrication effects, etc. Despite previous efforts, reaction wheel disturbances are still expected to represent a significant contribution to the overall pointing budget on many future precision pointing spacecraft missions.

1.1 Objective

The fundamental objective of this work is the development of an active control methodology capable of rejecting disturbances with narrowband nonstationary spectral distributions. The development will be in the context of narrowband nonstationary disturbances associated with reaction wheel imbalances, but extensions to other types of narrowband nonstationary disturbances are possible. Fundamentally, the disturbance rejection methodology developed in this work involves two basic steps. The first step involves developing parametric models of the nonstationary reaction wheel disturbances using a combination of physics-based modeling, together with experimental identification and model updating. Once the validated parameterized disturbance model has been characterized, the second step involves using an optimal control formulation to yield parameterized control gains. The intent is to define control gains in terms of the same parameters used to define the disturbance model. Using either direct measurements or real-time estimates of these parameters, the parameterized control gains may then be used to schedule optimal disturbance accommodating control. In the case of reaction wheel imbalances, wheel speed is the most obvious scheduling parameter and is generally accessible from a tachometer signal, but

scheduling control using other parameters such as disturbance magnitude and phase is also possible.

1.2 Previously Published Work

Disturbance rejection is one of the fundamental objectives of active control and has been intensely studied for many decades. In fact, research into disturbance rejection control met its beginnings almost in concert with basic control design theory. As a result, numerous techniques for disturbance rejection have evolved over time. A list of some of the most well known techniques is given below:

- Classical control
- Filtered-x Least Mean Squares adaptive feed-forward control
- Higher Harmonic Control
- Predictive feed-forward control and "Clear-Box" methods
- Optimal control

The methods developed in this work will focus on optimal control, but many of the analysis and design interpretation concepts from classical control apply and will provide important insights to the underlying commonality among many of the methods listed above.

1.2.1 Classical Control

The basic structure of a feedback control system is given in Figure 1.1. The symbols $G(s)$ and $K(s)$ are the transfer function matrix representations of the linear time invariant plant and compensator, respectively. The plant, $G(s)$, in general is a multi-input, multi-output (MIMO) matrix consisting of rational transfer function elements for the various input/output channels. The structure of the control system illustrated in Figure 1.1 accommodates four different design objectives: reference input tracking, set-point regulation, reference output tracking, and disturbance rejection. In terms of disturbance rejection, the structure in Figure 1.1 assumes that the disturbance, $d(t)$, may be represented as acting directly on the output, $z(t)$, as

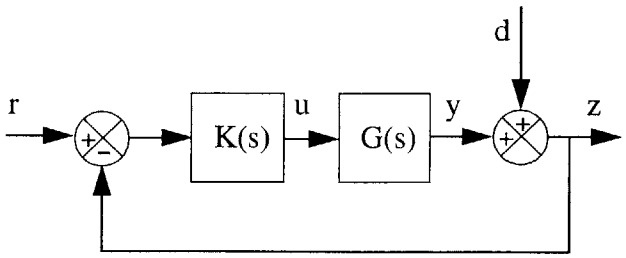

Figure 1.1 Classical Feedback Control Structure

$$z(t) = y(t) + d(t) \tag{1.1}$$

The output, $z(s)$, may be represented in terms of the closed-loop dynamics as

$$z(s) = [I + G(s)K(s)]^{-1} d(s) = S(s)d(s) \tag{1.2}$$

where $S(s)$ is defined as the sensitivity transfer function [Ogata, 1970]. The sensitivity transfer function plays a critical role in disturbance rejection. See [Mallory, 2000] for an excellent review of the properties of the sensitivity transfer function. From Equation 1.2, it is clear that if the design objective is to minimize the transmission of the disturbance to the performance, the compensator should be chosen to minimize $S(s)$ in the bandwidth of interest. For the MIMO systems, minimization of $S(s)$ may be achieved by minimizing its maximum singular value. For the single-input, single-output (SISO) case, $S(s)$ is

$$S(s) = \frac{1}{1 + G(s)K(s)} \tag{1.3}$$

and its maximum achievable attenuation at any given frequency is simply $|S(s)|_{s=j\Omega}$, where Ω is the frequency of interest. When the disturbance is narrowband, the obvious choice for the compensator is

$$K(s) = \frac{a(s+b)}{s^2 + \Omega^2} \tag{1.4}$$

Since $|S(j\Omega)| = 0$, a compensator of the form given in Equation 1.4 obtains perfect asymptotic rejection of a sinusoidal disturbance with frequency Ω. The coefficients a and

b are chosen to set the narrowband compensator bandwidth and stability requirements, respectively. A thorough review of SISO and MIMO design techniques for this class of compensator is presented in [Sievers, 1992]. An alternate way to view the compensator given in Equation 1.4 is that it places zeros in the sensitivity transfer function thereby blocking the transmission of the sinusoidal disturbance at that frequency. As simple as it may seem, the compensator given in Equation 1.4 has been shown to be the basis for many narrowband disturbance rejection techniques.

1.2.2 Filtered-x Least Mean Squares Adaptive Feed-Forward Control

The filtered-x Least Mean Squares (LMS) algorithm [Burgess, 1981], [Widrow, et al, 1985], and [Elliott, et al., 1987] has received much attention for its ability to adaptively reject narrowband disturbances. The algorithm is generally presented in discrete-time, but equivalent continuous-time versions have been developed. Figure 1.2 presents a discrete-time adaptive feed-forward control architecture employing the filtered-x LMS algorithm.

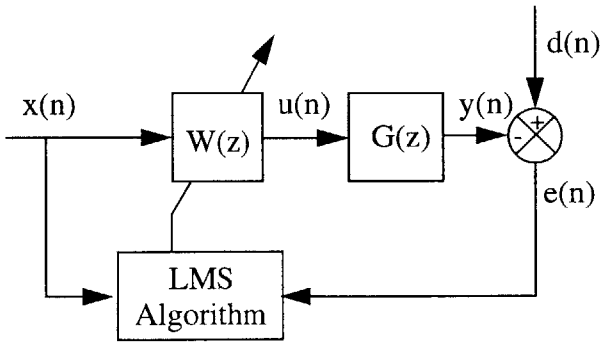

Figure 1.2 Adaptive feed-forward control

The filter input, $x(n)$, which is a disturbance correlated signal, is multiplied by the coefficients of a tap delay line, $W(z)$, to produce the control signal $u(n)$. The LMS algorithm adapts the coefficients of a tap delay line so that the sum of the mean square error is minimized. [Sievers, 1992] and [MacMartin, 1994] discuss the steady state properties of the

filtered-x LMS algorithm for a fixed-frequency disturbance and give the following expression for the equivalent linear time-invariant compensator:

$$K(s) = \frac{2\alpha(as + b\Omega)}{s^2 + \Omega^2} \tag{1.5}$$

where a and b are related to estimates of the plant's gain and phase at the disturbance frequency. Specifically, if an estimate of the plant at Ω is $G=Ae^{j\phi}$, then $a=A\cos(\phi)$ and $b=A\sin(\phi)$. The parameter, α, controls the adaptation rate of the algorithm. As in Equation 1.4, the gain of the equivalent linear LMS compensator is infinite at the disturbance frequency, yielding perfect asymptotic disturbance rejection. For small adaptation gains, the bandwidth is small and the system is gain stabilized at regions outside this bandwidth. It should be clear that a control system based upon the filtered-x LMS algorithm is fundamentally nonlinear. The analysis leading to the equivalent linear compensator is only valid during steady state conditions. Some references have shown that for slowly varying disturbances, the algorithm performs well, but analyzing stability or disturbance rejection properties is very difficult. Stability issues for systems employing the filtered-x LMS algorithm are well known. In fact, even in the steady state case, stability requires limiting the adaptation rate, α, in the presence of model errors in the plant estimate [Sievers, 1992].

1.2.3 Higher Harmonic Control

Another popular narrowband disturbance rejection methodology is called Higher Harmonic Control (HHC) [Shaw, 1980], [Shaw, 1981], and [Shaw, 1989]. HHC was initially developed to actively reject harmonic disturbances in helicopter rotor systems, but has found applications in general narrowband disturbance rejection [Scribner, 1993]. A linear time-invariant analysis, including the impact of modeling error on HHC performance is presented in [Hall, 1989]. A block diagram of a single-harmonic continuous time version of HHC, as developed in [Hall, 1989], is presented in Figure 1.3. The matrix T contains information about the plant model evaluated at the disturbance frequency Ω. Specifically, the elements are defined as

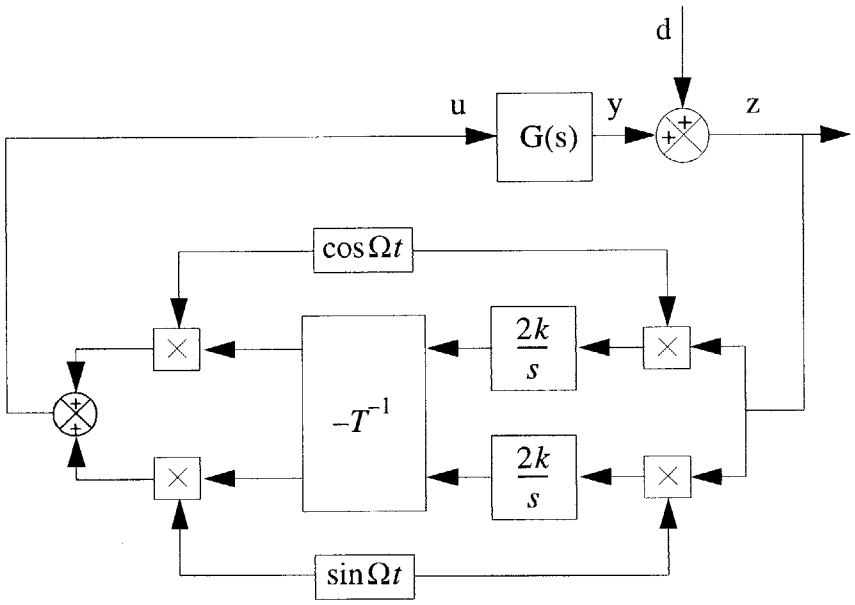

Figure 1.3 Continuous time implementation of higher harmonic control.

$$T^{-1} = \begin{bmatrix} A\cos(\phi) & A\sin(\phi) \\ -A\sin(\phi) & A\cos(\phi) \end{bmatrix} \tag{1.6}$$

where A and ϕ are related to an estimate of the plant at Ω by $G=Ae^{j\phi}$. The linear time-invariant equivalent compensator is given by

$$K(s) = \frac{2k(as + b\Omega)}{s^2 + \Omega^2} \tag{1.7}$$

The HHC LTI equivalent compensator is exactly the same form as those presented in Equations 1.4 and 1.5. An implementation using a time varying (frequency ramp) disturbance was presented in [Scribner, 1993]. This reference neglects to discuss many of the important aspects of the time varying implementation and does not discuss the possible stability issues that exist in the closed-loop system. A more complete implementation of time-varying HHC is given in [Nixon et al., 1997]. However, in this reference, airspeed and rotor speed are allowed to only vary slowly from their nominal values, achieving acceptable performance with and without updating the plant definition in T.

1.2.4 Predictive Feed-Forward Control and "Clear-Box" Methods

Recently, there has been substantial interest in developing disturbance accommodating control architectures that incorporate both system identification and feed-forward disturbance rejection in a single unified environment. [Hyland, 1996] and [Davis, 1997] have developed a multiple-tone noise cancellation technique for MIMO linear systems that requires no prior modeling information and has the ability to recover from sensor and actuator faults. The approach utilizes adaptive neural networks to perform online system identification and feed-forward disturbance rejection. Like LMS and HHC, the adaptive neural feed-forward control requires measurement of a disturbance-correlated signal. This approach has been applied to the large-order flexible test article described in [Abhyankar, 1993] and was reported to perform well in the presence of three fixed-frequency tones. The system took approximately ten minutes to identify the disturbance before achieving 20-40 dB attenuation over the open-loop system. Results for frequencies with stationary spectral distributions are very promising, but application to highly nonstationary disturbances is still an open issue.

Another approach to simultaneous system identification and feed-forward disturbance rejection is called "Clear-Box" [Goodzeit, 2000] and [Phan, 1997]. The Clear-Box approach differs from LMS, HHC, and adaptive neural feed-forward control in that it does not require a disturbance correlated signal. This approach focuses on system identification in the presence of unknown disturbances and then uses the identification results to solve the related disturbance rejection control problem. No a priori knowledge of the system or measurements of the disturbance are required. The approach requires only the excitation control inputs and the disturbance-corrupted outputs. Because it is fundamentally an identification technique it is not well suited to respond to highly nonstationary disturbances. Furthermore, optimality of control resources is not currently implemented.

[Juang, 1998] developed the generalized predictive control (GPC) methodology. The approach has many similarities to the system identification and feed-forward disturbance approach discussed above. Although similar, fundamental differences do exist. Specifi-

cally, GPC incorporates control energy considerations directly into the computation of the feed-forward control, and when it exists, takes advantage of a disturbance-correlated signal. The approach relies on the ability to predict future plant outputs, which requires that certain assumptions be made about the future control and disturbance inputs. These assumptions result in defining two parameters: a prediction horizon and a control horizon. In practice, these two parameters together with a control penalty parameter are adjusted to achieve stability and suitable performance. GPC has been successfully applied to a number of experimental test articles. Stability and performance of GPC in the presence of highly nonstationary disturbances requires further study.

1.2.5 Optimal Control

A large body of work in disturbance rejection is based upon various formulations of the optimal control problem. Some of the earliest references include [Athans, 1966] and [Johnson, 1971]. [Gupta, 1980] was responsible for developing a method of incorporating frequency shaping into the linear quadratic regulator problem. The work of [Gupta, 1980] has been widely referenced and has been the subject of many publications. This work is generally referred to as Frequency Shaped Cost Functionals (FSCF). The advantage of FSCF over conventional static state feedback optimal control is that it provides much more freedom to shape the dynamic response of the closed-loop system.

Narrowband disturbance rejection is achieved with FSCF by incorporating notch-like weighting filters on either the states or controls. [Sievers, 1991] provides guidelines on how to design MIMO narrowband disturbance rejecting controllers using FSCF. It was also shown in [Sievers, 1991] that the form of the compensator resulting from narrowband design using FSCF is the same as those given in Equations 1.4, 1.5 and 1.7. [Sievers, 1989] presents a comparison of two Linear-Quadratic-Gaussian (LQG) methods for stationary narrowband disturbance rejection. Comparisons between FSCF and a method termed *disturbance modeling* (DM) [Kwakernaak and Sivan, 1972] and [Suhardjo, 1989] were considered. It was discovered that although the design philosophies used to develop

the two LQG-based designs were very different, a duality between them exists. This discovery was important since insights drawn from one design approach might prove valuable in the other approach.

The work presented in this thesis extends the DM narrowband disturbance rejection approach in two ways. First, a new control gain synthesis approach is developed that provides closed-form analytically exact expressions of feed-forward gains for parameterized disturbance models. The second extension is the treatment of nonstationary narrowband disturbances associated with spacecraft reaction wheel imbalance problems. It will be shown that the DM-based control structure has a decoupled optimal control solution, not present in FSCF, that can be exploited to facilitate nonstationary narrowband disturbance rejection.

1.3 Thesis Outline

The fundamental concepts of optimal control are reviewed in Chapter 2. The review starts with a presentation of the necessary conditions for optimality assuming a general cost function with a general nonlinear time-varying plant. Various simplifying assumptions are applied, ultimately leading to the well-know continuous-time algebraic Riccati equation for linear time-invariant plants with quadratic cost functionals. Finally, the concept of frequency shaped cost functionals for both frequency-dependent state and control weighting matrices is reviewed.

Chapter 3 presents the underlying physics associated with reaction wheel imbalances and the form of the narrowband disturbance model structure that is used throughout this work. The development of a closed-form parameterized feed-forward control gain synthesis technique will be presented. A demonstration of this parameterized feed-forward control methodology using a low-order system is also provided.

A treatment of nonstationary narrowband disturbances associated with spacecraft reaction wheel imbalances is presented in Chapter 4. The treatment employs the properties of

Bessel functions to arrive at a finite-term series representation of the time-varying imbalance disturbances. A simplified online wheel state identification technique is developed to demonstrate feasibility of the approach.

Chapter 5 introduces an experimental test article that has been designed and fabricated to validate the optimal feed-forward control methodology developed in this work. The experimental apparatus consists of a very compliant hub-beam employing a variety of spacecraft-traceable sensors and actuators. A reaction wheel is located at the tip of the beam and serves as a harmonic imbalance disturbance source.

The focus of Chapter 6 is on experimental identification of parametric reaction wheel models. Two methods for reaction wheel imbalance identification using steady-state measurement data will be presented. The first method assumes minimal a priori knowledge about the system and the disturbance, but is limited to SIMO systems. The second method requires specific plant information, but is applicable to MIMO systems. Both approaches are validated using simulation and experimentally obtained data.

Chapter 7 presents an experimental demonstration of the effectiveness of the optimal feed-forward control methodology applied to the flexible beam test article. The practical issues and recommendations on the form of state estimation to be employed for this class of disturbances are also considered in this chapter.

Finally, Chapter 8 presents a summary of the thesis followed by a listing of the contributions of the thesis and recommendations for future work.

Chapter 2

OPTIMAL CONTROL FOR LINEAR SYSTEMS

The basic objective of control is to keep the components of the state vector $x(t)$, or some measure of performance formed as a linear combinations of the states, i.e., $y(t) = Cx(t)$, near zero or a reference value r(t), without excessive expenditure of control energy. Over the past four decades researchers have focused on developing methods to accomplish this objective. As a result, formal methods in optimal control theory have been developed and successfully deployed on a great number of aerospace missions. This chapter presents an overview of these methods and establishes the mathematical tools that will be employed in subsequent chapters.

2.1 The Optimal Control Problem

This section will present the solution to the optimal control problem for a general nonlinear time-varying system. The approach used here will be to present the necessary conditions for optimality for a general cost functional followed by those used with quadratic cost functionals. For a complete treatment of the necessary and sufficient conditions for optimality see [Anderson, 1971, and Kirk, 1970]. Consider the plant described by the nonlinear time-varying dynamical equation

$$\dot{x}(t) = f(x(t), u(t), t) \tag{2.1}$$

with state $x(t) \in \Re^n$ and control input function $u(t) \in \Re^m$. The optimal control problem is to determine an admissible $u(t)$ that minimizes the performance index $J(u)$. Consider the following performance index

$$J(u) = \Psi(x(t_1)) + \int_{t_0}^{t_1} L(x(t), u(t), t)dt \tag{2.2}$$

where $\Psi(x)$ and $L(x, u, t)$ are continuous real-valued scalar functions. The terminal time weighting function, $\Psi(x)$, depends on the final state $x(t_1)$, whereas the weighting function, $L(x, u, t)$, depends on the state and input at intermediate times in $[t_0, t_1]$. The type of optimal control problem considered in this work is referred to as a fixed final time with free final states and is directly applicable to structural control. The condition of free final states implies that there are no explicit final time state constraints, i.e., the state at t_1 is not constrained to a lie on any particular surface. Fixed final state problems are very typical in optimal rendezvous and docking, and targeting problems where the value of the states at t_1 are mission critical. Rarely in structural control is there a need to constrain the final states in this manner and therefore fixed final state problems will not be addressed in this work.

In presenting the necessary conditions for optimality, it is convenient to define the scalar function H (the Hamiltonian function) as

$$H = L(x(t), u(t), t) + p^T(t)f(x(t), u(t), t) \tag{2.3}$$

where $p(t) \in \Re^n$ are Lagrange multiplier functions (also called the costate). Introducing the Hamiltonian into Equation 2.2 gives

$$J(u) = \Psi(x(t_1)) + \int_{t_0}^{t_1} (H(x(t), p(t), u(t), t) - p^T(t)\dot{x}(t))dt \tag{2.4}$$

The necessary conditions for an optimal solution of Equation 2.4 subject to Equation 2.1 are

$$\dot{x}(t) = \frac{\partial}{\partial p}H(x(t), u(t), p(t), t) \tag{2.5}$$

$$\dot{p}(t) = -\frac{\partial}{\partial x}H(x(t), u(t), p(t), t) \tag{2.6}$$

$$\frac{\partial}{\partial u}H(x(t), u(t), p(t), t) = 0 \tag{2.7}$$

which are valid for all $t \in [t_0, t_1]$. The following boundary terms are needed to uniquely specify the solutions $x(t)$ and $p(t)$ to Equations 2.5 and 2.6

$$x(t_0) = x_0 \quad \text{and} \quad \frac{\partial}{\partial x}\Psi x(t_1) - p(t_1) = 0 \tag{2.8}$$

Equations 2.5 through 2.8 define a $2n$ set of nonlinear first order differential equations with split boundary conditions at t_0 and t_1. Nonlinear differential equations with split boundary terms, i.e., nonlinear two-point boundary-value problems, are in general very difficult to solve. This work will not address the solution of such problems, but instead apply Equations 2.5 through 2.8 to linear time-varying and time-invariant systems for the purpose of mitigating the influence of disturbances.

2.2 Linear Time-Varying Optimal Control

In this section, the general necessary conditions for optimality presented in Section 2.1 will be applied to a linear time-varying system with a quadratic performance index. The dynamical system of interest is as follows:

$$\dot{x}(t) = A(t)x(t) + B_u(t)u(t) \tag{2.9}$$

with state $x(t) \in \Re^n$, and control input function $u(t) \in \Re^m$. The quadratic performance index considered in this section has the following form

$$J(u) = \frac{1}{2}x^T(t_1)Fx(t_1) + \frac{1}{2}\int_{t_0}^{t_1}(x^T(t)Q(t)x(t) + u^T(t)R(t)u(t))dt \tag{2.10}$$

where $Q(t)$ and F are symmetric and positive semi-definite and $R(t)$ is symmetric positive definite, i.e., $Q(t) \geq 0$, $F \geq 0$ and $R(t) > 0$. The Hamiltonian function associated with optimal control problem defined by Equations 2.9 and 2.10 is

$$H = \frac{1}{2}(x^T(t)Qx(t) + u^T(t)Ru(t)) + (A(t)x(t) + B_u(t)u(t))^T p(t) \tag{2.11}$$

Applying the necessary conditions for optimality, i.e., Equations 2.5 through 2.8, results in the following linear time-varying two point boundary value problem

$$\dot{x}(t) = A(t)x(t) + B_u(t)u(t) \tag{2.12}$$

$$\dot{p}(t) = -Q(t)x(t) - A^T(t)p(t) \tag{2.13}$$

$$R(t)u(t) + B_u^T(t)p(t) = 0 \tag{2.14}$$

$$x(t_0) = x_0 \quad \text{and} \quad Fx(t_1) - p(t_1) = 0 \tag{2.15}$$

Solving for the optimal control in Equation 2.14 and substituting into Equation 2.12 gives the following $2n$ set of coupled first-order homogenous differential equations

$$\begin{bmatrix} \dot{x}(t) \\ \dot{p}(t) \end{bmatrix} = \begin{bmatrix} A(t) & -B(t)R^{-1}(t)B^T(t) \\ -Q(t) & -A^T(t) \end{bmatrix} \begin{bmatrix} x(t) \\ p(t) \end{bmatrix} \tag{2.16}$$

The coefficient matrix is called the continuous-time Hamiltonian matrix and has some very special properties that will be discussed in Section 2.3. Since Equation 2.16 is linear, its solution can be expressed in terms of its state transition matrix, $\Phi(t, \tau)$. Using the state transition matrix, the solution of Equation 2.16 can be written as

$$\begin{bmatrix} x(t) \\ p(t) \end{bmatrix} = \begin{bmatrix} \Phi_{11}(t, \tau) & \Phi_{12}(t, \tau) \\ \Phi_{21}(t, \tau) & \Phi_{22}(t, \tau) \end{bmatrix} \begin{bmatrix} x(\tau) \\ p(\tau) \end{bmatrix} \tag{2.17}$$

where $\Phi_{ij}(t, \tau)$ are $n \times n$ partitions of $\Phi(t, \tau)$. Expanding Equation 2.17 and employing the terminal time boundary conditions gives the relationship

$$F\Phi_{11}(t_1, t)x(t) + F\Phi_{12}(t_1, t)p(t) = \Phi_{21}(t_1, t)x(t) + \Phi_{22}(t_1, t)p(t) \tag{2.18}$$

Solving Equation for $p(t)$ gives

$$p(t) = [\Phi_{22}(t_1, t) - F\Phi_{12}(t_1, t)]^{-1}[F\Phi_{11}(t_1, t)x(t) - \Phi_{21}(t_1, t)]x(t) \tag{2.19}$$

Equation 2.19 suggests that there is a linear $n \times n$ time-vary matrix that linearly relates the costate to the state. This relationship can be written as

$$p(t) = S(t)x(t) \tag{2.20}$$

where

$$S(t) = [\Phi_{22}(t_1, t) - F\Phi_{12}(t_1, t)]^{-1}[F\Phi_{11}(t_1, t)x(t) - \Phi_{21}(t_1, t)] \tag{2.21}$$

with terminal condition $S(t_1) = F$. It is important to notice that $S(t)$ in Equation 2.21 depends on the terminal time penalty matrix F and terminal time t_1 and is independent of $x(t)$. We may therefore precompute $S(t)$ and use it to define the optimal state feedback control law $u(t)$ by using Equations 2.14 and 2.20

$$u(t) = -R^{-1}(t)B_u^T(t)p(t) = -R^{-1}(t)B_u^T(t)S(t)x(t) \tag{2.22}$$

Equation 2.22 states that the optimal control for a linear time-varying system with a quadratic performance index is linear. Furthermore, for finite-time horizon problems we see from Equation 2.21 that $S(t)$ is time-varying even if A, B_u, Q, and R are time-invariant.

The symmetric positive definite matrix $S(t)$ can also be obtained by solving the following matrix differential equation

$$\dot{S}(t) = -S(t)A(t) - A^T(t)S(t) + S(t)B_u(t)R^{-1}(t)B_u^T(t)S(t) - Q(t) \tag{2.23}$$

which may be obtained by taking the time derivative of Equation 2.20 and using Equation 2.16. Equation 2.23 is called the matrix Riccati equation and is valid for $t \in [t_0, t_1]$ and has the terminal time condition $S(t_1) = F$. The solution $S(t)$ of the nonlinear (quadratic in $S(t)$) time-varying differential equation is typically obtained by numerically integrating Equation 2.23. Alternately, if the state transition matrix for Equation 2.16 can be determined, Equation 2.21 can be used to directly compute $S(t)$.

2.3 The Steady State Solution

As mentioned in the previous section dealing with finite-time horizon optimal control problems, even if the matrices A, B_u, Q, and R are time-invariant, the matrix Riccati solution $S(t)$ will still be time-varying. However, [Kalman, 1960] has shown that for (A, B_u) stabilizable, $(A, \sqrt{Q})$ detectable, and $F = 0$, $S(t) \rightarrow S$ as $t \rightarrow \infty$. In steady state, the matrix Riccati simplifies to the following:

$$SA + A^T S - SB_u R^{-1} B_u^T S + Q = 0 \tag{2.24}$$

Equation 2.24 is called the continuous-time algebraic Riccati equation (CARE). The steady state solution for Equation 2.24 can be obtained by manipulating the matrix exponential of the constant coefficient differential equation

$$\begin{bmatrix} \dot{x}(t) \\ \dot{p}(t) \end{bmatrix} = \begin{bmatrix} A & -BR^{-1}B^T \\ -Q & -A^T \end{bmatrix} \begin{bmatrix} x(t) \\ p(t) \end{bmatrix} \tag{2.25}$$

Before pursuing the matrix exponential solution for Equation 2.25, it is important to present some special properties of general Hamiltonian matrices and show how they may be exploited to assist in solving for the steady state Riccati solution.

Define a real $2nx2n$ matrix of the form:

$$H = \begin{bmatrix} A & G \\ E & -A^T \end{bmatrix}_{2nx2n} \tag{2.26}$$

The matrix H is called Hamiltonian if $A \in \Re^{nxn}$, $G^T = G \in \Re^{nxn}$, and $E^T = E \in \Re^{nxn}$.

Consider the following transformation matrix:

$$J = \begin{bmatrix} 0 & I \\ -I & 0 \end{bmatrix}_{2nx2n} \tag{2.27}$$

Clearly, J has the following properties

$$J^T = J^{-1} = -J \tag{2.28}$$

Applying the above transformation to H gives:

$$J^T H J = -H^T \tag{2.29}$$

The transformation used above reveals that H and $-H^T$ are similar, therefore if μ is an eigenvalue of H, then so is $-\mu$, i.e., the eigenvalues of H are completely symmetric in the complex plane, where an example of complete symmetry is indicated in Figure 2.1.

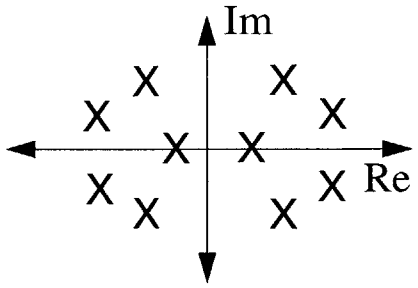

Figure 2.1 Eigenvalues of a General Hamiltonian Matrix

Using the above eigenvalue property for Hamiltonian matrices, the eigenproblem may be expressed as

$$\begin{bmatrix} A & -BR^{-1}B^T \\ -Q & -A^T \end{bmatrix} \begin{bmatrix} \bar{V}_1 & \bar{V}_2 \\ \bar{V}_3 & \bar{V}_4 \end{bmatrix} = \begin{bmatrix} \bar{V}_1 & \bar{V}_2 \\ \bar{V}_3 & \bar{V}_4 \end{bmatrix} \begin{bmatrix} \Lambda_1 & 0 \\ 0 & \Lambda_2 \end{bmatrix} \tag{2.30}$$

or

$$\begin{bmatrix} U_1 & U_2 \\ U_3 & U_4 \end{bmatrix} \begin{bmatrix} A & -BR^{-1}B^T \\ -Q & -A^T \end{bmatrix} = \begin{bmatrix} \Lambda_1 & 0 \\ 0 & \Lambda_2 \end{bmatrix} \begin{bmatrix} U_1 & U_2 \\ U_3 & U_4 \end{bmatrix} \tag{2.31}$$

where Λ_1 and Λ_2 correspond to the left (stable) and right (unstable) half-plane eigenvalues of H, respectively. Using Equations 2.30 and 2.31, the coefficient matrix in Equation 2.25 can be written as

$$H = \begin{bmatrix} A & -BR^{-1}B^T \\ -Q & -A^T \end{bmatrix}_{2n \times 2n} = \begin{bmatrix} \bar{V}_1 & \bar{V}_2 \\ \bar{V}_3 & \bar{V}_4 \end{bmatrix} \begin{bmatrix} \Lambda_1 & 0 \\ 0 & \Lambda_2 \end{bmatrix} \begin{bmatrix} U_1 & U_2 \\ U_3 & U_4 \end{bmatrix} \tag{2.32}$$

Equation 2.32 may be used to determine the matrix exponential of the differential equation presented in Equation 2.25. This matrix exponential can then be used to solve for the state and costate at time t_f as follows:

$$\begin{bmatrix} x(t_1) \\ p(t_1) \end{bmatrix} = \begin{bmatrix} \bar{V}_1 & \bar{V}_2 \\ \bar{V}_3 & \bar{V}_4 \end{bmatrix} \begin{bmatrix} e^{\Lambda_1 \tau} & 0 \\ 0 & e^{\Lambda_2 \tau} \end{bmatrix} \begin{bmatrix} U_1 & U_2 \\ U_3 & U_4 \end{bmatrix} \begin{bmatrix} x(t) \\ p(t) \end{bmatrix} \tag{2.33}$$

with $\tau = t_1 - t$. Expanding the first row in Equation 2.33 gives

$$x(t_1) = (\bar{V}_1 e^{\Lambda_1 \tau} U_1 + \bar{V}_2 e^{\Lambda_2 \tau} U_3) x(t) + (\bar{V}_1 e^{\Lambda_1 \tau} U_2 + \bar{V}_2 e^{\Lambda_2 \tau} U_4) p(t) \tag{2.34}$$

In order for $x(t_1) \to 0$ in steady state, we need the terms involving the increasing exponentials to vanish. This implies that

$$\bar{V}_2 e^{\Lambda_2 \tau} U_3 x(t) + \bar{V}_2 e^{\Lambda_2 \tau} U_4 p(t) = 0 \tag{2.35}$$

or

$$p(t) = -U_4^{-1} U_3 x(t) \tag{2.36}$$

From Equation 2.36 we see that the spectral factorization, $\bar{V}\Lambda U$, appropriately partitioned into stable and unstable eigenvalues, yields the steady state solution, S, to the matrix Riccati equation. The solution has the form:

$$S = -U_4^{-1} U_3 \tag{2.37}$$

Using a matrix inversion identity, the solution may be conveniently rewritten in terms of partitions in $\bar{V}$ as:

$$S = \bar{V}_3 \bar{V}_1^{-1} \tag{2.38}$$

From Equation 2.38 we see that the steady state solution to the CARE can be expressed in terms of the vectors that span the invariant subspace corresponding to the stable eigenvalues of H. For more information on the solution to algebraic Riccati equations see [Potter, 1966 and Laub, 1979].

2.4 Finite-Time Optimal Control Solutions for LTI Matrices

Previously we have presented optimal control solutions for the linear time-varying plant with finite-time horizon and for the linear time invariant plant with infinite-time horizon. In this section we will present a solution to the optimal control problem for linear time-invariant plants over a finite-time horizon. Recall the matrix Riccati equation corresponding to this problem is given as (see Equation 2.23)

$$\dot{S}(t) = -S(t)A - A^T S(t) + S(t)B_u R^{-1} B_u^T S(t) - Q \tag{2.39}$$

with terminal time condition $S(t_1) = F$. Also recall that the symmetric positive definite solution $S(t)$ is obtained by numerically integrating Equation 2.39, or alternately, from the state transition matrix for Equation 2.16. For the case when the matrices A, B_u, Q,

and R are time-invariant with t_1 bounded, an alternate solution may be obtained, [Junkins, 1986]. Assume $S(t)$ can be written as

$$S(t) = S + Z(t)^{-1} \tag{2.40}$$

where S is the solution to the steady state CARE (Equation 2.24) and $Z(t)$ is an undetermined symmetric positive definite matrix. Differentiating Equation 2.40 gives

$$\dot{S}(t) = \dot{Z}(t)^{-1} = -Z(t)^{-1}\dot{Z}(t)Z(t)^{-1} \tag{2.41}$$

Substituting Equations 2.40 and 2.41 into Equation 2.39 gives

$$\dot{Z}(t) = (A - B_u R^{-1} B_u^T S)Z(t) + Z(t)(A^T - SB_u R^{-1} B_u^T) - B_u R^{-1} B_u^T \tag{2.42}$$

with terminal condition $Z(t_1) = [S(t_1) - S]^{-1} = [F - S]^{-1}$. Notice that Equation 2.42 is a linear constant coefficient differential equation as opposed to Equation 2.39 which is a nonlinear differential equation. The solution to Equation 2.42 [Davison, 1975] can be shown by direct substitution to be

$$Z(t) = Z_{ss} + e^{A_{cl}(t-t_1)}[Z(t_1) - Z_{ss}]e^{A_{cl}^T(t-t_1)} \tag{2.43}$$

where $A_{cl} = A - B_u R^{-1} B_u^T S$, and Z_{ss} must satisfy the matrix algebraic equation

$$A_{cl}Z_{ss} + Z_{ss}A_{cl}^T - B_u R^{-1} B_u^T = 0 \tag{2.44}$$

Notice that although Equation 2.43 is mathematically well-posed, computing $Z(t)$ numerically may be difficult. The difficulty arises from the numerical values in the two exponential terms. Since the closed-loop plant matrix, A_{cl}, is strictly stable and $(t - t_1)$ is always negative the matrix exponentials may not be representable by IEEE double precision engineering software. The solution to the problem is to compute $Z(t)^{-1}$ directly as opposed to computing the inverse of $Z(t)$ at every time step. The inverse of $Z(t)$ may be written as

$$Z(t)^{-1} = W(t)^{-1}(I - (Z_{ss}^{-1} + W(t)^{-1})^{-1} W(t)^{-1}) \tag{2.45}$$

where $W(t)^{-1}$ is defined as

$$W(t)^{-1} = e^{A_{cl}^T(t_1-t)}[Z(t_1)-Z_{ss}]^{-1}e^{A_{cl}(t_1-t)} \tag{2.46}$$

Notice, that the matrix exponentials in Equation 2.46 are numerically well posed for all values of (t_1-t).

Considering Equation 2.40, the optimal control has the following form

$$u(t) = -R^{-1}B_u^T S(t)x(t) = -R^{-1}B_u^T Sx(t) - R^{-1}B_u^T Z(t)^{-1}x(t) \tag{2.47}$$

Notice that Equation 2.47 consists of a steady state portion (identical to the steady state solution presented in Section 2.3) and a transient portion. The transient portion decays in a few time constants of the closed-loop plant A_{cl}.

2.5 Stochastic Linear Optimal Control

The standard regulator problem, i.e., driving the states to zero from some initial condition, for many control applications provides sufficient performance. However, for systems subject to persistent disturbances alternate techniques may be necessary. An important step in deriving optimal disturbance accommodating controllers is to understand optimal control for systems that are subject to persistent random excitation. The class of systems of interest are defined as

$$\dot{x}(t) = A(t)x(t) + B_u(t)u(t) + B_w(t)w(t) \tag{2.48}$$

where $w(t)$ is assumed to be a stationary zero mean white-noise process with a correlation matrix

$$E[w(t)w^T(\tau)] = W\delta(t-\tau) \tag{2.49}$$

with $W = const$ and the symbol $E[\ ]$ denoting the expected value. Due to the stochastic nature of the disturbance, the state, $x(t)$, is a random process for any control law. Since

$x(t)$ is a random process, the performance index given in Equation 2.10 is a random function and no longer represents a meaningful objective function for minimization. Therefore, given the stochastic nature of the state and hence the performance index, a meaningful objective is to minimize

$$J = E\left[\frac{1}{2}x^T(t_1)Fx(t_1) + \frac{1}{2}\int_{t_0}^{t_1}(x^T(t)Q(t)x(t) + u^T(t)R(t)u(t))dt\right] \tag{2.50}$$

Most textbooks dealing with stochastic optimal control present solution techniques for Equation 2.50, but for the sake of completeness a method employing the Hamilton-Jacobi-Bellman (HJB) equation [Stengel, 1986] is presented. The HJB equation is essentially a formal statement of the minimum principle [Pontryagin, et al., 1962] which provides a global criterion for optimality. The HJB equation associated with performance index Equation 2.50 and dynamic system Equation 2.48 is given as

$$\frac{\partial}{\partial t}V(x(t), t) = -\left\{\frac{1}{2}(x^TQx + u^{*T}Ru^*) + \frac{\partial V}{\partial x}(Ax + B_u u^*) + \frac{1}{2}Tr\left(\frac{\partial^2 V}{\partial x^2}B_w W B_w^T\right)\right\} \tag{2.51}$$

where $u^*(t)$ is denoted as the optimal control and Tr is defined as the trace operator. It should be noted that as a result of the problem formulation leading to the HJB equation, the value function, $V(x(t), t)$, in Equation 2.51 is not considered a function of $u(t)$. Equation 2.51 can be rewritten as

$$\frac{\partial}{\partial t}V(x(t), t) = \min_u\left\{\frac{1}{2}(x^TQx + u^TRu) + \frac{\partial V}{\partial x}(Ax + B_u u) + \frac{1}{2}Tr\left(\frac{\partial^2 V}{\partial x^2}B_w W B_w^T\right)\right\} \tag{2.52}$$

In an attempt to reach a useful solution to the above HJB, a general form of the optimal index must be assumed as

$$V(x(t), t) = \frac{1}{2}x^T(t)S(t)x(t) + v(t) \tag{2.53}$$

The rational for the functional form of Equation 2.53 is formally justified for the deterministic case in [Anderson, 1971], while [Stengel, 1986] extends it to the stochastic problem. In [Stengel, 1986], the term $v(t)$ is called the stochastic value function increment and can be shown, see [Kwakernaak and Sivan, 1972], to have the form

$$v(t) = \frac{1}{2}\int_{t}^{t_1} Tr\left(\frac{\partial^2 V}{\partial x^2} B_w W B_w^T\right) dt \tag{2.54}$$

The left-hand side of the Equation 2.52 can be obtained by differentiating Equation 2.53 which gives

$$\frac{\partial V}{\partial t} = \frac{dV}{dt} - \frac{\partial V}{\partial x}\frac{dx}{dt} = \frac{1}{2}x^T(t)\dot{S}x(t) + \dot{v}(t) \tag{2.55}$$

Using the stochastic value function increment in the above expression gives

$$\frac{\partial V}{\partial t} = \frac{1}{2}x^T(t)\dot{S}x(t) - \frac{1}{2}Tr\left(\frac{\partial^2 V}{\partial x^2} B_w W B_w^T\right) \tag{2.56}$$

The minimum of the right-hand side of the Equation 2.52 can be obtained by differentiating with respect to $u(t)$ and setting the result equal to zero. This process results in the expression

$$u(t) = -R^{-1}B_u^T\left(\frac{\partial V}{\partial x}\right)^T = -R^{-1}B_u^T S(t)x(t) \tag{2.57}$$

Substituting Equations 2.56 and 2.57 into Equation 2.52 gives

$$\frac{1}{2}x^T\dot{S}x - \frac{1}{2}Tr\left(\frac{\partial^2 V}{\partial x^2} B_w W B_w^T\right) = -\frac{1}{2}x^T(Q + 2SA - SB_u R^{-1}B_u^T S)x - \frac{1}{2}Tr\left(\frac{\partial^2 V}{\partial x^2} B_w W B_w^T\right) \tag{2.58}$$

Due to the quadratic form of Equation 2.58, the non-symmetric term SA may be replaced by $\frac{1}{2}(SA + A^T S)$, resulting in

$$x^T \dot{S} x = -x^T (Q + SA + A^T S - S B_u R^{-1} B_u^T S) x \tag{2.59}$$

or

$$\dot{S}(t) = -S(t)A - A^T S(t) + S(t) B_u R^{-1} B_u^T S(t) - Q \tag{2.60}$$

Notice that the matrix Riccati equation in Equation 2.60 is identical to that given in Equation 2.23 for the deterministic case. This suggests that optimality is obtained for a system excited by white noise by simply ignoring the disturbance. We will see in Chapter 3 that alternate techniques are available for systems excited by non-white disturbances. It should also be noted that the above formulation also applies to the steady-state stochastic optimal control problem. In steady-state, the stochastic optimal control is obtained by solving CARE, Equation 2.24.

2.6 Frequency Shaped Cost Functionals

In many applications, the methods for optimal control of LTI systems presented in this chapter result in controllers with acceptable performance. However, there may be cases when the required loop dynamics cannot be achieved using conventional LQR design methods. For these cases alternate optimal control design strategies are needed. In reference [Gupta, 1980], a method is developed that allows designers to add frequency-dependent state and control weighting matrices to the standard linear quadratic optimal control problem. Using frequency shaped cost functionals, a control designer may explicitly shape the loop dynamics by selecting state and/or control weighting functions. Adding explicit roll-off to limit controller bandwidth, adding attenuation in control authority in a region of model uncertainty, and adding narrow-band amplification of control authority to account for disturbances are just a few examples of loop shaping.

The frequency-weighted optimal control is most easily understood by casting the infinite time horizon version of Equation 2.10 into the frequency domain using Parseval's theorem

$$J = \frac{1}{2\pi}\int_{-\infty}^{\infty}(x^H(j\omega)Q(j\omega)x(j\omega) + u^H(j\omega)R(j\omega)u(j\omega))d\omega \tag{2.61}$$

The frequency domain weighting functions $Q(j\omega)$ and $R(j\omega)$ may be rewritten as

$$Q(j\omega) = W_s^H(j\omega)W_s(j\omega) \tag{2.62}$$

and

$$R(j\omega) = W_c^H(j\omega)W_c(j\omega) \tag{2.63}$$

where $W_s(j\omega)$ and $W_c(j\omega)$ are at least proper, realizable transfer function matrices.

Substituting Equations 2.62 and 2.63 into 2.61 results in the following frequency domain cost functional

$$J = \frac{1}{2\pi}\int_{-\infty}^{\infty}(x^H(j\omega)W_s^H(j\omega)W_s(j\omega)x(j\omega) + u^H(j\omega)W_c^H(j\omega)W_c(j\omega)u(j\omega))d\omega \tag{2.64}$$

We may now introduce the following notation

$$Z_s(j\omega) = W_s(j\omega)x(j\omega) \tag{2.65}$$

and

$$Z_c(j\omega) = W_c(j\omega)u(j\omega) \tag{2.66}$$

resulting in the following frequency domain cost functional

$$J = \frac{1}{2\pi}\int_{-\infty}^{\infty}(Z_s{}^H(j\omega)Z_s(j\omega) + Z_c{}^H(j\omega)Z_c(j\omega))d\omega \tag{2.67}$$

Using Parseval's theorem, Equation 2.67 may be transformed back to the time domain as

$$J = \lim_{T\to\infty}\frac{1}{2T}\int_0^T(Z_s{}^T(t)Z_s(t) + Z_c{}^T(t)Z_c(t))dt \tag{2.68}$$

In order to solve Equation 2.68 using conventional LQR solution techniques, $Z_s(t)$ and $Z_c(t)$ must be modeled as the outputs of two state-space systems.

$$\dot{x}_s(t) = A_s x_s(t) + B_s x(t) \tag{2.69}$$

$$Z_s(t) = C_s x_s(t) + D_s x(t) \tag{2.70}$$

$$\dot{x}_c(t) = A_c x_c(t) + B_c u(t) \tag{2.71}$$

$$Z_c(t) = C_c x_c(t) + D_c u(t) \tag{2.72}$$

Given the above state-space realizations, the transfer function matrices from Equations 2.65 and 2.66 are defined as

$$W_s(j\omega) = C_s(j\omega I - A_s)^{-1} B_s + D_s \tag{2.73}$$

$$W_c(j\omega) = C_c(j\omega I - A_c)^{-1} B_c + D_c \tag{2.74}$$

Now that the basic structure of the state and control weighting filters has been prescribed, i.e., Equations 2.73 and 2.74, the closed-loop system dynamics are shaped by appropriately selecting the elements of the state-space systems given in Equations 2.69 through 2.72.

Combining the weighting filter dynamics with the nominal plant dynamics results in the following augmented state-space system

$$\begin{bmatrix} \dot{x} \\ \dot{x}_s \\ \dot{x}_c \end{bmatrix} = \begin{bmatrix} A & 0 & 0 \\ B_s & A_s & 0 \\ 0 & 0 & A_c \end{bmatrix} \begin{bmatrix} x \\ x_s \\ x_c \end{bmatrix} + \begin{bmatrix} B \\ 0 \\ B_c \end{bmatrix} u \tag{2.75}$$

$$\begin{bmatrix} Z_s \\ Z_c \end{bmatrix} = \begin{bmatrix} D_s & C_s & 0 \\ 0 & 0 & C_c \end{bmatrix} \begin{bmatrix} x \\ x_s \\ x_c \end{bmatrix} + \begin{bmatrix} 0 \\ D_c \end{bmatrix} u \tag{2.76}$$

Notice that the integrand in the cost functional of Equation 2.68 may be represented as the inner product of Equation 2.76. Performing this inner product results in the following representation of the time-domain cost functional

$$J = \lim_{T\to\infty} \frac{1}{2T}\int_0^T \left(\begin{bmatrix} X^T & u^T \end{bmatrix} \left[\begin{array}{ccc|c} D_s^T D_s & D_s^T C_s & 0 & 0 \\ C_s^T D_s & C_s^T C_s & 0 & 0 \\ 0 & 0 & C_c^T C_c & C_c^T D_c \\ \hline 0 & 0 & D_c^T C_c & D_c^T D_c \end{array}\right] \begin{bmatrix} X \\ u \end{bmatrix} \right) dt \tag{2.77}$$

Equation 2.77 is exactly the form of a general performance integral as given in [Friedland, 1986], which may be expressed as

$$J = \lim_{T\to\infty} \frac{1}{2T}\int_0^T (X^T(t)QX(t) + 2X^T(t)Nu(t) + u^T(t)Ru(t))dt \tag{2.78}$$

where

$$Q = \begin{bmatrix} D_s^T D_s & D_s^T C_s & 0 \\ C_s^T D_s & C_s^T C_s & 0 \\ 0 & 0 & C_c^T C_c \end{bmatrix}, N = \begin{bmatrix} 0 \\ 0 \\ C_c^T D_c \end{bmatrix}, R = D_c^T D_c \tag{2.79}$$

The optimal feedback gain associated with this problem is

$$\bar{K} = R^{-1}(B^T S + N^T) = \begin{bmatrix} K & K_s & K_c \end{bmatrix} \tag{2.80}$$

with a corresponding feedback control of

$$u(t) = -(Kx(t) + K_s x_s(t) + K_c x_c(t)) \tag{2.81}$$

From Equation 2.81 we see that the feedback control signal consists of three terms: a nominal plant state term, a state weighting term, and a control weighting term. Assuming full-state feedback, the nominal plant state term, $Kx(t)$, is formed from plant measurements,

but the state weighting term, $K_s x_s(t)$, and control weighting term, $K_c x_c(t)$, must be simulated (propagated) in real-time to provide the necessary signals required by the control law. For this reason, frequency-weighted optimal control is considered a form of dynamic compensation. For most real-world systems, particularly structural systems, full state is generally not available and a state estimator must be included in both design and implementation. Therefore, due to its similarity, frequency-weighted optimal control fits nicely into the standard control system implementation model while also providing the design freedom to explicitly shape the closed-loop dynamics.

2.7 Summary

This chapter has presented an overview of the fundamental concepts of optimal control. The presentation begins with the most general nonlinear time-varying plant and presents the corresponding necessary conditions for optimality. The general case is then simplified to linear time-varying and then linear time-invariant plants with quadratic cost indices. The continuous-time algebraic Riccati equation is introduced and solutions to the finite-horizon optimal control problem are given. The Hamilton-Jacobi-Bellman (HJB) equations are presented and used to provide a solution to the stochastic linear optimal control problem. Finally, the concept of loop shaping is presented in the discussion on frequency shaped cost functionals.

Chapter 3

OPTIMAL REJECTION OF QUASI-STATIONARY DISTURBANCES

In Chapter 2 we reviewed some of the fundamental formulations for various types of optimal control problems and discussed their solution methodologies. In this chapter we will integrate concepts of disturbance modeling with optimal control to form optimal disturbance accommodating controllers. A methodology for rejecting slowly time-varying, multi-tonal narrow-band disturbances, typical of those associated with rotating imbalances will be developed. Of particular interest to this research are the multi-tonal disturbances associated with spacecraft reaction wheel imbalances.

The methodology developed in this chapter utilizes optimal control theory to minimize a standard quadratic performance index. One of the fundamental differences between this approach and typical optimal control is that the focus in this work will be on obtaining parameterized closed-form symbolic expressions for the optimal control gains instead of the standard point-wise numeric solutions. In the case of the reaction wheel disturbance rejection problem, the symbolic optimal control gains are parameterized in terms of disturbance model parameters, enabling continuous and analytically exact gain adjustments as a function of the scheduling parameters. Typical scheduling parameters for the reaction wheel imbalance problem may be wheel spin rate, imbalance magnitudes, and imbalance phase angles.

An essential element in this approach is the necessity to analytically model the reaction wheel disturbances. Recent works [Bialke, 1997], [Bialke, 1998] and [Masterson, et al.,

1999] have presented analytic expressions for reaction wheel imbalance harmonics as a function of wheel speed and imbalance magnitudes. These models provide a basis for the mathematical models used in this control design and implementation methodology.

3.1 Reaction Wheel Imbalance Models

The structure of the analytic disturbance models to be used for control design will be presented in this Section. For an excellent treatment of dynamics of reaction wheel imbalances see [Masterson, et al., 1999 and Elias, 2001]. The modeling approach taken in this work is to employ generic disturbance models whose coefficients and parameters may be refined and enhanced as necessary through experimental data analysis. In this chapter, a steady-state analytic model of the disturbances resulting from a reaction wheel imbalance is assumed to have the form

$$w(t) = \sum_{i=1}^{p} M_i(\Omega_i)\sin(\Omega_i t + \phi_i) \tag{3.1}$$

where $M_i(\Omega_i)$ is a frequency dependent, i.e., spin-rate dependent magnitude function, Ω_i is a discrete frequency value, and ϕ_i is a general phase shift. It should be noted that for reaction wheel imbalances the frequency terms, Ω_i, are typically, but not limited to, integer multiples of the wheel spin rate. The non-integer frequency terms are usually related to shaft bearing effects, shaft lubrication effects, as well as other effects. Considering that Equation 3.1 is essentially a Fourier Series expansion of $w(t)$, it therefore needs little justification. The Fourier Series is particularly well-suited to represent functions whose spectral content closely approximates delta functions in the frequency domain. As an example of the spectral content of reaction wheel imbalance forces, a power spectral density (PSD) analysis of the MACE [Miller et al., 1996] reaction wheel cluster is given in Figure 3.1. The spectral waterfall plot presented in this figure was obtained by repeatedly performing a PSD analysis at selected discrete wheel speeds. This steady-state data was obtained experimentally using a 6 axis force/moment load cell. This data clearly shows multiple harmonics, with a dominate first harmonic. It should be noted that the load cell/mounting

fixture had a flexible mode near 40 Hz which explains the non-speed dependent spectral content at or near 40 Hz. It will be shown in Chapter 6 that data of the form presented in Figure 3.1 can be used to identify the model parameters required in Equation 3.1.

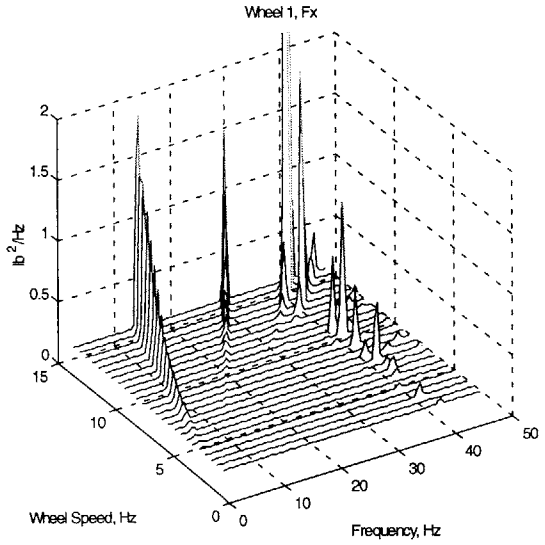

Figure 3.1 MACE reaction wheel imbalance.

Further justification of Equation 3.1 is seen by examining an idealization of a static imbalance on a simple spring-mass-damper system given in Figure 3.2. The equations of motion that describe this system are

$$(M+m)\ddot{x}(t) + C\dot{x}(t) + Kx(t) = me(\dot{\theta}^2 \sin(\theta(t)) - \ddot{\theta}\cos(\theta(t))) \tag{3.2}$$

or

$$(M+m)\ddot{x}(t) + C\dot{x}(t) + Kx(t) = w(t) \tag{3.3}$$

where $w(t)$ is defined as

$$w(t) = me(\dot{\theta}^2 \sin(\theta(t)) - \ddot{\theta}\cos(\theta(t))) \tag{3.4}$$

Notice that for a constant wheel speed ($\dot{\theta} = \Omega = const$), Equation 3.4 reduces to

$$w(t) = me\Omega^2 \sin(\Omega t + \theta_0) \tag{3.5}$$

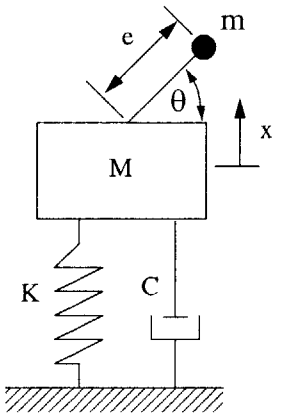

Figure 3.2 Idealization of a static imbalance.

A similar expression to that given in Equation 3.4 is obtained when modeling a dynamic imbalance. A dynamic imbalance results from an angular misalignment between the principal axes of inertia of a body with its spin axis. In Figure 3.3 the principal axes of inertia

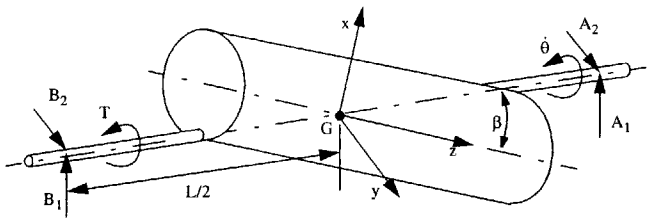

Figure 3.3 Idealization of a dynamic imbalance.

of the body are skewed from the spin axis by the constant angle β. In this example both the shaft and cylinder are assumed to be rigid and are supported by bearings at points A

and B. Furthermore, the center of mass, G, lies on the spin axis and therefore does not experience any acceleration. The bearing reaction forces expressed in an inertially fixed reference frame are given as

$$F_{Ax} = \frac{\sin(2\beta)(I_{xx} - I_{zz})}{2L}(\ddot{\theta}\cos\theta(t) - \dot{\theta}^2\sin\theta(t)) \tag{3.6}$$

$$F_{Ay} = \frac{\sin(2\beta)(I_{xx} - I_{zz})}{2L}(\dot{\theta}^2\cos\theta(t) + \ddot{\theta}\sin\theta(t)) \tag{3.7}$$

$$F_{Bx} = -F_{Ax} \tag{3.8}$$

$$F_{By} = -F_{Ay} \tag{3.9}$$

Notice the similarity between Equations 3.6 and 3.7 and Equation 3.4. Both static and dynamic imbalances manifest themselves in terms of forces (or moments) whose steady-state magnitudes are functions of the wheel spin rate squared. Furthermore, both of these imbalances produce only a once-per-rev disturbance, with higher harmonics resulting from bearings, lubrication, nonlinearities, and other motor related effects.

In many applications it is convenient to model the disturbance as the output of a known dynamical system. For the steady-state wheel speed case this turns out to be very straight forward. To this end, let us first consider $w(t)$ in the Laplace domain. Taking the Laplace transform of Equation 3.1 gives

$$w(s) = \frac{M(\Omega)}{s^2 + \Omega^2}(s\sin\phi + \Omega\cos\phi) \tag{3.10}$$

A linear time-invariant state-space model of the disturbance is assumed to be

$$\dot{x}_1(t) = A_1 x_1(t) + B_1\xi(t) \tag{3.11}$$

$$w(t) = C_1 x_1(t) \tag{3.12}$$

Taking the Laplace transform of Equations 3.11 and 3.12 gives

$$w(s) = [C_1(sI - A_1)^{-1}B_1]\xi(s) = H(s)\xi(s) \tag{3.13}$$

Since there is not an unique state-space realization of the disturbance, the matrices (A_1, B_1, C_1) in Equation 3.13 may be chosen to exactly model $w(s)$ from Equation 3.10 as follows

$$A_1 = \begin{bmatrix} 0 & 1 \\ -\Omega^2 & 0 \end{bmatrix} \quad B_1 = \begin{bmatrix} \sin\theta_0 \\ \Omega\cos\theta_0 \end{bmatrix} M(\Omega) \quad C_1 = \begin{bmatrix} 1 & 0 \end{bmatrix} \tag{3.14}$$

Which gives $H(s) = \dfrac{M(\Omega)}{s^2 + \Omega^2}[s(\sin\theta_0) + \Omega(\cos\theta_0)]$ as desired.

For the general case with multiple harmonics, the disturbance plant matrices take the following structure

$$A_1 = \begin{bmatrix} A_{1_1} & 0 & \cdots & 0 \\ 0 & A_{1_2} & \cdots & 0 \\ \vdots & \cdots & \ddots & \vdots \\ 0 & \cdots & \cdots & A_{1_p} \end{bmatrix} \quad B_1 = \begin{bmatrix} B_{1_1} & 0 & \cdots & 0 \\ 0 & B_{1_2} & \cdots & 0 \\ \vdots & \cdots & \ddots & \vdots \\ 0 & \cdots & \cdots & B_{1_p} \end{bmatrix} \quad C_1 = \begin{bmatrix} C_{1_1} & C_{1_2} & \cdots & C_{1_p} \end{bmatrix} \tag{3.15}$$

where the structure of the individual blocks $(A_{1_i}, B_{1_i}, C_{1_i})$ is identical to those given in Equation 3.14.

As will become apparent later, the eigenvalues and eigenvectors of the disturbance plant matrix play an important role in the optimal control solution. The right eigenvalues/vectors of A_1, or the eigensolution of $A_1 V_1 = V_1 D_1$, have the following form

$$\begin{bmatrix} 0 & 1 \\ -\Omega^2 & 0 \end{bmatrix} \begin{bmatrix} 1 & 1 \\ i\Omega & -i\Omega \end{bmatrix} = \begin{bmatrix} 1 & 1 \\ i\Omega & -i\Omega \end{bmatrix} \begin{bmatrix} i\Omega & 0 \\ 0 & -i\Omega \end{bmatrix} \tag{3.16}$$

The left eigenvalues/vectors of A_1, or the eigensolution of $A_1^T \Psi_1 = \Psi_1 D_1$, have the following form

$$\begin{bmatrix} 0 & -\Omega^2 \\ 1 & 0 \end{bmatrix} \begin{bmatrix} \frac{1}{2} & \frac{1}{2} \\ \frac{1}{2i\Omega} & \frac{-1}{2i\Omega} \end{bmatrix} = \begin{bmatrix} \frac{1}{2} & \frac{1}{2} \\ \frac{1}{2i\Omega} & \frac{-1}{2i\Omega} \end{bmatrix} \begin{bmatrix} i\Omega & 0 \\ 0 & -i\Omega \end{bmatrix} \tag{3.17}$$

It should be noted that as a result of the block diagonal structure of the multi-harmonic disturbance plant matrix, A_1, (see Equation 3.15) its corresponding eigensystem (eigenvalues plus right and left eigenvectors) may be obtained by inspection. This suggests that symbolic eigensolutions for the disturbance plant are not restricted to low dimensional disturbance models.

3.2 Optimal Rejection of Narrowband Disturbances for LTI Systems

The goal of this section is to develop a gain scheduling control design methodology to optimally reject disturbances that possess stationary or slowly varying narrow-band spectral distributions. Reaction wheel disturbances with stationary or slowly varying wheel spin rates naturally fall into this classification (see Figure 3.1). The disturbance accommodation goal will be achieved by combining optimal control theory with parameterized models of the disturbance. The disturbance model parameters, i.e., typically magnitude and frequency as presented in Section 3.1, will be used to schedule the disturbance accommodating controllers. The basic approach will yield a two-part control signal consisting of a gain scheduled feed-forward component and a static state feedback component. It will be shown that the parameterized feed-forward gains can be solved analytically for arbitrarily large disturbance models.

The design approach developed here utilizes a plant augmentation technique called *disturbance modeling* (DM) [Kwakernaak and Sivan, 1972], and is similar in a sense to the frequency shaped cost functional (FSCF) approach presented in Section 2.6. In the FSCF approach the nominal state and/or control signals are augmented with additional dynamics in an attempt to achieve certain loop dynamics. In the approach presented here, the plant is

augmented with a model of the disturbance and this augmented system is then used in an optimal control formulation to achieve improved disturbance rejection performance. Both methods result in a dynamic compensation scheme, with FSCF being completely closed-loop whereas the approach presented here consists of both feed-forward and feedback. A completely feedback implementation of DM is considered in Chapter 7.

To begin the development, recall from Section 2.5 that a system subject to persistent random excitation may be modeled as

$$\dot{x}_2(t) = A_2 x_2(t) + B_u u(t) + B_w w(t) \tag{3.18}$$

where the subscript "2" is used to designate the nominal plant system. Furthermore, recall that $w(t)$ is assumed to be a stationary zero mean white-noise process. In Section 3.1 we have shown that a linear time-invariant state-space model of the disturbance may be given by

$$\dot{x}_1(t) = A_1 x_1(t) + B_1 \xi(t) \tag{3.19}$$

$$w(t) = C_1 x_1(t) \tag{3.20}$$

Where the elements in (A_1, B_1, C_1) are chosen to adequately model the spectral content of $w(t)$. For notational purposes, assume $A_2 \in \Re^{nxn}$ and $A_1 \in \Re^{pxp}$. In most structural systems, $n \gg p$, but no assumptions regarding the relative orders of n and p are necessary in this work. Furthermore, the premise used in the remainder of this work is that the plant defined by (A_2, B_u, B_w) is a linear time invariant system with fully numeric matrices, and that symbolic parameterizations are only in the (A_1, B_1, C_1) disturbance models. The plant and disturbance systems may be combined to yield an augmented plant/disturbance system. The augmented system is given as

$$\begin{bmatrix} \dot{x}_1 \\ \dot{x}_2 \end{bmatrix} = \begin{bmatrix} A_1 & 0 \\ B_w C_1 & A_2 \end{bmatrix} \begin{bmatrix} x_1 \\ x_2 \end{bmatrix} + \begin{bmatrix} B_1 \\ 0 \end{bmatrix} \xi + \begin{bmatrix} 0 \\ B_u \end{bmatrix} u \tag{3.21}$$

The combined system described by Equation 3.21 is precisely the same form as the system used in Section 2.5 on stochastic linear optimal control and therefore the optimal control is obtained by solving the matrix Riccati equation, Equation 2.60.

$$\dot{S}(t) = -S(t)A - A^T S(t) + S(t)BR^{-1}B^T S(t) - Q \tag{3.22}$$

where (A, B) are now the augmented plant given in Equation 3.21.

It is important to notice that the (A_1, B_1) disturbance plant enters in as an uncontrollable subsystem to the augmented plant. This feature will be used later to simplify the Riccati equation solution process.

Recall from Chapter 2 that the optimal control has the form

$$u(t) = -R^{-1}B_u^T S(t)x(t) = -K(t)x(t) \tag{3.23}$$

For the augmented system in Equation 3.21, the control vector can also be represented in a partitioned way as

$$u(t) = -R^{-1}\begin{bmatrix} 0 & B_u^T \end{bmatrix}\begin{bmatrix} S_{11} & S_{12} \\ S_{12}^T & S_{22} \end{bmatrix}\begin{bmatrix} x_1(t) \\ x_2(t) \end{bmatrix} = -R^{-1}B_u^T\begin{bmatrix} S_{12}^T & S_{22} \end{bmatrix}\begin{bmatrix} x_1(t) \\ x_2(t) \end{bmatrix} \tag{3.24}$$

or

$$u(t) = -\begin{bmatrix} K_1(t) & K_2(t) \end{bmatrix}\begin{bmatrix} x_1(t) \\ x_2(t) \end{bmatrix} \tag{3.25}$$

Equation 3.24 clearly shows that the optimal control consists of two components; a component that is a linear combination of the original state, $x_2(t)$, and a component that is a linear combination of the disturbance plant state, $x_1(t)$. Since the Riccati solution is independent of the state vector, the conclusion is reached that the optimal control is a combination of a feedback term $K_2(t)x_2(t)$, and a feed-forward term $K_1(t)x_1(t)$. In fact, as will

be shown below, the feedback term is exactly the same term that would be present in the unaugmented system.

The equation representing the combined feedback/feed-forward system is obtained by combining Equations 3.18 and 3.25, as follows

$$\dot{x}_2(t) = (A_2 - B_u K_2(t))x_2(t) - B_u K_1(t)x_1(t) + B_w w(t) \tag{3.26}$$

It's important to note that the feed-forward signal, $K_1(t)x_1(t)$, in addition to $K_1(t)$, also requires the solution of Equation 3.11 or its equivalent, in real-time, to provide the proper phasing and amplitude of the signal. This issue will be addressed in more detail in Section 3.3.

A block diagram representing the feedback/feed-forward system is given in Figure 3.4.

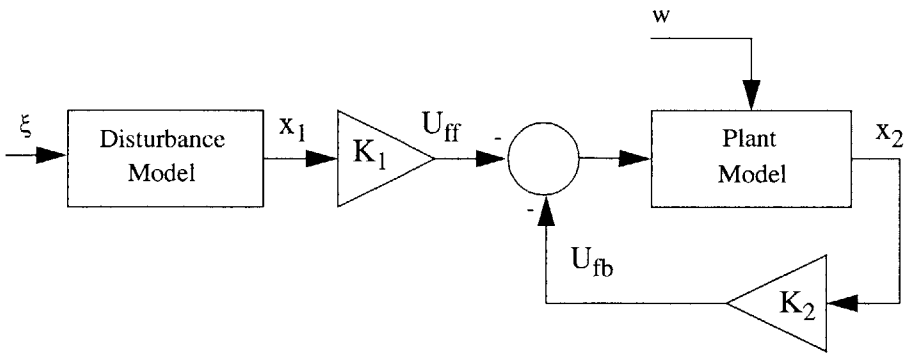

Figure 3.4 Combined feedback/feed-forward control system.

The decoupled nature of the feedback and feed-forward signals may be explored further by examining the partitioned form the matrix Riccati equation. Expanding Equation 3.22 in terms of its block partitions gives

$$\dot{S}_{11} = -S_{11}A_1 - A_1^T S_{11} - S_{12}A_{21} - A_{21}^T S_{12}^T + S_{12}B_u R^{-1} B_u^T S_{12} \tag{3.27}$$

$$\dot{S}_{12}^T = -S_{12}^T A_1 - S_{22}A_{21} - (A_2 - B_u K_2)^T S_{12}^T \tag{3.28}$$

$$\dot{S}_{22} = -S_{22}A_2 - A_2^T S_{22} + S_{22}B_u R^{-1} B_u^T S_{22} - Q_{22} \tag{3.29}$$

Notice that Equation 3.29 is completely decoupled from Equations 3.27 and 3.28 and in fact, is exactly the same Riccati equation that would result if the disturbance was not considered. Since $S_{22}(t)$ can be obtained independently, it may be used directly to solve for $S_{12}(t)$ in Equation 3.28. The differential equation for $S_{12}(t)$ is in fact linear. Specifically, Equation 3.28 is known as a matrix Lyapunov differential equation [Junkins, 1986], [Davison, 1975], and [Bellman, 1960]. In [Davison, 1975] the general solution to a matrix Lyapunov differential equation of the form

$$\dot{X} = M_1 X + X M_2 + M_3, \quad X(0) = C \tag{3.30}$$

is given by

$$X(t) = e^{M_1 t}(C - E)e^{M_2 t} + E \tag{3.31}$$

where E satisfies the matrix Lyapunov equation

$$M_1 E + E M_2 + M_3 = 0 \tag{3.32}$$

It is well-known that a necessary and sufficient condition for Equation 3.32 to have a solution for all M_3 is

$$\lambda_i + \mu_j \neq 0 \tag{3.33}$$

for all i, j where λ_i are the eigenvalues of M_1 and μ_j are the eigenvalues of M_2. In [Junkins, 1986], an alternate solution to Equation 3.32 is presented that does not require $\lambda_i + \mu_j \neq 0$, but instead requires that M_1 and M_2 do not possess repeated eigenvalues. In fact, the solution presented in [Junkins, 1986] may be generalized to include all matrices M_1 and M_2 that possess complete sets of linearly independent eigenvectors. The general form of this solution is

$$X(t) = e^{\lambda t}(C - W(t))e^{\mu t} \tag{3.34}$$

where λ and μ are diagonal matrices of the eigenvalues of M_1 and M_2, respectively and $W(t)$ is defined as

$$W(t) = \int_0^t e^{-\lambda r} N e^{-\mu r} dr \tag{3.35}$$

where N is a constant matrix related to M_3 in Equation 3.30.

In many control applications, particularly those with long operating times, persistent disturbances, or slowly varying narrowband disturbances, it makes sense to examine the steady-state nature of optimal control. Recall from Section 2.3 that the steady state solution, S, to the matrix Riccati equation can be expressed in terms of the vectors that span the invariant subspace corresponding to the stable eigenvalues of the Hamiltonian matrix H. The steady-state solution to Equation 3.29 is therefore

$$S_{22} = \bar{V}_3 \bar{V}_1^{-1} = -U_4^{-1} U_3 \tag{3.36}$$

where $\bar{V}_1$ and $\bar{V}_3$ are eigenvectors of

$$\begin{bmatrix} A_2 & -B_u R^{-1} B_u^T \\ -Q_{22} & -A_2^T \end{bmatrix} \begin{bmatrix} \bar{V}_1 & \bar{V}_2 \\ \bar{V}_3 & \bar{V}_4 \end{bmatrix} = \begin{bmatrix} \bar{V}_1 & \bar{V}_2 \\ \bar{V}_3 & \bar{V}_4 \end{bmatrix} \begin{bmatrix} D_s & 0 \\ 0 & D_u \end{bmatrix} \tag{3.37}$$

and U_4 and U_3 are eigenvectors of

$$\begin{bmatrix} U_1 & U_2 \\ U_3 & U_4 \end{bmatrix} \begin{bmatrix} A_2 & -B_u R^{-1} B_u^T \\ -Q_{22} & -A_2^T \end{bmatrix} = \begin{bmatrix} D_s & 0 \\ 0 & D_u \end{bmatrix} \begin{bmatrix} U_1 & U_2 \\ U_3 & U_4 \end{bmatrix} \tag{3.38}$$

where D_s and D_u are $n \times n$ diagonal matrices of the stable and unstable eigenvalues of H, respectively.

The steady-state solution to Equation 3.28 is obtained by solving the following Lyapunov equation.

$$S_{12}^T A_1 + S_{22} A_{21} + (A_2 - B_u K_2)^T S_{12}^T = 0 \tag{3.39}$$

Introducing the notational simplifications $A_{cl} = (A_2 - B_u K_2)$ and $M = S_{22} A_{21}$ into Equation 3.39 gives

$$S_{12}^T A_1 + A_{cl}^T S_{12}^T + M = 0_{n \times p} \tag{3.40}$$

Equation 3.40 may be transformed into a diagonal system of equations by using the right and left eigenvectors of A_{cl} and A_1. Lets introduce the following notation for the right, V_i, and left, Ψ_i, eigenvectors

$$A_1 V_1 = V_1 D_1 \tag{3.41}$$

$$A_1^T \Psi_1 = \Psi_1 D_1 \tag{3.42}$$

$$A_{cl} V_2 = V_2 D_2 \tag{3.43}$$

$$A_{cl}^T \Psi_2 = \Psi_2 D_2 \tag{3.44}$$

where V_i and Ψ_i are normalized such that

$$\Psi_i^T V_i = I \tag{3.45}$$

Using the above property, Equation 3.40 can be rewritten as

$$S_{12}^T V_1 D_1 \Psi_1^T + \Psi_2 D_2 V_2^T S_{12}^T + M = 0 \tag{3.46}$$

Pre-multiplying Equation 3.46 by V_2^T and post multiplying by V_1 gives

$$V_2^T S_{12}^T V_1 D_1 + D_2 V_2^T S_{12}^T V_1 + V_2^T M V_1 = 0 \tag{3.47}$$

Now, define an $n \times p$ matrix as $Y = V_2^T S_{12}^T V_1$ and substitute into Equation 3.47

$$Y D_1 + D_2 Y + N = 0 \tag{3.48}$$

where $N = V_2^T M V_1$. Solving for the Y_{ij} elements has been greatly simplified as a result of the diagonal coefficient matrices. Expanding Equation 3.48 in terms of the individual elements of the matrix-matrix products gives

$$\begin{bmatrix} Y_{11} & Y_{12} & \cdots & Y_{1p} \\ Y_{21} & Y_{22} & \cdots & Y_{2p} \\ \vdots & \cdots & \ddots & \vdots \\ Y_{n1} & Y_{n2} & \cdots & Y_{np} \end{bmatrix} \begin{bmatrix} D_{11} & 0 & \cdots & 0 \\ 0 & D_{12} & \cdots & 0 \\ \vdots & \cdots & \ddots & \vdots \\ 0 & \cdots & 0 & D_{1p} \end{bmatrix} + \begin{bmatrix} D_{21} & 0 & \cdots & 0 \\ 0 & D_{22} & \cdots & 0 \\ \vdots & \cdots & \ddots & \vdots \\ 0 & 0 & \cdots & D_{2n} \end{bmatrix} \begin{bmatrix} Y_{11} & Y_{12} & \cdots & Y_{1p} \\ Y_{21} & Y_{22} & \cdots & Y_{2p} \\ \vdots & \cdots & \ddots & \vdots \\ Y_{n1} & Y_{n2} & \cdots & Y_{np} \end{bmatrix} \tag{3.49}$$
$$= -\begin{bmatrix} N_{11} & N_{12} & \cdots & N_{1p} \\ N_{21} & N_{22} & \cdots & N_{2p} \\ \vdots & \cdots & \ddots & \vdots \\ N_{n1} & N_{n2} & \cdots & N_{np} \end{bmatrix}$$

Explicitly performing the matrix products in Equation 3.49 gives

$$\begin{bmatrix} D_{11}Y_{11} & D_{12}Y_{12} & \cdots & D_{1p}Y_{1p} \\ D_{11}Y_{21} & D_{12}Y_{22} & \cdots & D_{1p}Y_{2p} \\ \vdots & \cdots & \ddots & \vdots \\ D_{11}Y_{n1} & D_{12}Y_{n2} & \cdots & D_{1p}Y_{np} \end{bmatrix} + \begin{bmatrix} D_{21}Y_{11} & D_{21}Y_{12} & \cdots & D_{21}Y_{1p} \\ D_{22}Y_{21} & D_{22}Y_{22} & \cdots & D_{22}Y_{2p} \\ \vdots & \cdots & \ddots & \vdots \\ D_{2n}Y_{n1} & D_{2n}Y_{n2} & \cdots & D_{2n}Y_{np} \end{bmatrix} \tag{3.50}$$
$$= -\begin{bmatrix} N_{11} & N_{12} & \cdots & N_{1p} \\ N_{21} & N_{22} & \cdots & N_{2p} \\ \vdots & \cdots & \ddots & \vdots \\ N_{n1} & N_{n2} & \cdots & N_{np} \end{bmatrix}$$

From Equation 3.50 it follows that the p-individual columns of Y may be solved with the following matrix-vector equation

$$\begin{bmatrix} D_{1i}+D_{21} & 0 & \cdots & 0 \\ 0 & D_{1i}+D_{22} & \cdots & 0 \\ \vdots & \cdots & \ddots & \vdots \\ 0 & \cdots & \cdots & D_{1i}+D_{2n} \end{bmatrix} \begin{bmatrix} Y_{1i} \\ Y_{2i} \\ \vdots \\ Y_{ni} \end{bmatrix} = -\begin{bmatrix} N_{1i} \\ N_{2i} \\ \vdots \\ N_{ni} \end{bmatrix} \tag{3.51}$$

Notice that the necessary and sufficient condition for the solution of a general Lyapunov equation as given in Equation 3.33 is stated in Equation 3.51 as

$$D_{1i} + D_{2j} \neq 0 \tag{3.52}$$

with $i = 1 \ldots p$ and $j = 1 \ldots n$. Recall from linear quadratic regulator theory with (A_2, B_u) stabilizable and $(A_2, \sqrt{Q_{22}})$ detectable that the eigenvalues of the closed-loop system, D_2, are guaranteed to be stable. Therefore, for Equation 3.52 to be violated, the disturbance model's eigenvalues would have to lie at the mirror images in the complex plane of the D_2 eigenvalues. Recall that the disturbance models presented in Section 3.1 are inherently stable and therefore the solvability condition of Equation 3.52 is always satisfied.

Notice that once the p-individual columns of Y have been obtained using Equation 3.51, they may then be used to solve to for the desired S_{12}^T partition as follows

$$S_{12}^T = \Psi_2 Y \Psi_1^T \tag{3.53}$$

which yields a feed-forward gain of

$$K_1 = R^{-1} B_u^T \Psi_2 Y \Psi_1^T \tag{3.54}$$

Notice that in the computation of S_{12}^T, the closed-loop eigenvector matrices Ψ_2 and V_2 from Equations 3.43 and 3.44 are required. It can be shown that once S_{22} has been computed, as shown in Equation 3.36, that Ψ_2 and V_2 can be obtained with very few additional floating point operations. To show this, one needs to first establish the relationship between Ψ_2 and V_2 and the right and left eigenvectors of the Hamiltonian. From Equation 3.37 we have

$$\begin{bmatrix} A_2 & -B_u R^{-1} B_u^T \\ -Q_{22} & -A_2^T \end{bmatrix} \begin{bmatrix} \bar{V}_1 \\ \bar{V}_3 \end{bmatrix} = \begin{bmatrix} \bar{V}_1 \\ \bar{V}_3 \end{bmatrix} D_s \tag{3.55}$$

or by expanding the first row of Equation 3.55 we get

$$A_2\bar{V}_1 - B_u R^{-1} B_u^T \bar{V}_3 = \bar{V}_1 D_s \tag{3.56}$$

Using Equation 3.36 gives

$$(A_2 - B_u R^{-1} B_u^T S_{22})\bar{V}_1 = (A_2 - B_u K_2)\bar{V}_1 = \bar{V}_1 D_s \tag{3.57}$$

From Equation 3.57 we see that $V_2 = \bar{V}_1$ and therefore once S_{22} has been computed, V_2 is obtained with no additional floating point calculations. Performing a similar analysis using Equation 3.38 gives the following relationship

$$(A_2 - B_u K_2)U_4^{-1} = U_4^{-1} D_s \tag{3.58}$$

From Equation 3.36 we know that S_{22} may be computed from partitions of either $\bar{V}$ or U. However, most eigensolvers do not provide both left and right eigenvectors simultaneously, and certainly not without additional computational expense. It therefore becomes beneficial to exploit relationships between these eigenvector matrices. Using block matrix inversion, we know that there is a relationship between U and $\bar{V}$. One element of this relationship is

$$U_4^{-1} = \bar{V}_4 - S_{22}\bar{V}_2 \tag{3.59}$$

Therefore, from Equations 3.44, 3.58 and 3.59 we find

$$U_4^{-1} = \Psi_2 = \bar{V}_4 - S_{22}\bar{V}_2 \tag{3.60}$$

Equation 3.60 suggests that once S_{22} has been computed Ψ_2 may be obtained with relatively few additional floating point operations.

Thus, we have shown in this section that the disturbance augmented plant results in a Riccati system that decouples into feedback and feed-forward components. Furthermore, we have shown that the feed-forward portion may be solved parametrically in terms of eigen-

parameters of the disturbance model and with few additional floating point operations. These parameterized feed-forward gains form the basis of the disturbance accommodating control methodology developed in this work. Before moving onto an application example, we show how disturbance accommodating control may be used together with loop-shaping control designs to achieve greater design freedom.

3.2.1 Combining Frequency Weighted LQR with Optimal Feed-forward

In this section, we will demonstrate how the frequency weighted cost functional approach (see Section 2.6) can be used together with the optimal feed-forward control to provide more design freedom and potentially higher overall feed-forward performance. Recall from Chapter 2 that the general form of frequency weighted control design included both state and control weighting filters. In this discussion, we will address only state weighting filters; however the methodology is applicable to general state/control weighting. An additional modification to the development presented in Chapter 2 is that the weighting filters will be placed on the performance output instead of purely on the states. The nominal plant augmented with performance output weighting is given as

$$\begin{bmatrix} \dot{x}_2 \\ \dot{x}_s \end{bmatrix} = \begin{bmatrix} A_2 & 0 \\ B_s C_z & A_s \end{bmatrix} \begin{bmatrix} x_2 \\ x_s \end{bmatrix} + \begin{bmatrix} B_u \\ 0 \end{bmatrix} u + \begin{bmatrix} B_w \\ 0 \end{bmatrix} w \tag{3.61}$$

The weighted performance output is given as

$$z = D_s C_z x_2 + C_s x_s \tag{3.62}$$

which gives an augmented Q matrix as

$$Q = \begin{bmatrix} (D_s C_z)^T \\ C_s^T \end{bmatrix} \begin{bmatrix} D_s C_z & C_s \end{bmatrix} = \begin{bmatrix} C_z^T D_s^T D_s C_z & C_z^T D_s^T C_s \\ C_s^T D_s C_z & C_s^T C_s \end{bmatrix} \tag{3.63}$$

Equation 3.61 may be rewritten as

$$\dot{\overline{x}}_2(t) = \overline{A}_2\overline{x}_2(t) + \overline{B}_u u(t) + \overline{B}_w w(t) \tag{3.64}$$

where

$$\overline{A}_2 = \begin{bmatrix} A_2 & 0 \\ B_s C_z & A_s \end{bmatrix}, \overline{B}_u = \begin{bmatrix} B_u \\ 0 \end{bmatrix}, \overline{B}_w = \begin{bmatrix} B_w \\ 0 \end{bmatrix} \tag{3.65}$$

The development of the feed-forward augmented control follows exactly as it did in Equation 3.21, but using the performance filter augmented plant in Equation 3.64 and the weighting matrix defined by Equation 3.63.

3.3 Low-Order Sample Problem

The system in Figure 3.5 will be used as a design example to demonstrate the parameterized feed-forward methodology presented in this chapter. The system consists of two masses interconnected by springs and dampers. This example will examine control topolo-

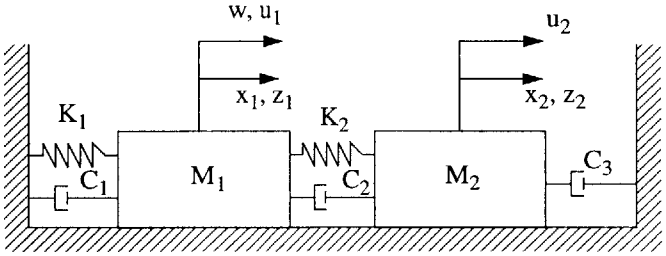

Figure 3.5 Spring-mass system

gies consisting of single input control designs, i.e., u_1 or u_2, with a single output performance metric consisting of a combination of displacement and velocity for either M_1 or M_2. All control designs will assume that the disturbance enters at M_1, which implies $G_{z_i w} = G_{z_i u_1}$. This control topology permits four unique design cases, see Table 3.1. In

TABLE 3.1 Spring-Mass Control Design Cases

Control Design Cases	
Case 1	$G_{z_1 u_1}$
Case 2	$G_{z_2 u_1}$
Case 3	$G_{z_1 u_2}$
Case 4	$G_{z_2 u_2}$

Case 1, the disturbance, control, and performance are collocated at M_1; this configuration is commonly referred to as input isolation. In Case 2, the disturbance and control are collocated at M_1 with performance at M_2. In Case 3, the disturbance and performance are collocated at M_1 with control at M_2. In Case 4, the performance and control are collocated at M_2 with disturbance at M_1; this configuration is commonly referred to as output isolation. For all cases, the state weighting matrix used in the optimal control problem was

$$Q = \begin{bmatrix} C_p & C_v \end{bmatrix}^T \begin{bmatrix} C_p \\ C_v \end{bmatrix} = \begin{bmatrix} C_p^T C_p & C_p^T C_v \\ C_v^T C_p & C_v^T C_v \end{bmatrix} \tag{3.66}$$

where C_p and C_v are position and velocity output influence matrices, respectively. The scalar control penalty weighting term used for all cases was: $\rho = 1/400$. When considering the results, it is important to realize that the uniform treatment of the state and control weighting terms across all cases may not represent the best (or even a good) performance index for all cases. This is particularly true for Case 4 which shows a performance degradation at certain frequencies when using feed-forward control.

The equations of motion for this system are

$$\begin{bmatrix} M_1 & 0 \\ 0 & M_2 \end{bmatrix} \begin{bmatrix} \ddot{x}_1 \\ \ddot{x}_2 \end{bmatrix} + \begin{bmatrix} C_1 + C_2 & -C_2 \\ -C_2 & C_2 + C_3 \end{bmatrix} \begin{bmatrix} \dot{x}_1 \\ \dot{x}_2 \end{bmatrix} + \begin{bmatrix} K_1 + K_2 & -K_2 \\ -K_2 & K_2 \end{bmatrix} \begin{bmatrix} x_1 \\ x_2 \end{bmatrix} = \begin{bmatrix} u_1 \\ u_2 \end{bmatrix} + \begin{bmatrix} w \\ 0 \end{bmatrix} \tag{3.67}$$

Notice that the structure of the damping matrix in Equation 3.67 permits diagonalization using the normal modes of the system. Diagonalization using the normal modes is possible because the damping matrix is in a form consistent with Rayleigh damping, i.e.,

$$C = \alpha M + \beta K \tag{3.68}$$

where constants α and β are chosen to provide the desired amount of modal damping.

The parameters of the system have been chosen to produce undamped natural frequencies of $\omega_1=\pi$ and $\omega_2=3\pi$ *rad/sec*, or $f_1=1/2$ and $f_2=3/2$ *Hz*, and modal damping ratios of $\zeta_1=\zeta_2=5/100$ ($\alpha=0.2356$ and $\beta=0.0080$). The numeric values for the mass and stiffness parameters are given in Table 3.2. Also in Table 3.2 are parameterized expressions for the

TABLE 3.2 Spring-Mass System Parameters

Parameter	Value
M_1	1
M_2	3/2
K_1	$\frac{\pi^2}{2}(10-\sqrt{10}) = 33.74$
K_2	$\frac{3\pi^2}{10}(10+\sqrt{10}) = 38.97$
C_1	$\frac{\pi}{8}(8+\sqrt{10})\zeta_1+\frac{3\pi}{8}(8-\sqrt{10})\zeta_2 = 0.5041$
C_2	$\frac{3\pi}{40}(10+\sqrt{10})(3\zeta_2-\zeta_1) = 0.3101$
C_3	$\frac{9\pi}{8}(3\zeta_1-\zeta_2) = 0.3534$

damping elements given in terms of the modal damping ratios ζ_1 and ζ_2. These parameterized expressions could be helpful if one wanted to study the impact of modal damping on system performance without transforming the system to modal coordinates. However, most structural systems, particularly large-order systems, are transformed to modal coor-

dinates using the normal modes of the system. The normal modes of the system are obtained from solving the following symmetric eigenproblem

$$K\Phi = M\Phi\omega^2 \tag{3.69}$$

where ω^2 is a real-valued diagonal matrix of the natural frequencies squared, and Φ is a matrix of mass-normalized mode shapes, i.e., $\Phi^T M\Phi = I$. The diagonalized equations of motion are

$$\ddot{q} = -2\zeta\omega\dot{q} - \omega^2 q + \Phi^T u + \bar{B}_w w \tag{3.70}$$

where $u^T = \begin{bmatrix} u_1 & u_2 \end{bmatrix}$, $\bar{B}_w = \Phi^T \begin{bmatrix} 1 & 0 \end{bmatrix}^T$, and $2\zeta\omega$ is a real-valued diagonal matrix. Equation 3.70 rewritten in state-space form is

$$\begin{bmatrix} \dot{q} \\ \ddot{q} \end{bmatrix} = \begin{bmatrix} 0 & I \\ -\omega^2 & -2\zeta\omega \end{bmatrix} \begin{bmatrix} q \\ \dot{q} \end{bmatrix} + \begin{bmatrix} 0 \\ \Phi^T \end{bmatrix} u + \begin{bmatrix} 0 \\ \bar{B}_w \end{bmatrix} w \tag{3.71}$$

The system given by Equation 3.71 in now in the form needed by Equation 3.18, with

$$A_2 = \begin{bmatrix} 0 & I \\ -\omega^2 & -2\zeta\omega \end{bmatrix}_{4\times 4} \quad B_u = \begin{bmatrix} 0 \\ \Phi^T \end{bmatrix}_{4\times 2} \quad \mathrm{B}_w = \begin{bmatrix} 0 \\ \bar{B}_w \end{bmatrix}_{4\times 1} \tag{3.72}$$

The form of the disturbance model, i.e., Equations 3.19 and 3.20, used in this example problem is similar to Equation 3.14, but with $M(\Omega) = \Omega^2$ and $\theta_0 = 0$

$$A_1 = \begin{bmatrix} 0 & 1 \\ -\Omega^2 & 0 \end{bmatrix}_{2\times 2} \quad B_1 = \begin{bmatrix} 0 \\ \Omega^3 \end{bmatrix}_{2\times 1} \quad C_1 = \begin{bmatrix} 1 & 0 \end{bmatrix}_{1\times 2} \tag{3.73}$$

$$w(t) = C_1 x_1(t) \tag{3.74}$$

It's interesting to note that with the above form of the disturbance model, the following relationships hold

$$x_{1_1}(t) = w(t) = \Omega^2 \sin(\Omega t) \tag{3.75}$$

and

$$x_{1_2}(t) = \dot{w}(t) = \Omega^3 \cos(\Omega t) \tag{3.76}$$

Using the relationships from Equations 3.75 and 3.76 in Equation 3.26 gives

$$\dot{x}_2(t) = (A_2 - B_u K_2)x_2(t) + (B_w - B_u K_{1_1})w(t) - B_u K_{1_2}\dot{w}(t) \tag{3.77}$$

From examining the input terms in Equation 3.77 we expect to see that when the disturbance and control are collocated that $K_{1_1} \rightarrow 1$ and $K_{1_2} \rightarrow 0$. This assumption turns out to be true for the "cheap" control case, i.e., for $\rho \rightarrow 0$. In other words, for the case of cheap controls with collocated disturbance and control, the disturbance is simply blocked from entering the system. It should be noted that these asymptotic values are not reached until the control weighting parameter, ρ, is reduced to a very small value, resulting in very large gains. This also suggests that optimality is achieved as a trade-off between totally blocking the disturbance and allowing a portion of it to enter while compensating for it with a quadrature component of the disturbance. Unfortunately this perfectly collocated situation is almost never encountered in real systems where the disturbances are caused by rotating imbalances. Furthermore, as a result of the need for stability margins in the controlled system, the cheap control case is almost never used in real missions where full-state information is not available.

A very different asymptotic feed-forward gain behavior is observed for the more general case when the disturbance and control are not collocated. For cheap controls, the performance integral reduces to one that considers only the output with no penalty on the control power and results in controls that drive *z(t)* to zero as quickly as possible. From Equation 3.77 we see that the performance output in the frequency domain can be represented as

$$z(s) = C(SI - A_{cl})^{-1}(B_w - B_u K_{1_1} - B_u K_{1_2} s)w(s) \tag{3.78}$$

or

$$z(s) = \bar{G}_{zw}(s)w(s) - \bar{G}_{zu}(s)(K_{1_1} + K_{1_2}s)w(s) \tag{3.79}$$

Solving Equation 3.79 with $z(s) = 0$ and $w(s)$ arbitrary gives

$$\bar{K}_{1_1}(\omega) + \bar{K}_{1_2}(\omega)j\omega = \bar{G}^{\dagger}{}_{zu}(j\omega)\bar{G}_{zw}(j\omega) \tag{3.80}$$

or

$$\bar{K}_{1_1}(\omega) = \Re e(\bar{G}^{\dagger}{}_{zu}(j\omega)\bar{G}_{zw}(j\omega)) \tag{3.81}$$

and

$$\bar{K}_{1_2}(\omega) = \Im m(\bar{G}^{\dagger}{}_{zu}(j\omega)\bar{G}_{zw}(j\omega))/\omega \tag{3.82}$$

where $\bar{G}^{\dagger}{}_{zu}(s)$ is in general the pseudo inverse of $\bar{G}_{zu}(s)$ and the overbar on K_1 is used to designate the feed-forward gains obtained by solving Equation 3.79. Figure 3.6 presents a plot of the ratios of the optimal feed-forward gains to those obtained using Equations 3.81 and 3.82. Notice that for higher values of the control penalty, ρ, there is significant difference between the gains, but at lower values of ρ, i.e., cheap control, the two gains asymptote to the same value.

3.3.1 Results for Low-Order Sample Problem

Time domain and frequency domain results for this problem will be presented. Since the theory developed in this work is based upon optimal linear quadratic control theory, the feed-forward results will be compared with those obtained using conventional LQR control without feed-forward. The time domain performance improvement may be accessed by comparing the performance output, $z(t) = C_z x_2(t) = \begin{bmatrix} C_p & C_v \end{bmatrix} x_2(t)$, of the feed-forward, i.e., Equation 3.77, to that of the nominal closed-loop system, i.e., conventional LQR control.

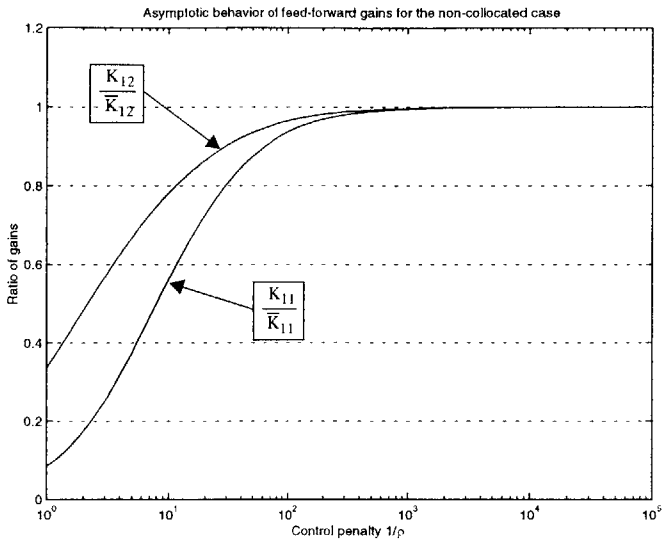

Figure 3.6 Asymptotic behavior of feed-forward gains

In the frequency domain, the transfer function of primary interest in optimally mitigating the propagation of disturbances through a dynamical system is G_{zw}. It therefore becomes beneficial to develop a frequency domain performance index that utilizes the G_{zw} channel. Frequency domain performance of the feed-forward system is

$$z(s)|_{s=j\omega} = C_z(sI - A_{cl})^{-1}(B_w - B_u K_{1_1}(\omega) - B_u K_{1_2}(\omega)s)w(s) = \bar{G}_{zw}w(s) \qquad (3.83)$$

and without feed-forward is

$$z(s)|_{s=j\omega} = C_z(sI - A_{cl})^{-1}B_w w(s) = G_{zw}w(s) \qquad (3.84)$$

Using Equations 3.83 and 3.84 we can define a feed-forward SISO performance index as follows

$$P(s)|_{s=j\omega} = \left|\frac{G_{zw}}{\bar{G}_{zw}}\right| \qquad (3.85)$$

with $P(s) > 1$ indicating a performance benefit using feed-forward control, and $P(s) < 1$ indicating a performance degradation.

The importance of the G_{zw} transfer function has been discussed above; however, it should also be clear that the transfer function G_{zu} also plays an important role, since all control inputs must be applied through B_u. Clearly, in frequency regions where G_{zu} exhibits significant attenuation one should not expect to see large performance improvements. This is particularly true for the case when attenuations in G_{zu} occur at or near frequencies with amplifications in G_{zw}.

Results of the optimal feed-forward control for each of the four cases are presented below. For each case, two separate figures, each with two subplots, are presented. The four plots for each case are: feed-forward gains K_{1_1} and ωK_{1_2}, G_{zu} transfer function, SISO performance index $P(j\omega)$, and time domain response due to a *1.5 Hz* disturbance.

For Case 1 in Figure 3.7, we see that the feed-forward control gains vary smoothly from near 0 *Hz* to past 3 *Hz*. Furthermore, we see that near 0.81 *Hz* the feed-forward gains approach zero. This near zero feed-forward signal is a result of the attenuation in both $G_{z_1u_1}$ and G_{z_1w} at this frequency. In fact, this is a demonstration of optimality because a disturbance cannot strongly enter the system nor can the control strongly react at this frequency to reject a disturbance, so the optimal solution simply turns off the feed-forward component at this frequency. In Figure 3.8 the feed-forward SISO performance index is plotted along with a time domain response of the system to a 1.5 *Hz* disturbance. From the performance index plot we see that at 1.5 *Hz* there is a 25 dB improvement using feed-forward control when compared to conventional LQR control.

In Figure 3.9 we see the parameterized feed-forward gains and $G_{z_2u_1}$ plotted for Case 2. Notice that the behavior of the feed-forward gains is unlike Case 1 where K_{1_1} and ωK_{1_2} simultaneously reduced in magnitude near the zero in the $G_{z_1u_1}$ transfer function. In this case, $G_{z_2u_1}$ does not possess the same transfer function zero and the optimal solution requires one or, for most frequencies, both gains to be non-zero throughout the operating range.

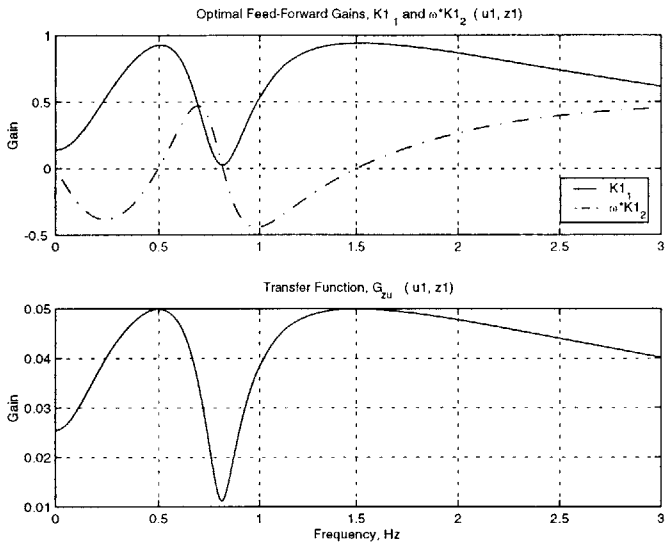

Figure 3.7 Feed-Forward Gains and G_{zu} Transfer Function Plots for Case 1

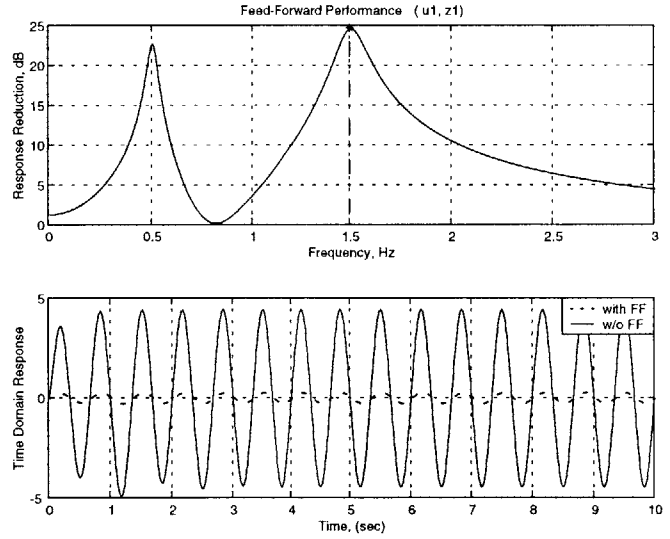

Figure 3.8 Performance plots for Case 1.

In Figure 3.10 we see that at 1.5 *Hz* there is a 17 dB improvement using feed-forward control when compared to conventional LQR control.

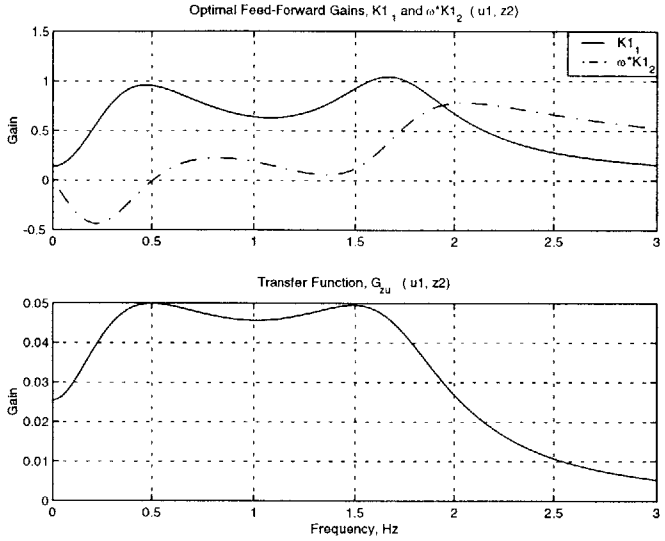

Figure 3.9 Feed-Forward Gains and G_{zu} Transfer Function Plots for Case 2

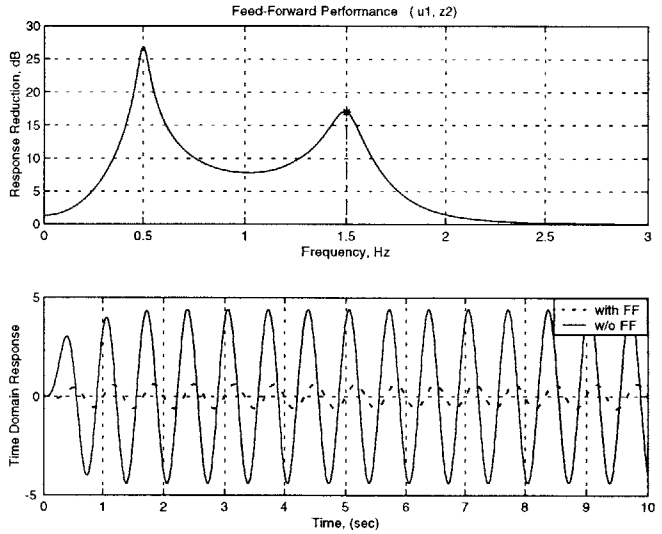

Figure 3.10 Performance Plots for Case 2

The G_{zu} transfer function for Case 3 is identical to that for Case 2, but results in different feed-forward gains (see Figure 3.11), because of the different performance metrics used in the optimal control problem. In Figure 3.12 the performance index plot shows significant performance improvement, with peaks near 40 dB of improvement. Notice that the perfor-

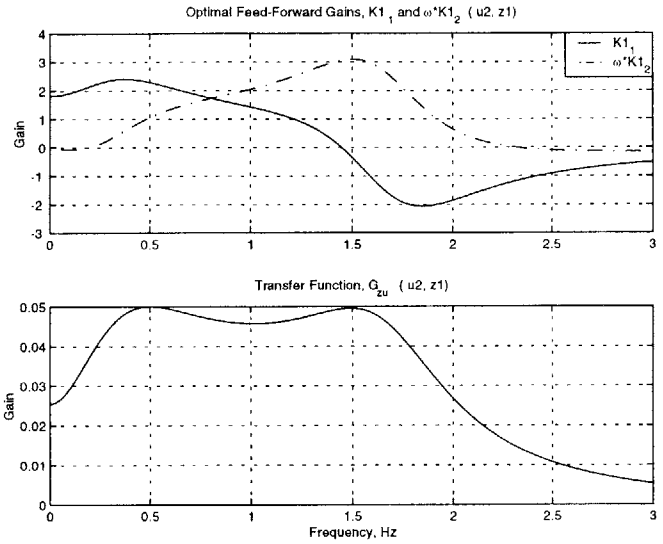

Figure 3.11 Feed-Forward Gains and G_{zu} Transfer Function Plots for Case 3

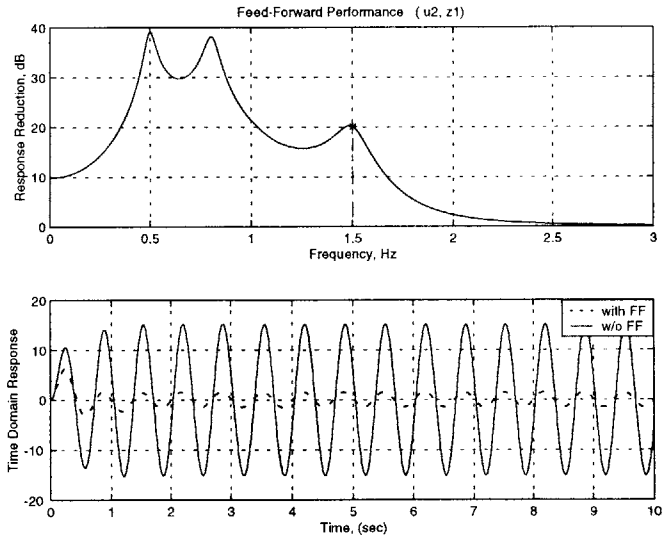

Figure 3.12 Performance plots for Case 3.

mance index for this case has three peaks: two near the open-loop poles of the system and a third at the zero of the $G_{z_1 w}$ transfer function. This third peak is a result of the optimization taking advantage of the attenuation in $G_{z_1 w}$ while still having authority in $G_{z_1 u_2}$. We

see that at 1.5 Hz there is a 20 dB improvement using feed-forward control when compared to conventional LQR control.

Figures 3.13 and 3.14 present the results for Case 4. We see in Figure 3.13 that the $G_{z_2 u_2}$ transfer function has significant attenuation between 1.0 to 1.5 Hz, while the $G_{z_2 w}$ from Figure 3.9 remains relatively flat through this range. The relative gain discrepancy between these transfer functions results in feed-forward gains that exhibit local extrema in this frequency region in an attempt to compensate for the reduced control authority. Furthermore, notice that the SISO performance index is actually negative in the low frequency region below 0.12 Hz and in the region between 1.15 to 1.4 Hz, which implies that the addition of feed-forward control actually makes the response of the system larger. Although this situation may not represent a desirable one, we must keep in mind that the optimization process considers both a weighted system response term plus a weighted control cost term, and that the sum of these two terms is the objective that is minimized.

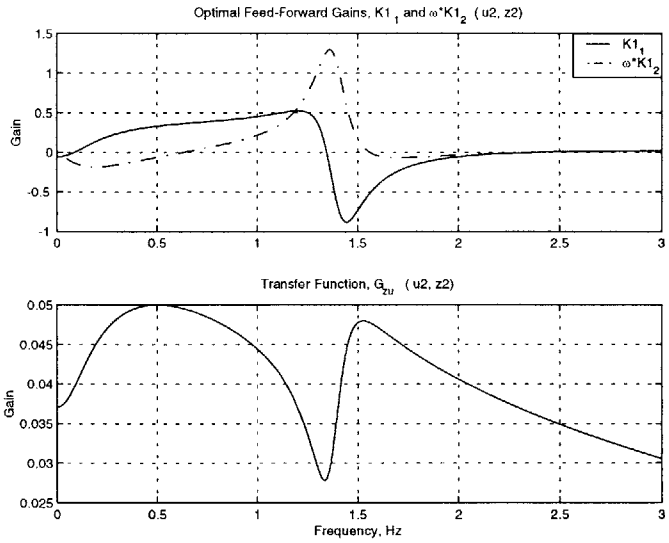

Figure 3.13 Feed-Forward Gains and G_{zu} Transfer Function Plots for Case 4

Comparing the cost function of standard LQR control to that of feed-forward augmented control, we see that for all four cases the feed-forward system results in lower cost func-

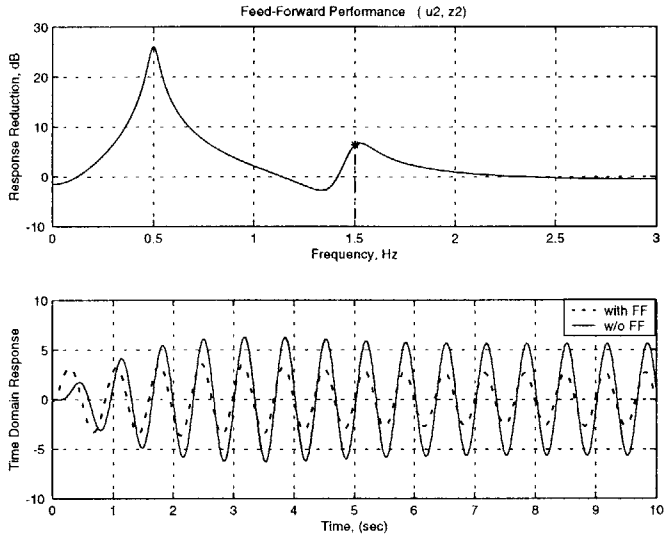

Figure 3.14 Performance plots for Case 4.

tion values. To demonstrate this, consider a frequency domain representation of the disturbance-driven cost functional with feed-forward

$$\tilde{J} = \frac{1}{2\pi}\int_{-\infty}^{\infty} w^H(j\omega)(\bar{G}_{xw}^H C_z^T C_z \bar{G}_{xw} + \bar{G}_{uw}^H \sqrt{\rho}\sqrt{\rho}\bar{G}_{uw})w(j\omega)d\omega \tag{3.86}$$

and without feed-forward

$$J = \frac{1}{2\pi}\int_{-\infty}^{\infty} w^H(j\omega)(G_{xw}^H C_z^T C_z G_{xw} + G_{uw}^H \sqrt{\rho}\sqrt{\rho}G_{uw})w(j\omega)d\omega \tag{3.87}$$

where the transfer function matrices in the above frequency domain cost functionals are described by Equations 3.88 through 3.91.

$$x_2(s)\big|_{s=j\omega} = (sI - A_{cl})^{-1}(B_w - B_u K_{1_1}(\omega) - B_u K_{1_2}(\omega)s)w(s) = \bar{G}_{xw}w(s) \tag{3.88}$$

$$u(s)\big|_{s=j\omega} = -(K_{1_1}(\omega) + K_{1_2}(\omega)s + K_2\bar{G}_{xw})w(s) = \bar{G}_{uw}w(s) \tag{3.89}$$

$$x_2(s)\big|_{s=j\omega} = (sI - A_{cl})^{-1} B_w w(s) = G_{xw} w(s) \tag{3.90}$$

$$u(s)\big|_{s=j\omega} = -K_2 G_{xw} w(s) = G_{uw} w(s) \tag{3.91}$$

The cost functionals given by Equation 3.86 and 3.87 have been computed numerically for all four cases and are presented in Table 3.3. Notice that the addition of feed-forward control reduces the cost functional. This is even true for Case 4, despite the localized performance degradation shown in Figure 3.14.

TABLE 3.3 Cost Functional Comparison

$100 \times (\bar{J} - J)/J$	
Case 1	-47.07 %
Case 2	-47.17 %
Case 3	-62.70 %
Case 4	-11.42 %

The results for Case 4 can be dramatically modified by simply changing the state and control weighting terms. However, a more generalized approach is to combine the frequency weighted cost functional approach with the feed-forward approach as discussed in Section 3.2.1. This combined control design approach will be presented in the next section.

As expected, the G_{zu} and G_{zw} transfer functions together have a large impact on the shape of the feed-forward gains and hence the resulting feed-forward performance. Furthermore, we have seen that for most cases the feed-forward control scheme results in significantly improved performance over conventional LQR control. The focus of the next section will be to demonstrate how the frequency weighted cost functional approach can be used to augment the optimal feed-forward control by adding additional freedom in shaping the G_{zu} and G_{zw} transfer functions.

3.3.2 Combined Frequency Weighted LQR with Optimal Feed-forward

We saw in the previous section that optimal feed-forward control alone resulted in substantial performance improvements over conventional LQR for most of the cases considered. However, for Case 4 the performance improvements were somewhat limited. It was stated (without example) that by simply modifying the state and control weighting terms the performance could be dramatically improved. In this section, we will demonstrate how the frequency weighted cost functional approach (see Section 2.6) can be used together with the optimal feed-forward control to achieve higher overall feed-forward performance. Case 4 will be used to demonstrate the combined control design methodology.

Recall from Chapter 2 that the general form of frequency weighted control design included both state and control weighting filters. In this demonstration, we will address only state weighting filters; however the methodology is applicable to general state/control weighting. An additional modification to the development presented in Chapter 2 is that the weighting filters will be placed on the performance output instead of purely on the states. The nominal plant augmented with performance output weighting is given as

$$\begin{bmatrix} \dot{x}_2 \\ \dot{x}_s \end{bmatrix} = \begin{bmatrix} A_2 & 0 \\ B_s C_z & A_s \end{bmatrix} \begin{bmatrix} x_2 \\ x_s \end{bmatrix} + \begin{bmatrix} B_u \\ 0 \end{bmatrix} u + \begin{bmatrix} B_w \\ 0 \end{bmatrix} w \tag{3.92}$$

The weighted performance output is given as

$$z = D_s C_z x_2 + C_s x_s \tag{3.93}$$

which gives an augmented Q matrix as

$$Q = \begin{bmatrix} (D_s C_z)^T \\ C_s^T \end{bmatrix} \begin{bmatrix} D_s C_z & C_s \end{bmatrix} = \begin{bmatrix} C_z^T D_s^T D_s C_z & C_z^T D_s^T C_s \\ C_s^T D_s C_z & C_s^T C_s \end{bmatrix} \tag{3.94}$$

The development of the feed-forward augmented control follows exactly as it did in Equation 3.21, but using the performance filter augmented plant in Equation 3.92 and the weighting matrix defined by Equation 3.94.

The results of the frequency weighted cost functional approach with the optimal feed-forward control are presented in Figures 3.15 through 3.17. The optimal feed-forward gains and performance weighting filter transfer function are shown in Figure 3.15. The weight-

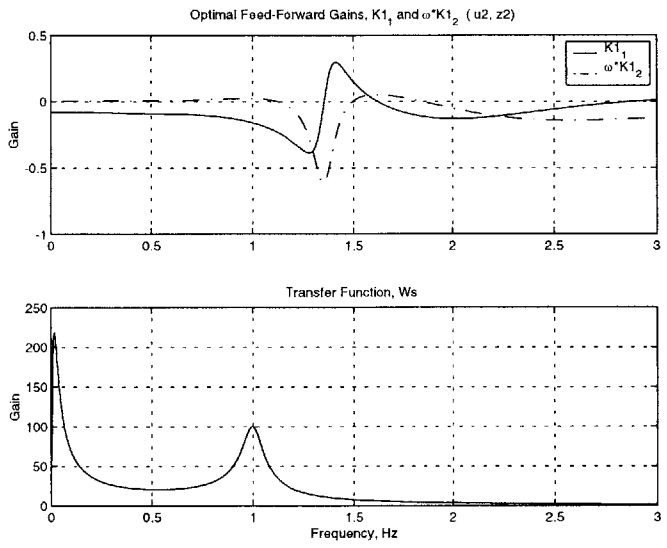

Figure 3.15 Feed-Forward Gains and W_sTransfer Function Plots for Case 4

ing filter chosen for this example was a fourth order model with the following poles and zeros

$$poles = \begin{bmatrix} 0.1 & 0.1 & 6.28 & 6.28 \end{bmatrix} \quad \text{rad/sec} \tag{3.95}$$

$$zeros = \begin{bmatrix} 3.0e-4 & 1.2 & 1.2 & 1.2 \end{bmatrix} \quad \text{rad/sec} \tag{3.96}$$

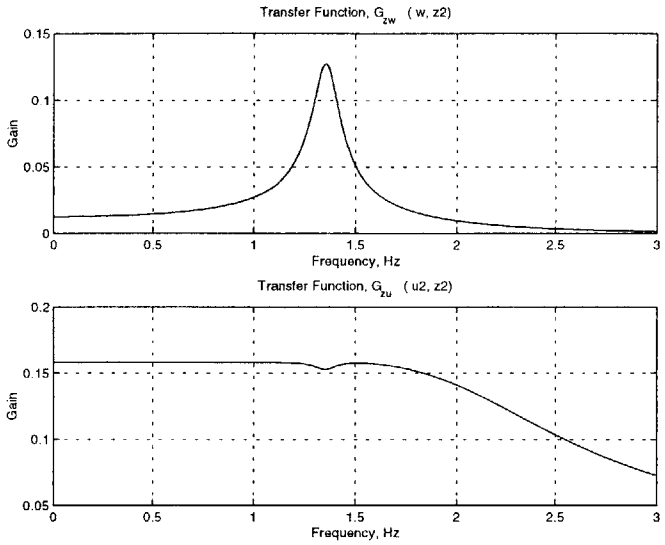

Figure 3.16 G_{zw} and G_{zu} Transfer Function Plots for Case 4

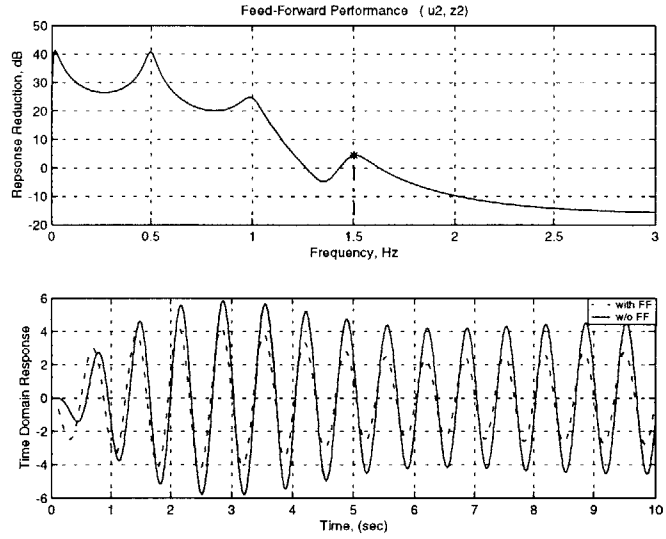

Figure 3.17 Performance Plots for Case 4 with Frequency Weighting

It should be noted that most of the performance gains resulting from the addition of the frequency weighting can be achieved with a lower-order filter. In fact, a second-order bandpass filter with a double pole at *0.1 rad/sec* and zeros at *3.0e-4* and *13.0 rad/sec* also performs well in the low frequency region. The additional two poles of the fourth-order

filter helps in the mid-frequency region performance. The closed-loop G_{zu} and G_{zw} transfer functions are shown in Figure 3.16. Both transfer functions demonstrate substantially different characteristics than those presented in Section 3.3.1. The most notable is that the low and mid-frequency improvements in G_{zu} come at the expense of amplified disturbance response in G_{zw} near the *1.3 Hz* region. The SISO performance index and time domain response to a *1.5 Hz* disturbance are shown in Figure 3.17. Notice that the addition of frequency weighting has dramatically improved the low to mid-frequency performance of the feed-forward controller. In fact, improvements of greater than *20 dB* from near *0 Hz* to just past *1.0 Hz* have been realized. The issue of degraded performance in the low to mid-frequency region has been eliminated, but the region near *1.3 Hz* still shows a performance degradation. The problem in the *1.3 Hz* region can also be eliminated with the proper selection of the frequency weighting, but as is typical for many systems, eliminating the problem in one region results in performance degradation in other regions. This turns out to be the case in this example as well.

3.4 Summary

The objective was to develop a gain scheduling control design methodology to optimally reject disturbances that possess stationary or slowly varying narrow-band spectral distributions. From Equation 3.53 we see that the S_{12}^T portion of the control, i.e., the feed-forward portion, is directly parameterized in terms of the eigenvalues and eigenvectors of the disturbance model. Furthermore, it was shown in Section 3.1, that for the class of disturbances of interest in this study, the disturbance model's eigensystem may be expressed analytically in terms of the individual harmonics of the disturbance. Therefore, by combining the disturbance modeling with the partitioned solution for the optimal control, we have achieved our objective of developing a gain scheduling disturbance rejection methodology. Of course, the control scheme developed here must be coupled with a disturbance identification scheme to fully prescribe the feed-forward control signal. Disturbance identification may be performed off-line or alternately in real-time to form an adaptive feed-

forward compensator. A discussion of disturbance identification methods will be presented in Chapter 6.

A demonstration of the optimal feed-forward control methodology was given using a low-order spring-mass system. Results using a stationary wheel speed were compared to conventional LQR designs. The results show that for most cases considered the feed-forward control scheme yields significantly improved performance over conventional LQR control alone - upwards of *40 dB* in selected frequency regions. A control design combining frequency weighting together with feed-forward was also demonstrated. This example demonstrated how loop-shaping control can be used to improve the performance of the feed-forward control.

The next chapter will focus on the nonstationary wheel speed case. It will be shown that the methodology developed here plays an important role in the time-varying case.

Chapter 4

OPTIMAL REJECTION OF TIME-VARYING DISTURBANCES

In Chapter 3 we developed optimal disturbance accommodating controllers for rejecting quasi-stationary multi-tonal narrow-band disturbances. For a large number of practical engineering applications the quasi-stationary approach yields excellent results. However, for disturbances whose spectral content is rapidly changing, the quasi-stationary approach may not be sufficient. The goal of this chapter is to develop a disturbance accommodating control for disturbances with arbitrarily fast dynamics.

4.1 Disturbance Accommodating Control

Recall from Section 3.2 that the quasi-stationary approach was based upon augmenting the plant with a model of the disturbance and using this augmented system in an optimal control formulation to achieve improved disturbance rejection performance. This section will forego the disturbance augmentation and treat the disturbance explicitly. The equations describing optimal disturbance accommodating control for this case will be presented. Steady state behavior and the limitations on their practical implementation will be discussed.

Consider the general time-varying disturbance-driven plant given as

$$\dot{x}_2(t) = A_2(t)x(t) + B_u(t)u(t) + B_w(t)w(t) \tag{4.1}$$

with known disturbance $w(t) \in \Re^p$. Retaining this explicit form of the disturbance-driven plant results in the following forced state and costate equations

$$\begin{bmatrix} \dot{x}_2(t) \\ \dot{p}(t) \end{bmatrix} = \begin{bmatrix} A_2(t) & -B(t)R^{-1}B^T(t) \\ -Q(t) & -A_2^T(t) \end{bmatrix} \begin{bmatrix} x_2(t) \\ p(t) \end{bmatrix} + \begin{bmatrix} B_w(t)w(t) \\ 0 \end{bmatrix} \tag{4.2}$$

Equation 4.2 is simply the forced version of the Hamiltonian system given in Equation 2.16. In general, the solution to the forced Hamiltonian at time t_1 can be expressed as

$$\begin{bmatrix} x_2(t_1) \\ p(t_1) \end{bmatrix} = \begin{bmatrix} \Phi_{11}(t_1, t) & \Phi_{12}(t_1, t) \\ \Phi_{21}(t_1, t) & \Phi_{22}(t_1, t) \end{bmatrix} \begin{bmatrix} x_2(t) \\ p(t) \end{bmatrix} + \int_t^{t_1} \begin{bmatrix} \Phi_{11}(t_1, \eta)B_w(\eta)w(\eta) \\ \Phi_{21}(t_1, \eta)B_w(\eta)w(\eta) \end{bmatrix} d\eta \tag{4.3}$$

To simplify, lets introduce the following notation

$$\begin{bmatrix} h_1(t) \\ h_2(t) \end{bmatrix} = \int_t^{t_1} \begin{bmatrix} \Phi_{11}(t_1, \eta)B_w(\eta)w(\eta) \\ \Phi_{21}(t_1, \eta)B_w(\eta)w(\eta) \end{bmatrix} d\eta \tag{4.4}$$

Substituting Equation 4.4 into Equation 4.3 gives

$$x_2(t_1) = \Phi_{11}(t_1, t)x_2(t) + \Phi_{12}(t_1, t)p(t) + h_1(t) \tag{4.5}$$

$$p(t_1) = Fx_2(t_1) = \Phi_{21}(t_1, t)x_2(t) + \Phi_{22}(t_1, t)p(t) + h_2(t) \tag{4.6}$$

Solving for $p(t)$ from Equations 4.5 and 4.6 gives

$$p(t) = S(t)x_2(t) - [\Phi_{22}(t_1, t) - F\Phi_{12}(t_1, t)]^{-1}(h_2(t) - Fh_1(t)) \tag{4.7}$$

where $S(t)$ is the same function as defined in Equation 2.21. To further simplify, lets introduce the notation

$$g(t) = [\Phi_{22}(t_1, t) - F\Phi_{12}(t_1, t)]^{-1}(h_2(t) - Fh_1(t)) \tag{4.8}$$

with $g(t) \in \Re^n$. Therefore the costate is

$$p(t) = S(t)x_2(t) - g(t) \tag{4.9}$$

Equation 4.9 implies that the costate is no longer simply a linear function of the state as it was in Equation 2.20, but an additional term $g(t)$ is present, resulting in a control law of the form

$$u(t) = -R^{-1}(t)B_u^T(t)p(t) = -R^{-1}(t)B_u^T(t)[S(t)x_2(t) - g(t)] \tag{4.10}$$

Notice the similarity between Equation 4.10 and Equation 3.24. Equation 4.10 clearly shows that the optimal control consists of two components, a component that is a linear combination of the original state, $x_2(t)$, and a component that is a linear combination of the newly introduced $g(t)$ state.

The closed-loop dynamics of the optimal trajectory $x_2(t)$ in the presence of an external disturbance $w(t)$ is given as (to conserve space, explicit time dependence is not shown)

$$\dot{x_2} = [A_2 - B_u R^{-1} B_u^T S]x_2 + B_w w + B_u R^{-1} B_u^T g \tag{4.11}$$

An alternate expression for $g(t)$ in Equation 4.8 can be derived by differentiating Equation 4.9

$$\dot{p}(t) = \dot{S}(t)x_2(t) + S(t)\dot{x_2}(t) - \dot{g}(t) \tag{4.12}$$

Substituting Equation 4.11 into Equation 4.12 gives (to conserve space, explicit time dependence is not shown)

$$\dot{p} = \dot{S}x_2 + S[(A_2 - B_u R^{-1} B_u^T S)x_2 + B_w w + B_u R^{-1} B_u^T g] - \dot{g} \tag{4.13}$$

From Equations 2.16 and 4.9, $\dot{p}(t)$ must also satisfy the following

$$\dot{p}(t) = -(Q(t) + A_2^T(t)S(t))x_2(t) + A_2^T(t)g(t) \tag{4.14}$$

Comparing Equations 4.13 and 4.14 suggests that the following relationships must hold

$$\dot{S}(t) = -S(t)A(t) - A^T(t)S(t) + S(t)B_u(t)R^{-1}(t)B_u^T(t)S(t) - Q(t) \tag{4.15}$$

and

$$\dot{g}(t) = -\left[A_2(t) - B_u(t)R^{-1}(t)B_u^T(t)S(t)\right]^T g(t) + S(t)B_w(t)w(t) \tag{4.16}$$

Equation 4.15 is exactly the same as Equation 2.23 and must also satisfy the same terminal condition, i.e., $S(t_1) = F$. Equation 4.16 is a linear time-varying differential equation that describes how $w(t)$ directly influences the control law (Equation 4.10). Notice that $g(t)$ does not depend on the state $x(t)$, and in this sense does not contribute a feedback term in the control law. Again, it has been shown that the control law consists of two terms: a feedback term plus a feed-forward term. The feed-forward term, $R^{-1}(t)B_u^T(t)g(t)$, is the output of a dynamical system that is being driven by the disturbance $w(t)$ and in this sense the dynamics of the disturbance are directly incorporated into the optimal control applied to the system. The difficulty in implementing Equation 4.16 is that it must satisfy the terminal time condition $g(t_1) = 0$ and therefore must be solved backwards in time. If $w(t)$ is known for $t \in [t_0, t_1]$ then solving for $g(t)$ does not pose a significant problem, however in many applications complete knowledge of $w(t)$ is not available.

Before we address the need for complete knowledge of $w(t)$, let's examine Equation 4.16 in more detail. First of all, since most integration routines solve differential equations in forward time, they cannot be used directly to solve Equation 4.16. The best approach when using conventional software is therefore to transform Equation 4.16 into an equation in forward time by using a time-shift of $\tau = t_1 - t$. Applying this time-shift to Equation 4.16 gives

$$\dot{g}(\tau) = \left[A_2(\tau) - B_u(\tau)R^{-1}(\tau)B_u^T(\tau)S(\tau)\right]^T g(\tau) - S(\tau)B_w(\tau)w(\tau) \tag{4.17}$$

with initial condition $g(\tau = 0) = 0$. Notice that the forward-time equation is stable, and in fact, has the same eigenvalues as the closed-loop plant from Equation 4.11. It therefore

follows that the transient behavior of the feed-forward control is defined by the plant's closed-loop dynamics.

In this work we are primarily concerned with linear time-invariant (LTI) systems. If we introduce the LTI assumption into Equation 4.16 we get

$$\dot{g}(t) = -[A_2 - B_u R^{-1} B_u^T S(t)]^T g(t) + S(t) B_w w(t) \tag{4.18}$$

Notice that despite the LTI assumption for the plant matrices, the system still is time-varying due to the presence of the time-varying Riccati matrix term, $S(t)$. Recall from Section 2.3 that under generally broad conditions $S(t) \rightarrow S$ as the terminal time becomes large. This is indeed the case in structural control where the terminal time is typically very large with respect to the plant's dynamics. Furthermore, from Section 2.4, it was shown that the transient portion of $S(t)$ decays at a rate related to the time constants of the closed-loop plant. As an example of the steady-state behavior of the Riccati solution, consider the gains corresponding to the low-order sample problem, Case 3, from Section 3.3. The time-varying gains are shown in Figure 4.1. Notice that in less than 2.0 *sec.* the gains have reached steady-state (the slowest closed-loop time constant for this system is 0.404 *sec.*). Therefore in most applications involving structural control we can safely assume that the feed-forward dynamics are defined as

$$\dot{g}(t) = -[A_2 - B_u R^{-1} B_u^T S]^T g(t) + S B_w w(t) \tag{4.19}$$

or more compactly written as

$$\dot{g}(t) = -A_{cl}^T g(t) + S B_w w(t) \tag{4.20}$$

$$U_{ff}(t) = R^{-1} B_u^T g(t) \tag{4.21}$$

Now that we have a fully LTI system we can examine its steady-state behavior. To this end, the frequency domain response of Equations 4.20 and 4.21 is given as

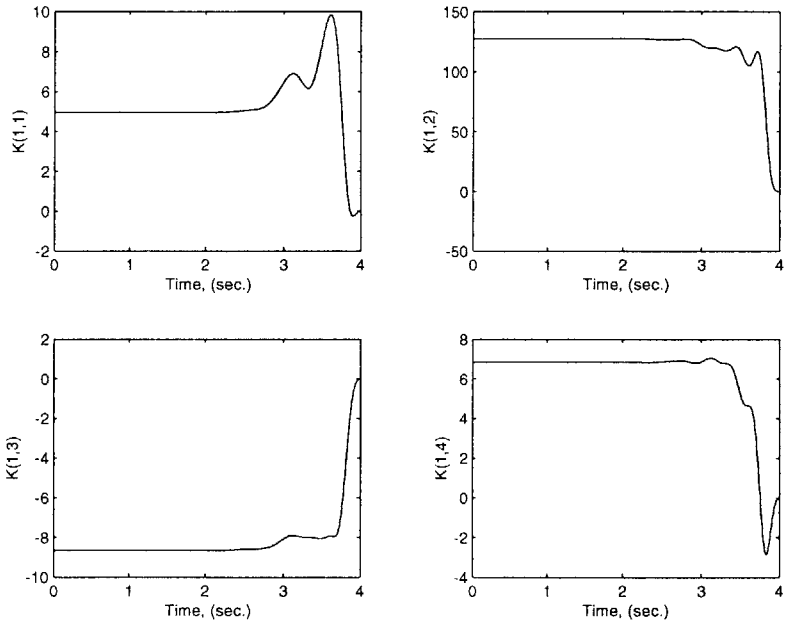

Figure 4.1 Time-varying feedback gains

$$U_{ff}(s) = R^{-1}B_u^T\Psi(s)SB_w w(s) \tag{4.22}$$

where $\Psi(s) = (sI + A_{cl}^T)^{-1}$. To compare the above expression with that given in Chapter 3, recall from Equation 3.24 that the feed-forward control was presented as

$$U_{ff}(t) = -R^{-1}B_u^T S_{12}^T x_1(t) \tag{4.23}$$

Furthermore, from Equation 3.73 for a single harmonic disturbance we know that disturbance state vector has the following components

$$x_1(t) = \begin{bmatrix} x_{11}(t) \\ x_{12}(t) \end{bmatrix} = \begin{bmatrix} x_{11}(t) \\ \dot{x}_{11}(t) \end{bmatrix} \tag{4.24}$$

Also, with $C_1 = \begin{bmatrix} 1 & 0 \end{bmatrix}$, we know that the $x_{11}(t)$ component is in-phase with the disturbance and the $x_{12}(t)$ is 90° out of phase. Using this information in the frequency domain representation of Equation 4.23 gives

$$U_{ff}(s) = -R^{-1}B_u^T S_{12}^T \begin{bmatrix} 1 \\ s \end{bmatrix} w(s) \tag{4.25}$$

In terms of the feed-forward gains $K1$, Equation 4.25 becomes

$$U_{ff}(s) = -\begin{bmatrix} K1_1 & K1_2 \end{bmatrix} \begin{bmatrix} 1 \\ s \end{bmatrix} w(s) = -(K1_1 + sK1_2)w(s) \tag{4.26}$$

Using $s = j\omega$ and comparing the above expression with Equation 4.23 yields the following expressions for the feed-forward gains

$$K1_1 = -\Re e(R^{-1}B_u^T \Psi(j\omega)SB_w) \tag{4.27}$$

$$\omega K1_2 = -\Im m(R^{-1}B_u^T \Psi(j\omega)SB_w) \tag{4.28}$$

From Equations 4.27 and 4.28, that result from the steady state solution of Equation 4.21, we see alternate expressions for the feed-forward gains given in Chapter 3. We may therefore conclude that there is a consistent relationship between Equations 4.21 and 4.23. This connection is now explored further. The feed-forward control is given by

$$U_{ff}(t) = -R^{-1}B_u^T S_{12}^T x_1(t) = R^{-1}B_u^T g(t) \tag{4.29}$$

which requires

$$-S_{12}^T x_1(t) = g(t) \tag{4.30}$$

It turns out, and will be shown below, that Equation 4.30 is an alternate statement of the Lyapunov equation given in 3.39. To show this, substitute Equation 4.30 into 4.20

$$\dot{g} = -S_{12}^T \dot{x}_1 = -S_{12}^T A_1 x_1 = -A_{cl}^T g + SB_w w = A_{cl}^T S_{12}^T x_1 + SB_w C_1 x_1 \tag{4.31}$$

Clearly, Equation 4.31 must hold for all $x_1(t)$ and therefore requires

$$S_{12}^T A_1 + A_{cl}^T S_{12}^T + S B_w C_1 = 0 \tag{4.32}$$

Therefore the steady-state equivalence of the feed-forward control of Equations 4.21 and 4.23 has been established.

4.2 Implementing Time-Varying Feed-Forward Control

In the previous section we developed the equations that define optimal feed-forward control for arbitrary disturbances and demonstrated how, in steady state, they reduce to the quasi-stationary solution presented in Chapter 3. We also pointed out the condition on when the time-varying solution could be implemented exactly without approximation. Let's now discuss this condition, i.e., the need for complete knowledge of $w(t)$ for $t \in [t_0, t_1]$, related to implementing Equation 4.16.

A case worth considering is applicable for missions that involve repetitive operations. The term operation is used to denote a given mission function for the system, e.g., spacecraft momentum bias compensation, spacecraft slew maneuver, etc. For such cases, it may be possible to develop, over an extended period of time, very good characterizations of the disturbance environment. Once the disturbance has been characterized for a given operation, this disturbance would be used in Equation 4.16 to obtain the feed-forward control signal. This approach may benefit from exploiting the linearity of Equation 4.16. Recall that $g(t)$, and hence the feed-forward control, is obtained by solving a linear time-varying system of equations. Despite the time-varying nature of the system, the system is linear and therefore superposition still holds. Superposition is stated as follows

$$g(t) = \sum_{i=1}^{n} C_i g_i(t) \tag{4.33}$$

where $g_i(t)$ are the solution of

$$\dot{g}_i(t) = -[A_2(t) - B_u(t)R^{-1}(t)B_u^T(t)S(t)]^T g_i(t) + S(t)B_w(t)w_i(t) \tag{4.34}$$

The individual disturbance terms, $w_i(t)$, effectively serve as basis functions for the disturbance associated with a given operation. Of course the C_i's in Equation 4.33 are obtained from matching the disturbance for the given operation with the basis set using

$$w(t) = \sum_{i=1}^{n} C_i w_i(t) \tag{4.35}$$

A catalog of disturbance basis functions could be generated and recalled as necessary to compose the feed-forward control for a given operation. This approach produces analytically exact results, but still relies upon the ability to model the disturbance over the time interval $t \in [t_0, t_1]$, i.e., pre-compute C_i's that are valid for the entire interval. Although this approach results in a realizable optimal control signal, it leaves us with no way to accommodate for local variations in the predicted disturbance. There is, in fact, no easy way to incorporate the need for realizability into the mathematical formulation used in optimal control. If we do not know precisely all future values of the disturbance we cannot react in an optimal manner to reject them. The alternative is to use an approximate value for the future disturbance signal resulting in sub-optimal feed-forward control [Juang, 1998].

4.2.1 Implementation Using Local Disturbance Approximations

The previous section presented an approach for optimal disturbance accommodating control for the case when the disturbance is fully characterized throughout the time interval of interest. This section will address the implementation of sub-optimal feed-forward control using local (in time) approximations of the disturbance.

One approach for implementing local approximations is obtained by extending the basis function approach presented in Equations 4.33, 4.34, and 4.35. The basic concept consists of obtaining locally valid C_i's using a real-time identification process. Once the local values of C_i's have been identified, the optimal feed-forward control is defined. However, this approach cannot be applied as stated to the reaction wheel imbalance problem because

the imbalance cannot be measured directly. Instead, the measurable quantities used to parameterize the imbalance forces and torques should be used to define future values of the disturbance. The fundamental measurable quantity for the reaction wheel imbalance problem is wheel speed, obtained using a tachometer or encoder.

It should be clear that using local estimates of the disturbance to predict future values will loose the anticipatory nature of the optimal feed-forward control. Also, the resulting optimal control will only be as good as our estimate. Furthermore, our ability to predict future events is a function of the prediction time interval. In other words, we are much more likely to correctly predict future quantities when the prediction interval is just a few sample points, rather than a few minutes. This leads to the necessity to keep the time horizon as short as possible, but still long enough to be unaffected by the terminal time condition $g(t_1) = 0$. These are clearly conflicting requirements and lead to the need for a sliding horizon control. Although achievable, the likelihood of accommodating these various complexities may pose a significant challenge. A cleaner solution is desired.

4.3 Sub-Optimal Feed-Forward Control

The solution proposed in this work exploits the nature of the disturbance with an effort to utilize the developments in Chapter 3. The basic approach exploits the fact that the wheel speed is always periodic and therefore can be generally represented by the following Fourier series

$$\omega(t) = \omega_o + \sum_{n=1}^{\infty} \beta_n \cos(\alpha_n t + \phi_n) \tag{4.36}$$

The above function is also used to define the wheel's angular position, $\theta(t)$, and its angular acceleration $\dot{\omega}(t)$. The angular position is given as

$$\theta(t) = \theta_o - \omega_o t_o - \sum_{n=1}^{\infty} \frac{\beta_n}{\alpha_n} \sin(\alpha_n t_o + \phi_n) + \omega_o t + \sum_{n=1}^{\infty} \frac{\beta_n}{\alpha_n} \sin(\alpha_n t + \phi_n) \tag{4.37}$$

or more compactly written as

$$\theta(t) = \Psi + \omega_o t + \sum_{n=1}^{\infty} \frac{\beta_n}{\alpha_n} \sin(\alpha_n t + \phi_n) \tag{4.38}$$

The angular acceleration is given as

$$\dot{\omega}(t) = -\sum_{n=1}^{\infty} \alpha_n \beta_n \sin(\alpha_n t + \phi_n) \tag{4.39}$$

Recall that the reaction wheel imbalance is assumed to have the form

$$w(t) = Me[\omega^2(t)\sin\theta(t) - \dot{\omega}(t)\cos\theta(t)] \tag{4.40}$$

where $\theta(t)$, $\omega(t)$, and $\dot{\omega}(t)$ are defined in Equations 4.38, 4.36, and 4.39, respectively. For the sake of clarity, we will proceed with the derivation assuming that the series in Equations 4.36 contains only one term and the acceleration term in Equation 4.40 can be neglected. Under these assumptions, Equation 4.40 reduces to

$$w(t) = Me\left[(\omega_o + \beta\cos(\alpha t + \phi))^2 \sin\left(\Psi + \omega_o t + \frac{\beta}{\alpha}\sin(\alpha t + \phi)\right)\right] \tag{4.41}$$

Notice that the disturbance consists of an amplitude modulation term, $\omega_o + \beta\cos(\alpha t + \phi)$, and frequency modulation term, $(\beta/\alpha)\sin(\alpha t + \phi)$. Signals of this type are commonly used in practical FM communication systems and have been the subject of much research, see [Cuccia, 1952 and Giacoletto, 1947]. Expanding Equation 4.41 gives

$$\begin{aligned} w(t) = {} & Me\omega_o^2 \sin\left(\Psi + \omega_o t + \frac{\beta}{\alpha}\sin(\alpha t + \phi)\right) \\ & + 2Me\beta\omega_o \cos(\alpha t + \phi)\sin\left(\Psi + \omega_o t + \frac{\beta}{\alpha}\sin(\alpha t + \phi)\right) \\ & + \frac{Me\beta^2}{2}\sin\left(\Psi + \omega_o t + \frac{\beta}{\alpha}\sin(\alpha t + \phi)\right) \\ & + \frac{Me\beta^2}{2}\cos(2\alpha t + 2\phi)\sin\left(\Psi + \omega_o t + \frac{\beta}{\alpha}\sin(\alpha t + \phi)\right) \end{aligned} \tag{4.42}$$

or more compactly

$$w(t) = w_1(t) + w_2(t) + w_3(t) + w_4(t) \tag{4.43}$$

Equation 4.42 may now be approximated term-by-term using a Fourier series. Let's consider the first term $w_1(t)$

$$w_1(t) = Me\omega_o{}^2 \sin\left(\Psi + \omega_o t + \frac{\beta}{\alpha}\sin(\alpha t + \phi)\right) \tag{4.44}$$

Rewriting Equation 4.44 using complex exponentials gives

$$w_1(t) = Me\omega_o{}^2 \Im m\left(e^{i(\Psi + \omega_o t)} e^{i\frac{\beta}{\alpha}\sin(\alpha t + \phi)}\right) \tag{4.45}$$

Notice that $e^{i\frac{\beta}{\alpha}\sin(\alpha t + \phi)}$ is periodic with fundamental frequency, $\frac{\alpha}{2\pi}$ *Hz*. It can be expanded in a Fourier series to yield

$$e^{i\frac{\beta}{\alpha}\sin(\alpha t + \phi)} = \sum_{n=-\infty}^{\infty} C_n e^{in(\alpha t + \phi)} \tag{4.46}$$

with C_n defined as

$$C_n = \frac{1}{T}\int_{-\frac{T}{2}}^{\frac{T}{2}} e^{i\frac{\beta}{\alpha}\sin(\alpha t + \phi)} e^{-in(\alpha t + \phi)} dt \tag{4.47}$$

This integral cannot be evaluated in closed form. It does however converge to some real value. Equation 4.47 is a function of n and β/α and is given the name *Bessel function of the first kind* and will be referenced as $J_n(\beta/\alpha)$. The ratio β/α is generally referred to in the literature as the frequency modulation index [Couch, 1993]. Before we proceed with the derivation, it is necessary to present the fundamental properties of Bessel functions. It can be shown that, for integer values of n

$$J_{-n}\left(\frac{\beta}{\alpha}\right) = (-1)^n J_n\left(\frac{\beta}{\alpha}\right) \tag{4.48}$$

This property tells us that we need only evaluate $J_n(\beta/\alpha)$ along the positive n axis. Figure 4.2 shows the behavior of $J_n(\beta/\alpha)$ as a function of n and β/α. Notice that for very small values of β/α, $J_0(\beta/\alpha)$ approaches unity while, $J_1(\beta/\alpha)$ and $J_2(\beta/\alpha)$ (as well as higher values of n) approach zero. Furthermore, notice that for a fixed value of β/α, $J_n(\beta/\alpha)$ eventually approaches zero as n increases. This will become an important observation in finding the bandwidth of the feed-forward control.

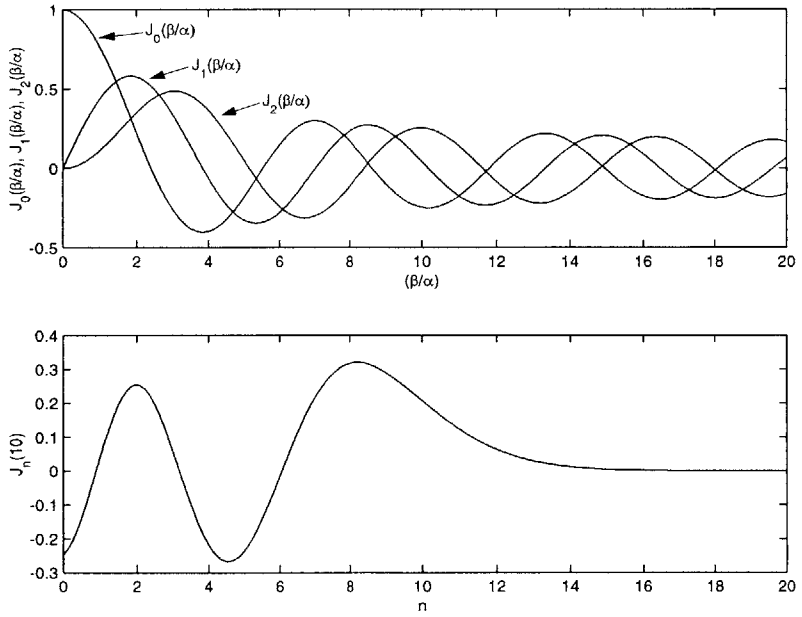

Figure 4.2 Bessel function behavior

Returning now to Equation 4.47 we see that this can be rewritten, using the Bessel function, as

$$C_n = J_n\left(\frac{\beta}{\alpha}\right) \tag{4.49}$$

Equation 4.45 becomes

$$w_1(t) = Me\omega_o{}^2 \Im m\left(e^{i(\Psi+\omega_o t)} \sum_{n=-\infty}^{\infty} J_n\left(\frac{\beta}{\alpha}\right) e^{in(\alpha t+\phi)}\right) \tag{4.50}$$

which becomes

$$w_1(t) = Me\omega_o{}^2\left(\sum_{n=-\infty}^{\infty} J_n\left(\frac{\beta}{\alpha}\right)\sin(\Psi + n\phi + (\omega_o + n\alpha)t)\right) \tag{4.51}$$

Now, lets consider the second term in Equation 4.42.

$$w_2(t) = 2Me\beta\omega_o\cos(\alpha t+\phi)\sin\left(\Psi + \omega_o t + \frac{\beta}{\alpha}\sin(\alpha t+\phi)\right) \tag{4.52}$$

The modulation theorem for the Fourier Transform states that the result of multiplying a time function by a pure sinusoid is a shift of the original transform both up and down by the frequency of the sinusoid, and reduction of the magnitude by half. Applying this theorem to Equation 4.52 and using the results of Equation 4.51 gives

$$\begin{aligned} w_2(t) = {} & Me\beta\omega_o\left(\sum_{n=-\infty}^{\infty} J_n\left(\frac{\beta}{\alpha}\right)\sin(\Psi + (n-1)\phi + (\omega_o + (n-1)\alpha)t)\right) \\ & + Me\beta\omega_o\left(\sum_{n=-\infty}^{\infty} J_n\left(\frac{\beta}{\alpha}\right)\sin(\Psi + (n+1)\phi + (\omega_o + (n+1)\alpha)t)\right) \end{aligned} \tag{4.53}$$

Using the results from the first two terms in Equation 4.42 gives the following expressions for the third and fourth terms:

$$w_3(t) = \frac{Me\beta^2}{2}\left(\sum_{n=-\infty}^{\infty} J_n\left(\frac{\beta}{\alpha}\right)\sin(\Psi + n\phi + (\omega_o + n\alpha)t)\right) \tag{4.54}$$

and

$$w_4(t) = \frac{Me\beta^2}{4}\left(\sum_{n=-\infty}^{\infty} J_n\left(\frac{\beta}{\alpha}\right)\sin(\Psi + (n-2)\phi + (\omega_o + (n-2)\alpha)t)\right) \qquad (4.55)$$
$$+ \frac{Me\beta^2}{4}\left(\sum_{n=-\infty}^{\infty} J_n\left(\frac{\beta}{\alpha}\right)\sin(\Psi + (n+2)\phi + (\omega_o + (n+2)\alpha)t)\right)$$

From Equations 4.51, 4.53 4.54, and 4.55 we see that we have expressed Equation 4.42 as a summation of pure sinusoids. If we truncate the summation to a finite number of terms, for example $n = -k \ldots k$, then the number of unique frequencies contained in Equations 4.51, 4.53 4.54, and 4.55 is $2k + 5$, and range from $\omega_o - (k+2)\alpha$ to $\omega_o + (k+2)\alpha$ with discrete increments of α. The question of how to select k needs to be addressed. To address this issue we must recall the behavior of the Bessel function as given in Figure 4.2. Notice that for small values of the frequency modulation index, i.e, $\beta/\alpha < 1$, we see that $J_0(\beta/\alpha)$ and $J_1(\beta/\alpha)$ are the only significant terms. At larger values of the frequency modulation index, i.e, $\beta/\alpha = 10$, we see that many more significant terms are present. The behavior of the Bessel between the extremes of low and high frequency modulation indices has been well studied and the following rule of thumb guidelines [Couch, 1993] have been developed. The bandwidth of the signal from Equations 4.51, 4.53 4.54, and 4.55 is approximately given as

$$BW \approx 2(\beta + \alpha) \qquad (4.56)$$

Using Equation 4.56 we can get an estimate for number of terms to retain in the summation as

$$k = ceil\left(\frac{2\beta}{\alpha}\right) \qquad (4.57)$$

where the $ceil(\ )$ function rounds its argument to the nearest integer towards infinity.

The important consequence of expressing Equation 4.42 as Equations 4.51, 4.53, 4.54, and 4.55 is that the formulation developed in Chapter 3 can now be applied to disturbances

that are time varying. Notice that when $\beta = 0$, i.e., no frequency modulation in $w(t)$, the terms $w_2(t) = w_3(t) = w_4(t) = 0$ and $w_1(t)$ defined as

$$w_1(t) = Me\omega_o^2 \sin(\omega_o t + \Psi) \tag{4.58}$$

which is the same form of the disturbance assumed in the quasi-stationary development in Chapter 3. To implement feed-forward control using the disturbance model of Equations 4.51, 4.53 4.54, and 4.55, we would need to identify, in real-time, the parameters that define instantaneous wheel speed given in Equation 4.36. Once these parameters have been identified, the $2(2k+5)$ (two gains per discrete frequency) feed-forward gains are computed using Equation 3.54 and implemented using Equation 4.23, where the $x_1(t)$ states are defined using Equations 4.51, 4.53 4.54, and 4.55 and their first time derivatives.

Before addressing real-time parameter identification of Equation 4.36, lets demonstrate the proposed technique on the low-order sample problem from Section 3.3, Case 3, and compare it to the exact time-varying solution given by Equation 4.10. This example will consider the system's response for three different frequency modulation indices, $\beta/\alpha = \begin{bmatrix} 4/40 & 4/8 & 8/4 \end{bmatrix} = \begin{bmatrix} 1/10 & 1/2 & 2 \end{bmatrix}$. The value of k for each of the three frequency modulation cases was computed using Equation 4.57. The results are presented in Figures 4.3 through 4.8. Two figures were generated for each simulation example, one for the performance output and one that describes the wheel trajectory and associated disturbance. In all examples, the wheel speed starts out at the constant nominal spin rate and then at *5 seconds* into the simulation switches to a modulation. The wheel speed is modulated according to its modulation index using a nominal spin rate of *1.5 Hz*. The time interval used to solve the time-varying problem was *10 seconds*. The start-up effect, i.e., $g(t_1) = 0$, at the terminal time can be observed in the time-varying results, particularly for the $\beta/\alpha = 1/10$ case, where the feed-forward portion of the control reduces to zero. In all cases the sub-optimal feed-forward control performs extremely well, despite its inability to anticipate the jump in wheel trajectory. For this particular set of examples, the anticipatory nature of the time-varying optimal solution is observable at its output, but not

pronounced. As an example of this, notice the slight phase shift in the time-varying solution near the switching point. It is also noticed, at least for the cases considered, that the sub-optimal approach performs slightly better than the time-varying approach through the switching point. However, it is better only when considering the performance outputs. Comparing the feed-forward control signals tells a very different story. Figure 4.9 presents a comparison of an expanded view around the switching point of the feed-forward control signals for the $\beta/\alpha = 2$ case. Notice that the anticipatory nature of the time-varying optimal control signal is dramatic and that the time-varying approach uses much less control authority through the wheel speed transition.

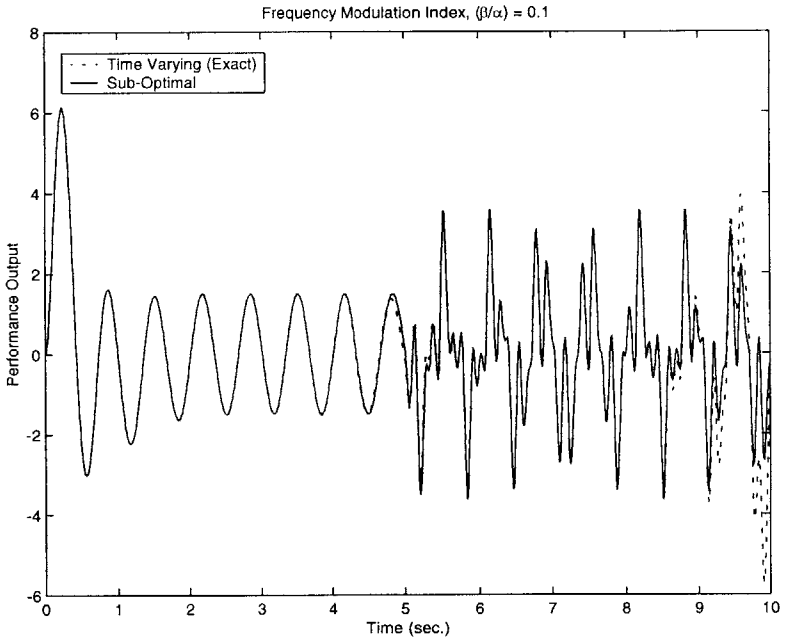

Figure 4.3 System performance for $\beta/\alpha=1/10$

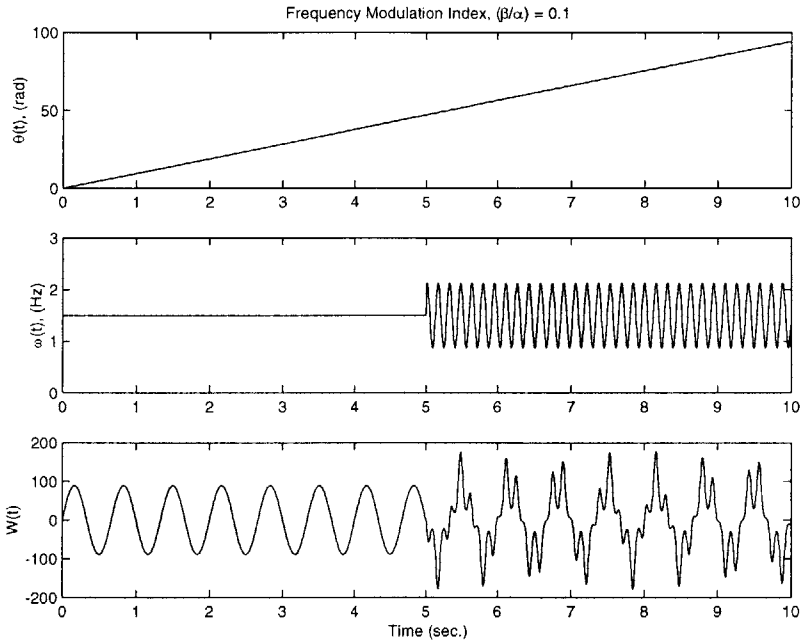

Figure 4.4 Imbalance angle, angular rate, and disturbance for $\beta/\alpha=1/10$

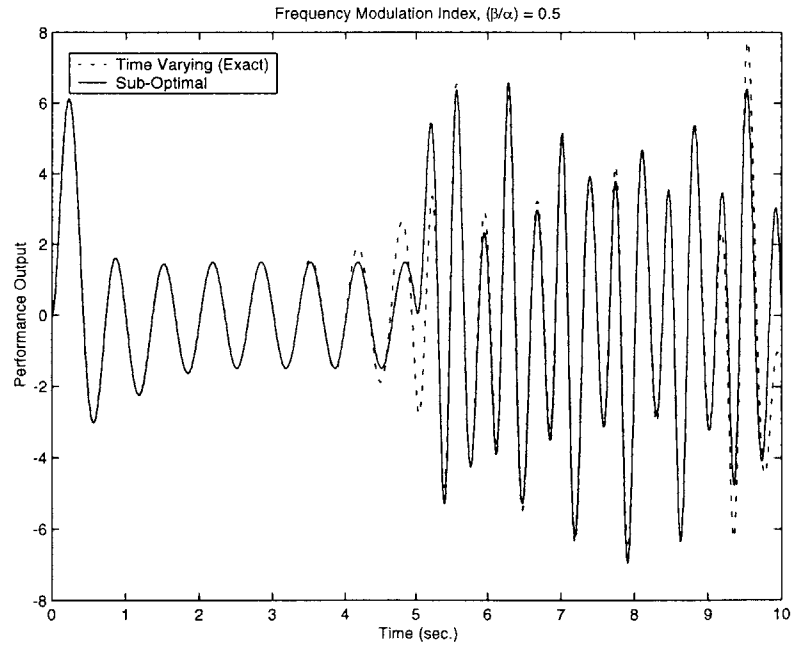

Figure 4.5 System performance for $\beta/\alpha=1/2$

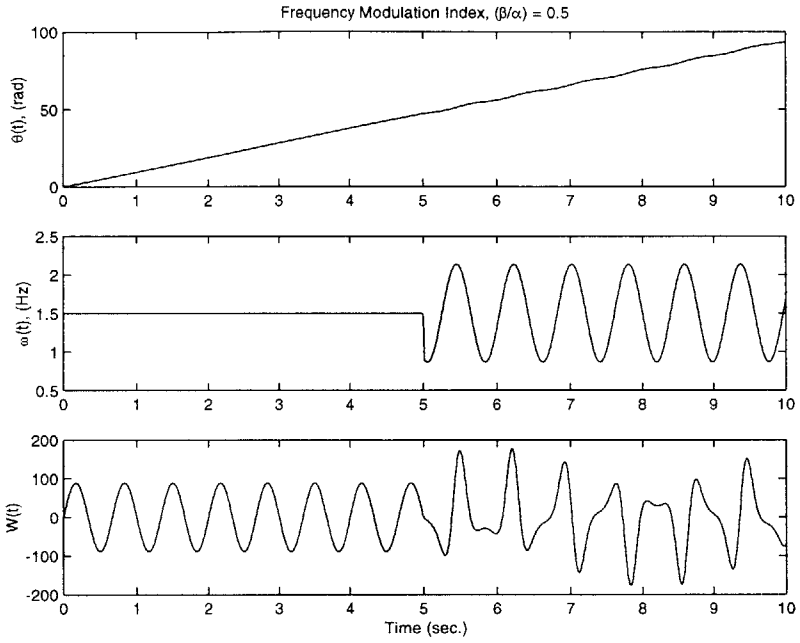

Figure 4.6 Imbalance angle, angular rate, and disturbance for $\beta/\alpha=1/2$

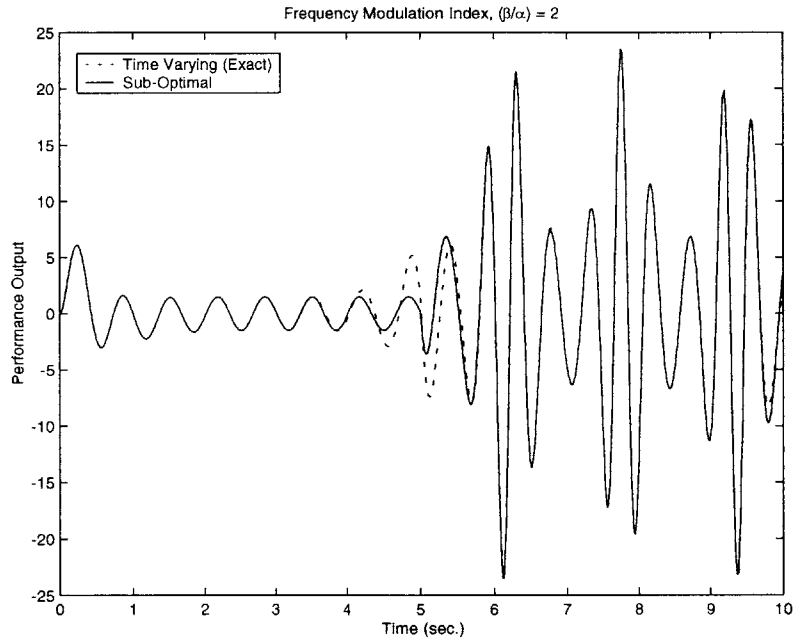

Figure 4.7 System performance for $\beta/\alpha=2$

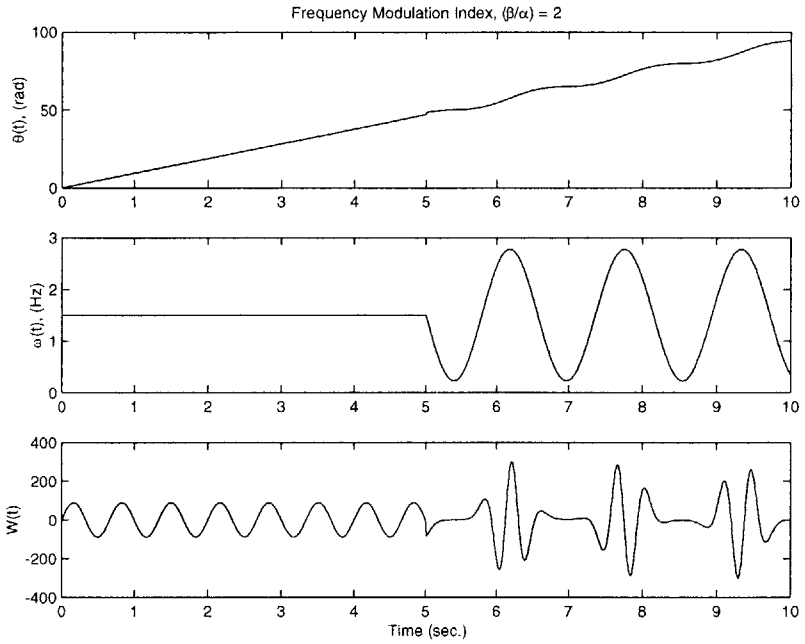

Figure 4.8 Imbalance angle, angular rate, and disturbance for $\beta/\alpha=2$

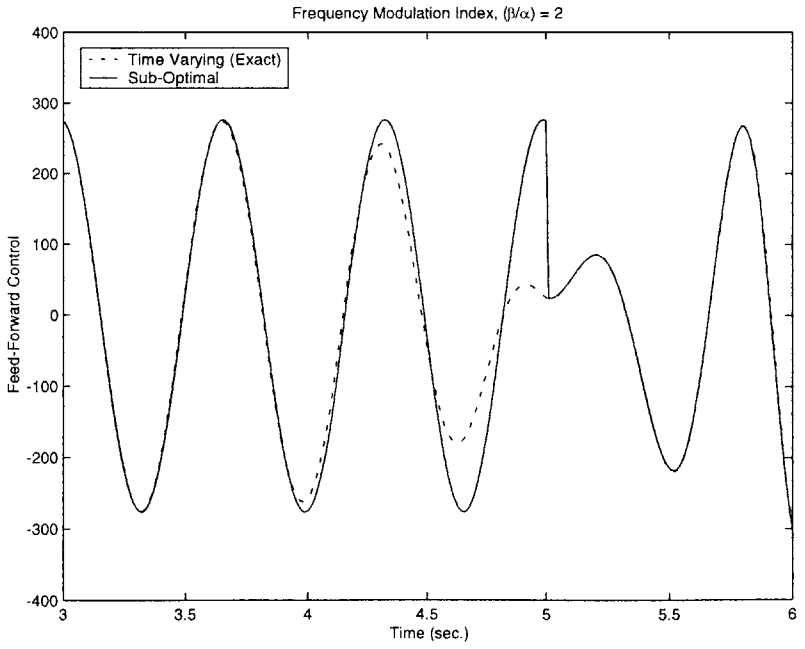

Figure 4.9 Comparison of feed-forward control signals

4.3.1 Online Sinusoidal Parameter Identification

Success of the sub-optimal feed-forward approach requires that we estimate, in real-time and with minimal phase delay, the parameters in Equation 4.36. Real-time sinusoidal parameter estimation has been the topic of extensive research [Annaswamy, 2000, Cao, 2002, Kay, 1993, Li, 1992, Quinn, 1991, Rahman, 1987, and Stoica, et al., 1989]. The goal here is not to develop new theory in sinusoidal parameter estimation, but to demonstrate the feasibility of a single technique through example. To this end, we will present a technique for identifying the parameters in Equation 4.36 for the case when $n = 1$, i.e, a single modulation frequency. For this case, Equation 4.36 reduces to

$$\omega(t) = \omega_o + \beta\cos(\alpha t + \phi) \tag{4.59}$$

Equation 4.59 can be represented using a Taylor series expansion about $t = t_0$ as

$$\omega(t) \approx \omega_o + \beta\cos(\alpha t_0 + \phi) - \beta\alpha\sin(\alpha t_0 + \phi)(t - t_0) - \frac{\beta\alpha^2}{2}\cos(\alpha t_0 + \phi)(t - t_0)^2 + \frac{\beta\alpha^3}{3!}\sin(\alpha t_0 + \phi)(t - t_0)^3 + \frac{\beta\alpha^4}{4!}\cos(\alpha t_0 + \phi)(t - t_0)^4 \tag{4.60}$$

Equation 4.60 may be expressed as

$$\omega(t) \approx \begin{bmatrix} 1 & -(t-t_0) & -\frac{(t-t_0)^2}{2} & \frac{(t-t_0)^3}{3!} & \frac{(t-t_0)^4}{4!} \end{bmatrix} \begin{bmatrix} \omega_o + \beta\cos(\alpha t_0 + \phi) \\ \beta\alpha\sin(\alpha t_0 + \phi) \\ \beta\alpha^2\cos(\alpha t_0 + \phi) \\ \beta\alpha^3\sin(\alpha t_0 + \phi) \\ \beta\alpha^4\cos(\alpha t_0 + \phi) \end{bmatrix} \tag{4.61}$$

If we define $t_k = k\Delta t$, $t_{k-1} = (k-1)\Delta t$, ..., $t_{k-n} = (k-n)\Delta t$, and $t_0 = t_{k-4}$, we can write Equation 4.61 at the current time plus the previous four time steps as

$$\begin{bmatrix} \omega_{k-4} \\ \omega_{k-3} \\ \omega_{k-2} \\ \omega_{k-1} \\ \omega_k \end{bmatrix} \approx \begin{bmatrix} 1 & 0 & 0 & 0 & 0 \\ 1 & -\Delta t & -\frac{\Delta t^2}{2} & \frac{\Delta t^3}{6} & \frac{\Delta t^4}{24} \\ 1 & -2\Delta t & -2\Delta t^2 & \frac{4\Delta t^3}{3} & \frac{2\Delta t^4}{3} \\ 1 & -3\Delta t & -\frac{9\Delta t^2}{2} & \frac{9\Delta t^3}{2} & \frac{27\Delta t^4}{8} \\ 1 & -4\Delta t & -8\Delta t^2 & \frac{32\Delta t^3}{3} & \frac{32\Delta t^4}{3} \end{bmatrix} \begin{bmatrix} \omega_o + \beta\cos(\alpha t_{k-4} + \phi) \\ \beta\alpha\sin(\alpha t_{k-4} + \phi) \\ \beta\alpha^2\cos(\alpha t_{k-4} + \phi) \\ \beta\alpha^3\sin(\alpha t_{k-4} + \phi) \\ \beta\alpha^4\cos(\alpha t_{k-4} + \phi) \end{bmatrix} \tag{4.62}$$

Equation 4.62 can be solved to give

$$\begin{bmatrix} x_1 \\ x_2 \\ x_3 \\ x_4 \\ x_5 \end{bmatrix} = \begin{bmatrix} 1 & 0 & 0 & 0 & 0 \\ \frac{25}{12\Delta t} & -\frac{4}{\Delta t} & \frac{3}{\Delta t} & -\frac{4}{3\Delta t} & \frac{1}{4\Delta t} \\ -\frac{35}{12\Delta t^2} & \frac{26}{3\Delta t^2} & -\frac{19}{2\Delta t^2} & \frac{14}{3\Delta t^2} & -\frac{11}{12\Delta t^2} \\ -\frac{5}{2\Delta t^3} & \frac{9}{\Delta t^3} & -\frac{12}{\Delta t^3} & \frac{7}{\Delta t^3} & -\frac{3}{2\Delta t^3} \\ \frac{1}{\Delta t^4} & -\frac{4}{\Delta t^4} & \frac{6}{\Delta t^4} & -\frac{4}{\Delta t^4} & \frac{1}{\Delta t^4} \end{bmatrix} \begin{bmatrix} \omega_{k-4} \\ \omega_{k-3} \\ \omega_{k-2} \\ \omega_{k-1} \\ \omega_k \end{bmatrix} \tag{4.63}$$

where

$$\begin{bmatrix} x_1 \\ x_2 \\ x_3 \\ x_4 \\ x_5 \end{bmatrix} \approx \begin{bmatrix} \omega_o + \beta\cos(\alpha t_{k-4} + \phi) \\ \beta\alpha\sin(\alpha t_{k-4} + \phi) \\ \beta\alpha^2\cos(\alpha t_{k-4} + \phi) \\ \beta\alpha^3\sin(\alpha t_{k-4} + \phi) \\ \beta\alpha^4\cos(\alpha t_{k-4} + \phi) \end{bmatrix} \tag{4.64}$$

If we require $\beta > 0$ and $0 < \alpha < \pi/\Delta t$, then Equation 4.64 gives the following unique solutions:

$$\alpha \approx \sqrt{\frac{x_4}{x_2}} = \sqrt{\frac{x_5}{x_3}} \tag{4.65}$$

$$\omega_o \approx x_1 - \frac{x_3}{\alpha^2} \tag{4.66}$$

$$\beta \approx \sqrt{(x_1 - \omega_o)^2 + \frac{x_2^2}{\alpha^2}} \tag{4.67}$$

$$\phi \approx \text{atan}\left(\frac{\alpha x_2}{x_3}\right) - \alpha(k-4)\Delta t \tag{4.68}$$

We now have expressions for the parameters in Equation 4.59 by solving a linear system of equations using the current plus four delayed wheel speed sensor outputs. The number of delays could be reduced to three, except that Equation 4.65 suffers from numerical conditioning associated with the zero crossing in x_2 and x_3. Accepting the additional delay provides a numerically well-conditioned solution for α because x_2 and x_3 do not cross through zero at the same time.

4.3.2 Simulation Example Using Online Parameter Identification

A simulink model implementing Equations 4.63 and 4.65 through 4.68 has been developed and is shown in Figure 4.10. The purpose of this model is to verify that feed-forward with sinusoidal parameter identification is feasible. If this model were an actual real-time implementation, the blocks labeled "Parameter Identification" and "Sub-Optimal Feed-Forward" would be the only ones needed to generate the feed-forward signals. For comparison purposes, the exact time-varying results were also generated using the pre-computed feed-forward solution in the block labeled "indata". Simulation results are generated using the same wheel speed scenario that was used to generate the results shown in Figure 4.7. A comparison of the performance output for the exact time-varying solution and the sub-optimal solution with parameter identification is presented in Figure 4.11.

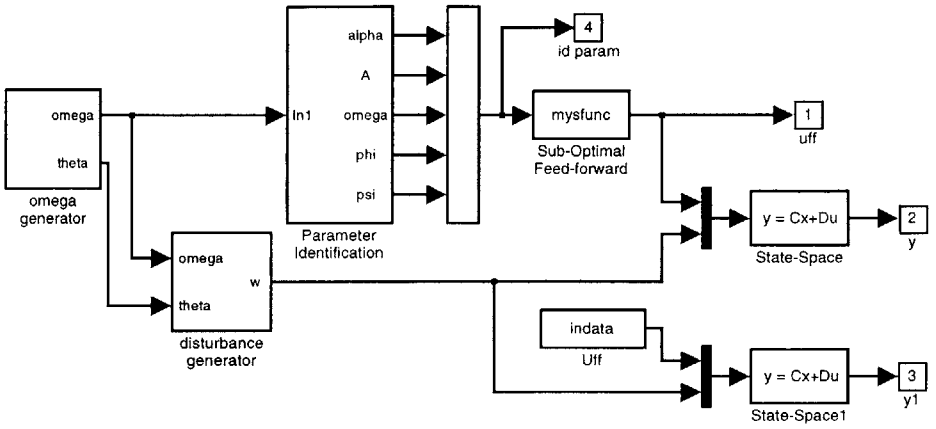

Figure 4.10 Block diagram of feed-forward control with parameter ID

Notice that the results are nearly identical to those given in Figure 4.7. A comparison of the feed-forward control signals is presented in Figure 4.12. Comparing Figure 4.12 with Figure 4.9 shows a nearly perfect match, with a slight difference in their peak values near *5.8 seconds*. Figure 4.13 presents the identified parameters of Equation 4.59. Notice that the parameter identification results are well-behaved and equal to their true values, with an exception at the switching point at *5 seconds*. Recall that the switching point involves a discontinuity in the wheel speed and therefore we should not expect the identification process to preform well across this point. In a physical device, the wheel speed could not respond instantaneously and therefore discontinuities of this type would not be an issue. Future work will include investigating the ability to accurately identify sinusoidal parameters with noisy sensor data.

4.4 Extension to Multiple Modulation Frequencies

Generality of the proposed sub-optimal implementation methodology requires that we demonstrate its extensibility to multiple modulation frequencies. This section will generalize the formulation given in Equation 4.36 for the case when $n>1$. Before we begin, an

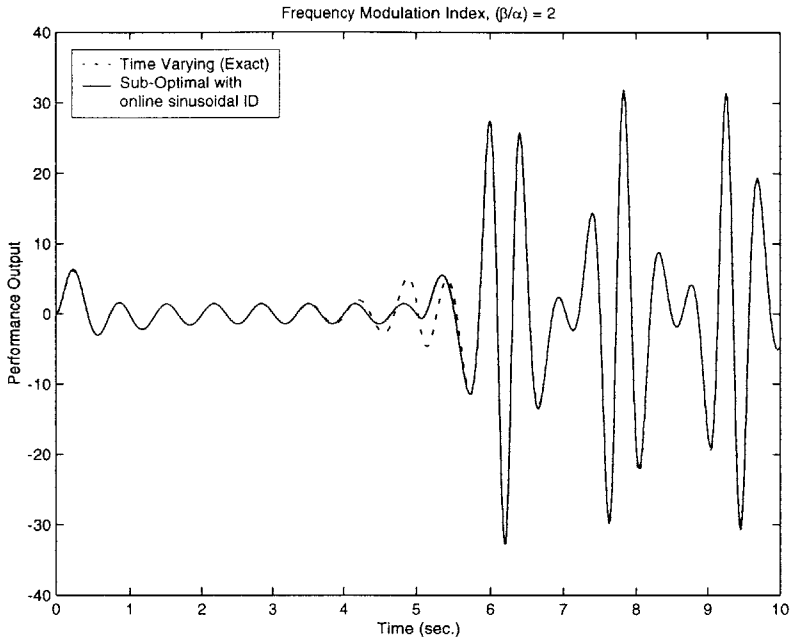

Figure 4.11 System performance for $\beta/\alpha=2$ using parameter ID

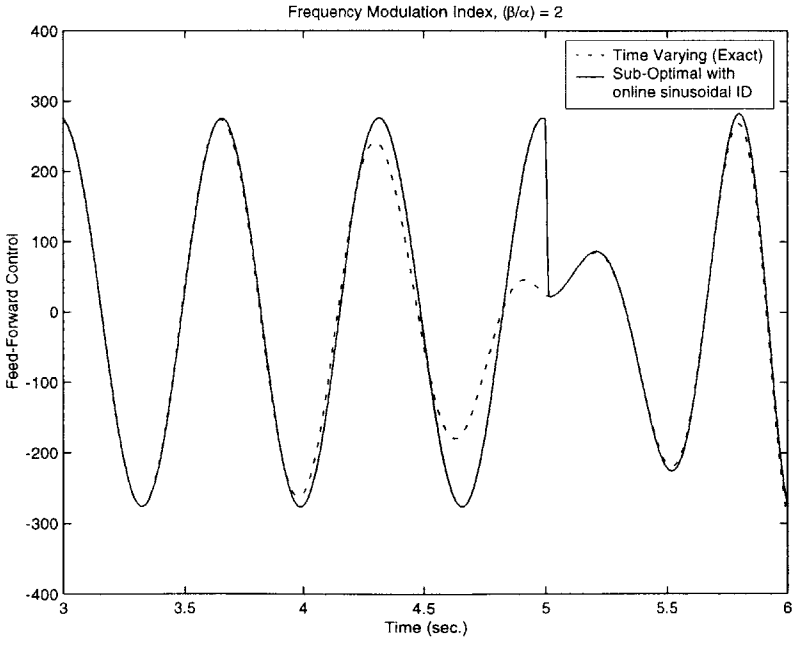

Figure 4.12 Comparison of feed-forward control signals with online ID

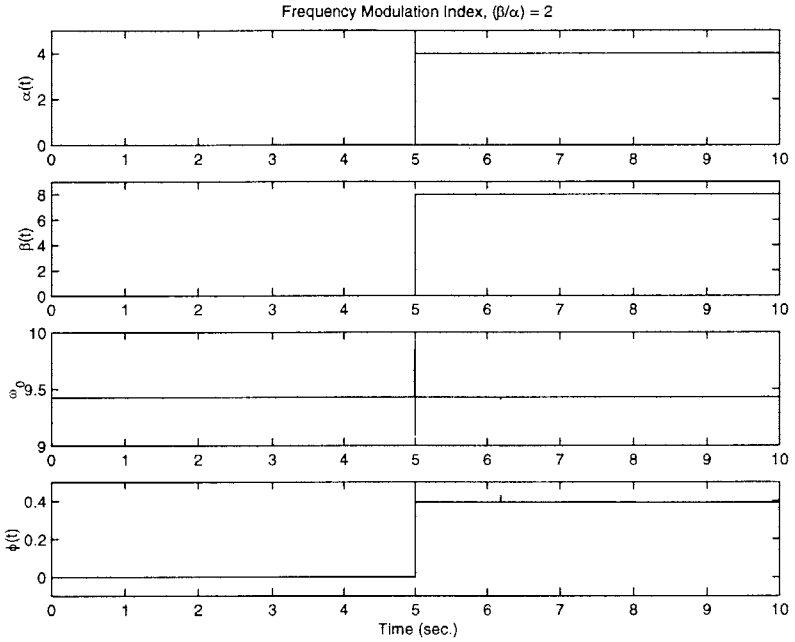

Figure 4.13 Identified wheel speed parameters

additional assumption specific to spacecraft reaction wheel operations will be introduced. In almost all reaction wheel based systems, the wheels are generally operated about a bias wheel speed to prevent zero wheel speed crossing events. We will take this mode of operation to imply that $\omega_0 >> \beta_i$. This assumption in no way limits the generality of the methodology; it just serves to simplify the resulting expressions. Further, we make no assumptions on the α_i frequency terms. Recall, Equation 4.36

$$\omega(t) = \omega_o + \sum_{n=1}^{N} \beta_n \cos(\alpha_n t + \phi_n) \tag{4.69}$$

The assumption $\omega_0 >> \beta_i$ results in

$$\omega(t)^2 \approx \omega_o^2 \tag{4.70}$$

Again, and without loss of generality we will assume that the effect of wheel acceleration is negligible on the imbalance force. Therefore, the imbalance is

$$w(t) = Me\omega_o^2 \sin\left(\Psi + \omega_o t + \sum_{n=1}^{N} \frac{\beta_n}{\alpha_n} \sin(\alpha_n t + \phi_n)\right) \tag{4.71}$$

Expanding using complex exponentials gives

$$w(t) = Me\omega_o{}^2 \Im m\left(e^{i(\Psi + \omega_o t)} e^{i\frac{\beta_1}{\alpha_1}\sin(\alpha_1 t + \phi_1)} e^{i\frac{\beta_2}{\alpha_2}\sin(\alpha_2 t + \phi_2)} \ldots e^{i\frac{\beta_N}{\alpha_N}\sin(\alpha_N t + \phi_N)}\right) \tag{4.72}$$

In term of Bessel functions

$$w(t) = Me\omega_o{}^2 \Im m\left(e^{i(\Psi + \omega_o t)} \sum_{n_1=-\infty}^{\infty} J_{n_1}\left(\frac{\beta_1}{\alpha_1}\right) e^{in_1(\alpha_1 t + \phi_1)} \ldots \sum_{n_N=-\infty}^{\infty} J_{n_N}\left(\frac{\beta_N}{\alpha_N}\right) e^{in_N(\alpha_2 t + \phi_2)}\right) \tag{4.73}$$

Alternately, using a more compact notation

$$w(t) = Me\omega_o{}^2 \Im m\left(e^{i(\Psi + \omega_o t)} \prod_{m=1}^{N} \sum_{n_m=-\infty}^{\infty} J_{n_m}\left(\frac{\beta_m}{\alpha_m}\right) e^{in_m(\alpha_m t + \phi_m)}\right) \tag{4.74}$$

Lets assume that we run each summation from *-k...k*. This would result in a total of $(2k+1)^N$ discrete frequencies (ignoring possible repeated values) with the following values

$$(\omega_o \pm h\alpha_1 \pm i\alpha_2 \pm \ldots \pm m\alpha_N) \tag{4.75}$$

where the indices *h,i,...m* vary independently from *-k...k*. This is of course assuming that the α_i's are not harmonically related. The coefficients on the individual frequencies have the general form

$$Me\omega_o{}^2 J_h\left(\frac{\beta_1}{\alpha_1}\right) J_i\left(\frac{\beta_2}{\alpha_2}\right) \ldots J_m\left(\frac{\beta_N}{\alpha_N}\right) \tag{4.76}$$

Notice that the amplitudes are determined by the product of multiple Bessel functions. This will result in the product terms reducing faster than the individual terms for increasing orders of k. Therefore, despite the potentially large number of terms present, the number of significant terms may be substantially smaller. For the case when α_i's are harmonically related, the number of unique frequency terms is dramatically reduced. For example, with $N=4$ and $k=4$, the number of unique frequency terms is *81*, substantially less than *6561* computed from $(2k+1)^N$. Furthermore, *81* is an upper bound to the number of frequencies and may be reduced to fewer significant terms by examining the magnitudes of the four-term Bessel function coefficients.

4.5 Summary

The general time-varying optimal feed-forward control problem was introduced. The formulation involved solving a forced Hamiltonian system with terminal time boundary conditions. It was shown that the transient behavior of the resulting feed-forward control was defined by the plant's closed-loop dynamics. Furthermore, its steady-state behavior was presented and the relationship to the theory developed in Chapter 3 was shown.

Limitations on the implementation of the fully time-varying solution were presented and several alternatives were given. The fundamental development in this chapter was the sub-optimal feed-forward control for the rejection of nonstationary reaction wheel imbalances. The formulation involved expanding the wheel angular states in terms of a general series representation. This series was further expanded using Bessel functions to arrive at an expression for the time-varying imbalance disturbances characterized by an infinite set of discrete frequencies. The properties of Bessel functions were employed to permit the practical truncation of the infinite series to a finite set of frequencies. Once the finite-set series representation was obtained, the methods of Chapter 3 were used to generate the feed-forward control signal.

Implementation of the sub-optimal feed-forward approach requires the online estimation of the parameters used in the series representation of the wheel states. A simplified param-

eter identification technique was developed and used to demonstrate the feasibility of the proposed sub-optimal implementation. Time domain simulations of the sub-optimal feed-forward control using online parameter identification were conducted. Results compared favorably to the exact time-varying solution.

Chapter 5

EXPERIMENTAL SETUP

The flexible beam test article, shown in Figure 5.1, has been designed to validate the optimal feed-forward control methodology developed in this work. The system consists of a very flexible thin aluminum blade, approximately one-meter long, attached at its base to a hub motor. The hub motor is the primary control effector for the system. At the tip of the beam is a reaction wheel. In general, this tip actuator can be used in two different operating modes, either as an additional control actuator for flexible-body control, or as a narrowband disturbance generator. For the validation effort here, the reaction wheel is used solely as a disturbance generator to provide the harmonic imbalance forces. An imbalance has been created by adding a small mass to the outer rim of the reaction wheel. The test article has nine sensors that may be used in any combination for either feedback or performance output monitoring.

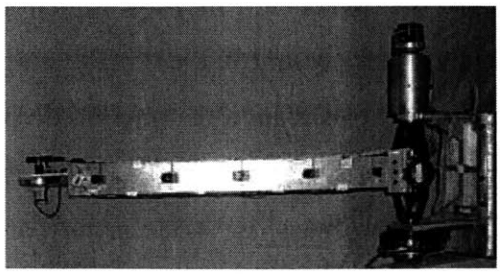

Figure 5.1 Flexible Beam Test Article

5.1 Structure

All structural elements of the flexible beam test article are constructed from aluminum. The structure consists of the following elements: hub assembly, beam attachment fixture, flexible beam, and tip bracket. The hub assembly consists of the hub base plate, shafts to permit rotation, and upper and lower bearing assemblies. Connected to the hub base plate is the beam attachment fixture. The beam attachment fixture consists of a pair of L-brackets with one L-bracket on each side of the beam. These brackets are secured to the hub base plate and to the base of the beam with machine screws. The L-brackets are constructed from standard 2-inch extruded aluminum L-channel and have been cut to match the width of the beam. The flexible beam is a homogenous section of aluminum measuring approximately $28\frac{9}{16}$ inches long by 3 inches wide by $\frac{3}{32}$ inches thick (material properties will be given in Section 5.5). The tip bracket is a homogenous section of aluminum with a machined slot to accept a portion of the beam. The bracket is secured to the beam with six set screws. The tip bracket has been designed to provide for mounting of the reaction wheel assembly and an accelerometer.

5.2 Actuators

The flexible beam test article has two actuators, one at the hub and one at the tip. The hub actuator is a direct drive DC motor capable of applying torque directly to the hub assembly. The tip actuator is also a direct drive DC motor that applies torque to the system, but unlike the hub motor, the tip motor applies a reactive torque as a result of accelerating a disk. As mentioned previously, the tip actuator may also function as a harmonic imbalance source using the nominal imbalances present in the disk/bearing system or it may be augmented with additional imbalances to enhance the magnitude of the imbalance forces. In the current study, an additional imbalance has been added using a known offset mass at a known offset distance. The offset mass is 4.38 *grams* at $5.2286e-2$ *meters*, or $2.290e-4$ KgM. Both actuators are commanded through current controlled amplifiers

to eliminate the need to model their back-emf properties. The motor constants and inertias are listed in Table 5.1.

TABLE 5.1 Actuator properties.

	Hub	**Tip**
Inertia	5.347e-3 KgM^2	4.648e-04 KgM^2
Motor Constants	0.35 $\frac{\text{N-M}}{Volt}$	1.67e-2 $\frac{\text{N-M}}{Volt}$

The inertia values listed in Table 5.1 reflect the total rotational inertia for each actuator. Specifically, for the hub, the number listed includes the inertia of the hub assembly plus the inertia of the motor. Likewise, for the tip actuator, the inertia includes the wheel inertia plus the motor inertia.

5.3 Sensors

As mentioned previously, the test article has nine sensors that may be used in any combination for either feedback or performance output monitoring. The nine sensors are: hub angular position, hub angular rate, five strain gauges distributed along the length of the beam, an accelerometer located at the tip of the beam, and a digital encoder to measure tip wheel position and speed (see Figure 5.2). Hub angular position is determined by processing $\sin\theta(t)$ and $\cos\theta(t)$ signals obtained from a sine/cosine resolver (see Figure 5.3). A tachometer device mounted to the base of the motor measures hub angular rate. The tachometer gain factor is $1.25\frac{\text{rad}/sec}{volt}$. Strain gauge locations and gauge factors are listed in Table 5.2. The position measurements given in Table 5.2 are measured from the axis of rotation (the centerline of the hub assembly).

The accelerometer is a Sundstrand model QA-900 and is located 0.8076 meters from the centerline of the hub assembly. The digital optical shaft encoder is a US Digital model S2-2000. The encoder is capable of tracking rotation rates in the range: 0 ± 165 Hz with an

TABLE 5.2 Strain gauge locations.

	SG1	SG2	SG3	SG4	SG5
Location (meter)	0.0797	0.2478	0.4167	0.5844	0.7525
Gauge Factor (volt/strain)	9984.0	10626.2	10390.1	11212.6	10175.6

angular resolution of 0.09 degrees. The encoder is coupled to the tip wheel by a flex coupling to accommodate minor angular misalignments between the encoder shaft and the reaction wheel shaft.

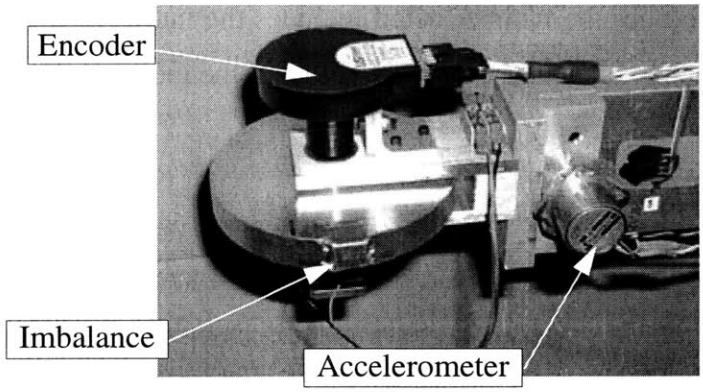

Figure 5.2 Reaction wheel and tip sensors

5.4 Real-Time Computing Environment

The real-time computing environment used with the flexible beam test article consists of both hardware and software elements. The hardware part of the environment is a dSPACE system consisting of the following components:

- DS1003 DSP board (TI's TMS320C40)
- DS2003 Multi-Channel A/D Board (32 Channels at 16-bit resolution)
- DS2103 Multi-Channel D/A Board (32 Channels at 14-bit resolution)

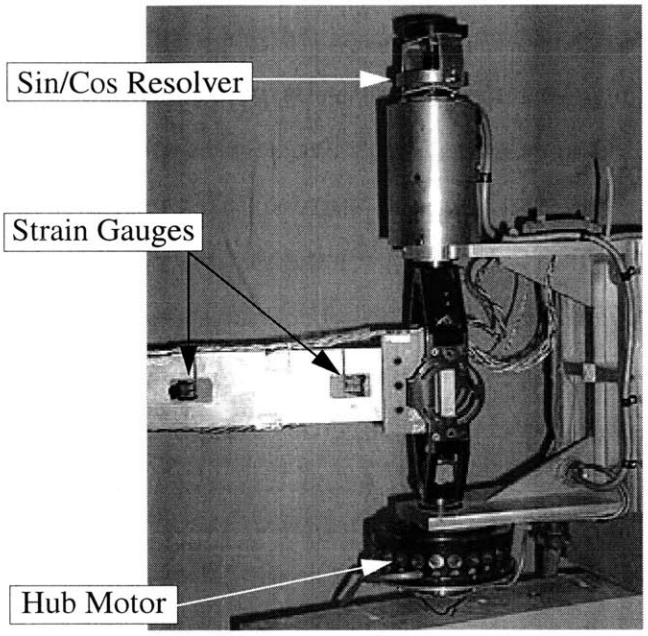

Figure 5.3 Hub assembly

- DS3001 Incremental Encoder Interface Board (5 Channels with a 24-bit position counter)

The software environment includes The Mathworks software products MATLAB and SIMULINK plus the Real-Time Workshop Toolbox. DSPACE's Real-Time Interface (RTI) handles the connection between the hardware and software. RTI is the link between dSPACE's real-time system and MATLAB's control system development software. The software environment has an additional component called ControlDesk by dSPACE that permits the user to monitor and interact with the experiment in real-time.

5.5 Modeling the Hub-Beam System

Modeling the hub-beam system may be handled using a variety of either analytical or empirical methods. In this work, the approach was taken to develop an analytical model and then validate this model against one obtained through experimental methods. This section will present the analytical model developed for the flexible beam test article and make comparisons to an experimentally obtained model.

5.5.1 Finite Element Model

The finite element method was chosen to model this system. The finite element code is based upon a simple implementation of Euler-Bernoulli planar beam elements. This code implements a two-node beam element, with two degrees of freedom at each node. A total of 116 elements were used in this model; thirty-six used to model the hub assembly and beam attachment fixture, thirty-two used for the flexible portion of the beam, and forty-eight used for the tip bracket and reaction wheel mounting fixture. Considering element connectivity and boundary conditions, the total number of degrees of freedom was 233. The material stiffness and mass density properties used for the beam elements are given in Table 5.3. Also in this table are the reaction wheel and the accelerometer assembly masses. The reaction wheel mass listed in Table 5.3 includes the mass of the motor (118.1 grams) plus the mass of the wheel (355.4 grams).

TABLE 5.3 Material properties.

Property	Value
Young's Modulus	65.33e9 N/m^2
Mass Density	2850 Kg/m^3
Reaction Wheel Mass	473.5 grams
Accelerometer with Bracket	100.0 grams

An eigensystem analysis was performed using the mass and stiffness matrices obtained from the finite element program. The undamped frequencies and mode shapes were used as the basis to generate the state-space modal models. The first eight modes were used to build the state-space model. Numerical values for the first eight undamped natural frequencies are given in Table 5.4.

5.5.2 System Identification Model

System identification was performed on the flexible beam test article. The purpose of this system identification was to experimentally identify the (SIMO) transfer functions between the hub actuator to eight output sensors. The outputs of interest included: hub angular position, hub angular rate, all strain gauges, and the accelerometer. The experimentally identified transfer functions were also used to update selected parameters in the finite element model. It should be noted that all parameters listed in this document are the updated values.

An image of the SIMULINK block diagram used for the identification is given in Figure 5.4. The excitation is a band-limited white noise source with a corner frequency of 450 Hz. All outputs were filtered using software fourth-order butterworth low-pass filters with a 450 Hz corner frequency. The sample period for the real-time process was 0.001 seconds. Although the real-time process was run at $1KHz$, the sensor data was downsampled to record every fourth data point resulting in an effective sample rate for the system ID model of 250 Hz. A total of 250 seconds of data were recorded for nine channels (eight outputs and one input). The 250 Hz rate was imposed to accommodate limited real-time data storage capacity of the dSPACE system.

Experimental transfer functions from the hub actuator to eight sensors were obtained. The finite element model was updated to match these experimentally obtained transfer functions. It should be noted that no attempt was made to update the disturbance to output transfer functions. Transfer function comparisons of the updated finite element model to those obtained experimentally are presented in Figure 5.5 through Figure 5.12. In general there is excellent agreement between the updated finite element model and the data. The discrepancies in Figure 5.5 are a result of poor angular resolution in the hub angle sensor. Ideally, white noise input to the hub motor should not produce a net angular motion, but instead the system should oscillate rapidly about its nominal position. Because of its quantization, this small angular motion is not captured well by the hub angle sensor. Quantization is not an issue in the other seven transfer functions primarily because six of them are

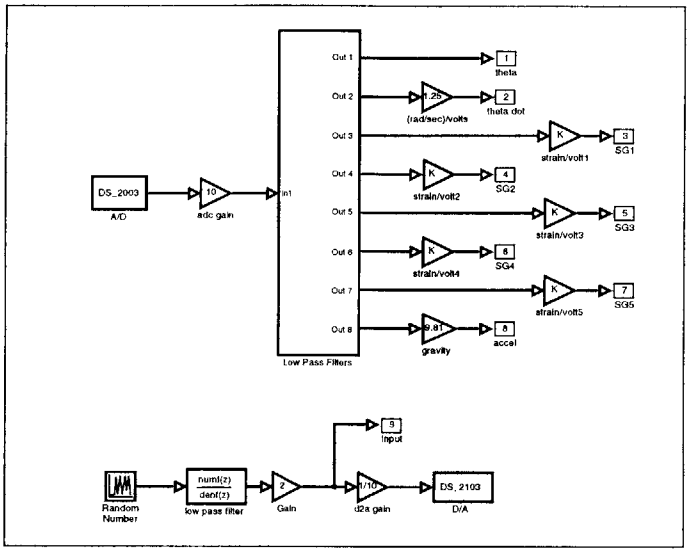

Figure 5.4 SIMULINK identification block diagram.

obtained using purely analog sensors and not subject to quantization. The hub tachometer however is a discrete device, but given the bandwidth of the excitation, its quantization does not pose a problem.

It should be noted that the finite element model used for comparison includes a phase delay to account for the 250 Hz sample rate.

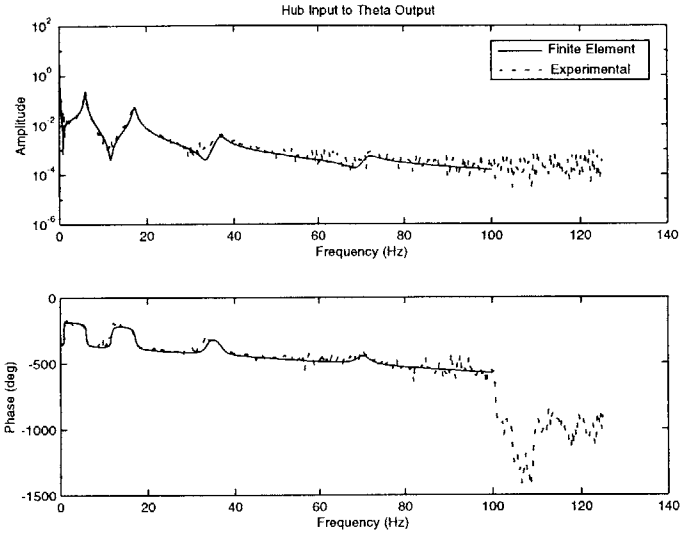

Figure 5.5 Hub input to hub angle transfer function.

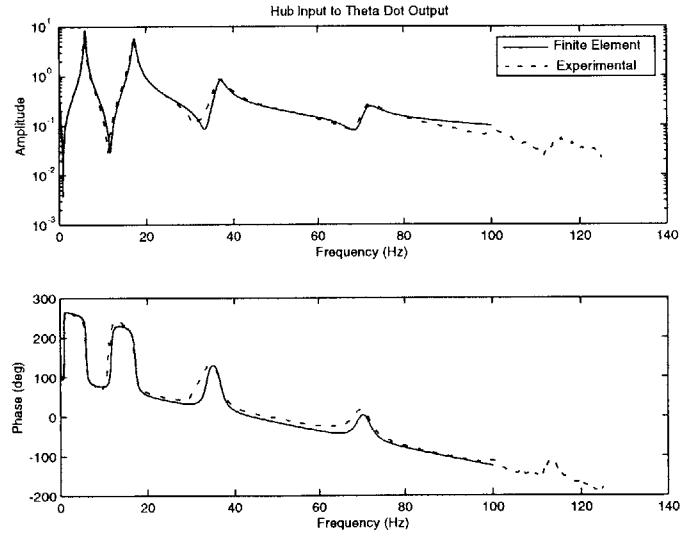

Figure 5.6 Hub input to hub angular rate transfer function.

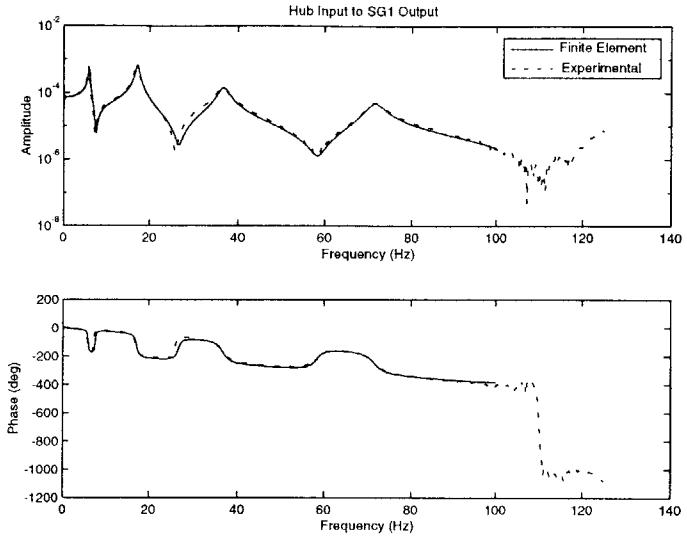

Figure 5.7 Hub input to strain gauge 1 transfer function.

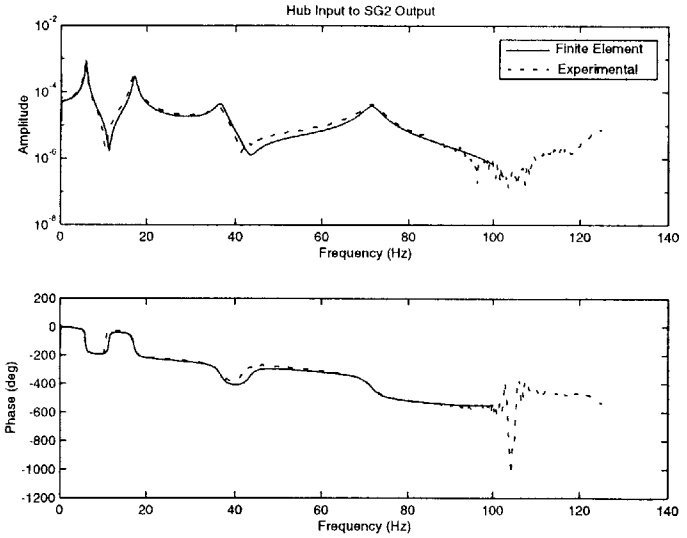

Figure 5.8 Hub input to strain gauge 2 transfer function.

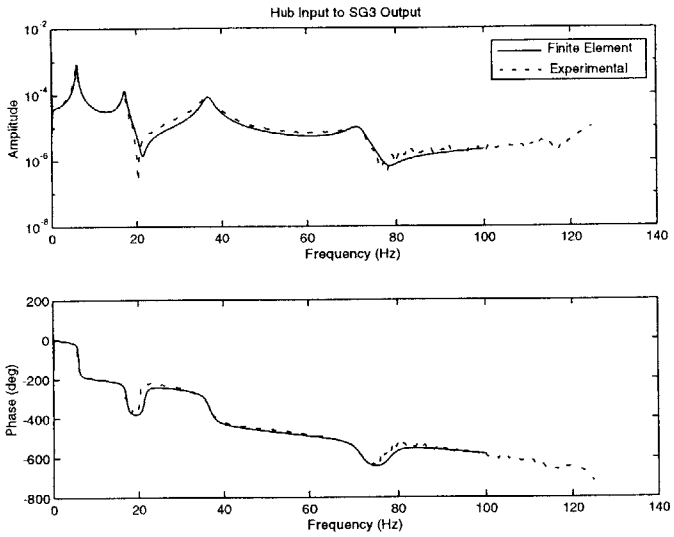

Figure 5.9 Hub input to strain gauge 3 transfer function.

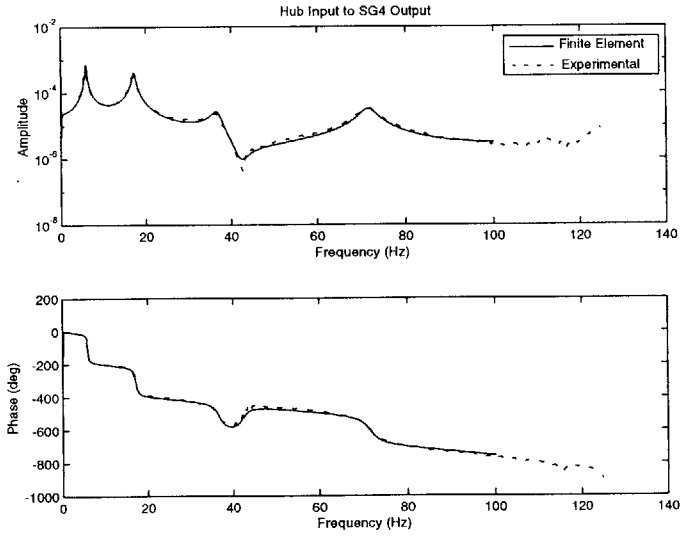

Figure 5.10 Hub input to strain gauge 4 transfer function.

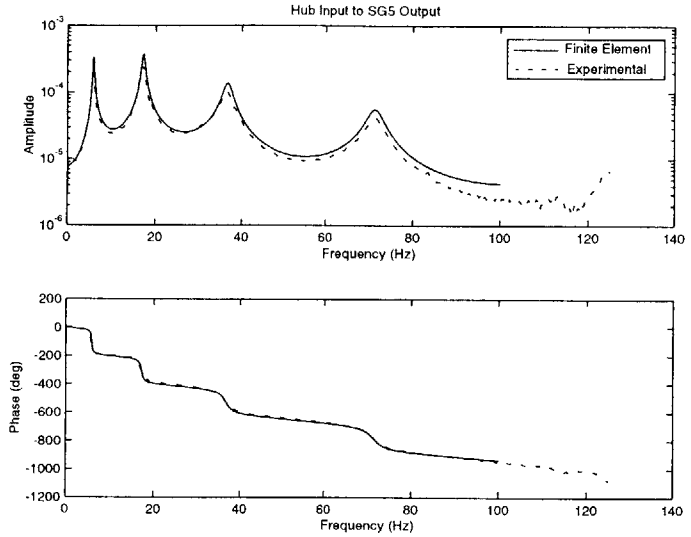

Figure 5.11 Hub input to strain gauge 5 transfer function.

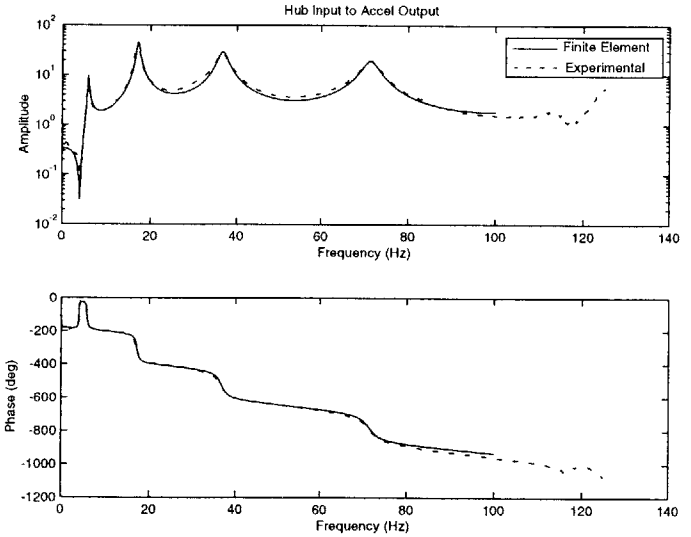

Figure 5.12 Hub Input to Tip Accelerometer Transfer Function

A comparison of the undamped frequencies of the finite element and experimental models is given in Table 5.4. The experimentally identified modal damping ratios for the first four flexible modes are given in Table 5.5. Modal parameters were obtained using the Eigensystem Realization Algorithm (ERA) [Juang, 1985].

TABLE 5.4 Undamped natural frequencies.

Mode Number	Finite Element Frequency (*Hz*)	Exper. Frequency (*Hz*)
1	0.000	0.001
2	5.903	5.718
3	17.157	17.016
4	36.738	36.520
5	71.448	71.476
6	125.744	125.260
7	199.960	---
8	293.665	---

TABLE 5.5 Experimentally determined modal damping ratios.

	Flexible Mode 1	Flexible Mode 2	Flexible Mode 3	Flexible Mode 4	Flexible Mode 5
Modal Damping	0.0315	0.0251	0.0380	0.0250	0.0644

5.6 Summary

The flexible beam test article has been designed for the primary purpose of validating the optimal feed-forward control methodology developed in this work. The system, a long thin very flexible aluminum blade is controlled using a direct current motor located at the base of the beam. A reaction wheel actuator located at the tip of the beam was designed as a disturbance generator to provide a harmonic imbalance source. A reaction wheel imbalance has been created by adding a known mass to the outer rim of the wheel. The test article has nine sensors that may be used for either feedback or performance output monitoring A finite element model has been developed and partially updated to match the experimentally obtained transfer functions.

Chapter 6

DISTURBANCE IDENTIFICATION WITH EXPERIMENTAL VALIDATION

As detailed in Chapter 3, the disturbance rejection methodology developed in this work requires an explicit model of the disturbance as well as models of disturbance influence matrices, B_w, D_w. This chapter will present two methods for characterizing the disturbance parameters necessary to fully prescribe an optimal feed-forward control signal. The first approach deals with SISO or SIMO systems and the most general case of both unknown disturbance influence matrices, B_w, D_w, with unknown disturbance magnitude and phase characteristics as defined in Equation 3.1. The second case, capable of handling MIMO systems, assumes that the disturbance influence matrices are known, but the disturbance magnitude and phase characteristics are unknown. Both approaches are capable of identifying multi-tonal sinusoidal disturbances from steady-state response data.

6.1 Identification with Unknown Disturbance Influence Matrices

There may be situations when the data necessary to characterize disturbance influence matrices, B_w, D_w, is not readily available. Many times, these situations occur in working systems which are incapable of generating the appropriate data for use in conventional identification techniques. For these systems, methods must be developed to accommodate for both unknown disturbance parameters and unknown disturbance influence matrices.

In the development that follows, it is assumed that the plant matrices A_2, C are known. Furthermore, it is assumed that steady state measurement data is known for a variety of wheel speeds. The disturbance influence matrices, B_w, D_w, phase, ϕ_i, and the disturbance magnitude, M_i, are all unknown. The problem can be stated as follows:

Given: steady state measurement data $y(t)$, plant matrices A_2, C, and wheel speed Ω

Determine: plant matrices B_w and D_w, and disturbance parameters M_i and ϕ_i.

Typical system identification algorithms such as those referenced in [Sima, 1999] and [Juang, 1985] require knowledge of the magnitude and the relative phase between the input and output signals to uniquely identify the plant parameters. In fact, if the magnitude and phase information were known, the problem of solving for the unknown plant matrices B_w and D_w simplifies to the following linear least squares problem,

$$G_{yw}(j\Omega) = \left[C(j\Omega I - A_2)^{-1} \; 1\right]\begin{bmatrix} B_w \\ D_w \end{bmatrix} \tag{6.1}$$

where $G_{yw}(s)$ is the transfer function from disturbance to measurements.

Unfortunately, for the reaction wheel imbalance problem, magnitude and phase information is not known and therefore alternate methods must be developed.

The approach developed here is applicable to the general parameterized steady state multi-tonal sinusoidal disturbance as given in Equation 3.1. However, for the sake of clarity of presentation, the following derivation will focus on single-tone static imbalance disturbances of the form

$$w(t) = M\Omega^2 \sin(\Omega t + \phi) \tag{6.2}$$

From linear system theory, the steady state response of the system to a single-tone static imbalance disturbance can be represented as

$$y(t) = M\Omega^2 \left| G_{yw}(j\Omega) \right| \sin(\Omega t + \phi + \angle G_{yw}(j\Omega)) \tag{6.3}$$

Designate the actual measurement signal as

$$y_{meas}(t) = \Gamma \sin(\Omega t + \Psi) \tag{6.4}$$

It is important to realize that Equation 6.4 is only valid for the steady state portion of the system's response. When collecting data, sufficient time must be given to allow for the transient portion of the signal to decay. In practice, visual monitoring of the response signals is generally sufficient; however, the process could be easily automated. The terms Γ and Ψ from Equation 6.4 are easily obtained using a least squares solution on the measurement data together with frequency information from either a spectral analysis of the steady state signal or directly from the wheel speed sensor.

The time index used in Equation 6.4 also requires some discussion. In this work, the time index is arbitrary. Arbitrary in the sense that it is not assumed to be correlated to a trigger level in the output signal and not assumed consistent between different data records. In the results that follow, the time index was reset to zero at the beginning of each steady state data record. Assuming an arbitrary time index greatly simplifies the data collection process, but adds complexity to the parameter identification process. To illustrate the effect of an arbitrary time index on signal phase definition it may be helpful to examine representative imbalance and response signals. Consider the following wheel angular profile

$$\begin{aligned} \theta(t) &= \theta_0 + \frac{\Omega}{2}\left(t - \frac{T}{2\pi}\sin\left(\frac{2\pi}{T}t\right)\right), & t \le \frac{T}{2} \\ \theta(t) &= \theta_0 + \Omega t - \frac{\Omega T}{4}, & t \ge \frac{T}{2} \end{aligned} \tag{6.5}$$

$$\omega(t) = \frac{\Omega}{2}\left(1 - \cos\left(\frac{2\pi}{T}t\right)\right), \quad t \leq \frac{T}{2} \tag{6.6}$$
$$\omega(t) = \Omega, \quad t \geq \frac{T}{2}$$

$$\dot{\omega}(t) = \frac{\Omega\pi}{T}\sin\left(\frac{2\pi}{T}t\right), \quad t \leq \frac{T}{2} \tag{6.7}$$
$$\dot{\omega}(t) = 0, \quad t \geq \frac{T}{2}$$

Where $\theta(t)$, $\omega(t)$, and $\dot{\omega}(t)$ are the angular position, velocity, and acceleration of the imbalance. Equations 6.5, 6.6, and 6.7 are plotted in Figure 6.1 with $T = 4$, $\theta_0 = \frac{\pi}{8}$, and

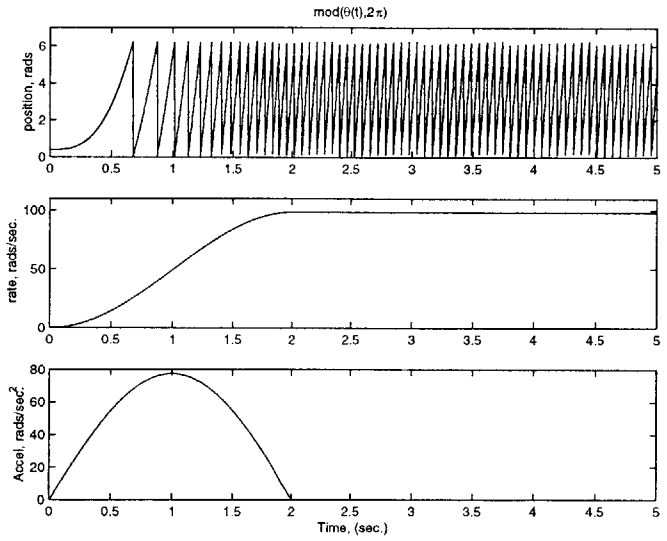

Figure 6.1 Sample wheel profile

$\Omega = 15.67\ Hz$. Figure 6.2 presents the disturbance, as given in Equation 3.4, corresponding to this imbalance profile as well as simulation data of the flexible beam's tip

acceleration response. The imbalance reaches its steady state value at $T/2 = 2$ seconds,

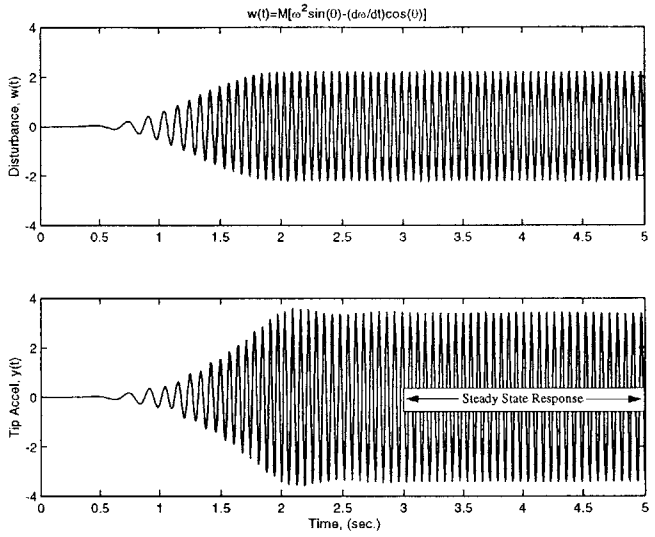

Figure 6.2 Disturbance and tip acceleration response.

while the system reaches a steady state level in approximately 3 seconds. If we started collecting data at exactly $t = 3.5$ seconds, and assumed a time index starting from zero at the first measurement, the phase of the output signal with respect to this time index would be $\Psi = 1.4667$ radians and the phase of the disturbance would be $\phi = 1.6103$ radians. If, on the other hand, we started collecting data at $t = 4$ seconds (again using the same scheme for the time index), the output and disturbance phases would be $\Psi = 0.4496$, and $\phi = 0.5932$, respectively. Of course the phase differences between the disturbance and response signals must be constant and equal to the phase of the transfer function evaluated at the excitation frequency. Explicitly evaluating the phase of the transfer function gives $\angle G_{yw}(j\Omega) = -0.1436 = \Psi - \phi$. It should be clear that either value for the disturbance phase is perfectly acceptable for creating a signal of the form given in Equation 6.2. Once a disturbance phase angle has been identified it may be used together with an angular encoder signal to identify the location of the imbalance. Once the imbalance location has been identified it can be used directly in Equation 6.2 for the creation of the feed-forward

signal. If an encoder signal is not available then the disturbance phase computations must be performed as a calibration step prior to the application of the feed-forward control.

Equations 6.3 and 6.4 will be used to form the basis for a disturbance/plant identification process. Comparing Equations 6.3 and 6.4 gives

$$M\Omega^2\left|G_{yw}(j\Omega)\right| = \Gamma \tag{6.8}$$

and

$$\phi + \angle G_{yw}(j\Omega) = \Psi \tag{6.9}$$

Assuming a SISO system and a disturbance of the form given in Equation 6.2, the number of unknowns that can be solved uniquely using Equations 6.8 and 6.9 is $n+2$. The total number of unknowns, however, is $n+3$; n unknowns from B_w and 1 unknown from D_w, with the disturbance parameters M and ϕ contributing two additional unknowns. It should be obvious that even in the absence of a feed-through term, D_w, the problem does not yield a unique solution. A solution to this fundamental limitation is to recast the problem in terms of scaled disturbance influence matrices. Specifically, assume the following structure,

$$\dot{x}_2(t) = A_2x_2(t) + B_u u(t) + \bar{B}_w\bar{w}(t) \tag{6.10}$$

and

$$y(t) = Cx_2(t) + D_u u(t) + \bar{D}_w\bar{w}(t) \tag{6.11}$$

where

$$\bar{w}(t) = \Omega^2\sin(\Omega t + \phi) \tag{6.12}$$

and

$$\bar{B}_w = B_wM \text{ and } \bar{D}_w = D_wM \tag{6.13}$$

Introducing the scaled disturbance influence matrices into Equations 6.8 and 6.9 gives the following two sets of equations

$$\Omega^2 \left| \bar{G}_{yw}(j\Omega) \right| = \Gamma \tag{6.14}$$

and

$$\phi + \angle \bar{G}_{yw}(j\Omega) = \Psi \tag{6.15}$$

For reasons that will be obvious later, it is convenient to cast Equation 6.14 as the square of the magnitude, i.e.,

$$\left| \bar{G}_{yw}(j\Omega) \right|^2 = \Gamma^2 / \Omega^4 \tag{6.16}$$

A solution using the scaled disturbance equations can be obtained by solving a nonlinear least squares optimization problem formed from Equations 6.15 and 6.16. The basic nonlinear least squares optimization problem is stated mathematically as follows:

$$\min_{v \in \Re^{n+k+1}} \quad f(v) = \frac{1}{2} \sum_{i}^{2k} F_i^2(v) \tag{6.17}$$

where k is the number of steady state measurements and v is the vector of unknown variables. Each measurement must be taken at either a unique frequency or on a separate output channel. When the measurements are taken at unique frequencies for the same output channel, $F_i's$ have the following form

$$F(v) = \begin{bmatrix} F_1 \\ F_2 \\ \vdots \\ F_k \\ F_{k+1} \\ F_{k+2} \\ \vdots \\ F_{2k} \end{bmatrix} = \begin{bmatrix} \left|\bar{G}_{yw}(j\Omega_1)\right|^2 - \Gamma_1^2/\Omega_1^4 \\ \left|\bar{G}_{yw}(j\Omega_2)\right|^2 - \Gamma_2^2/\Omega_2^4 \\ \vdots \\ \left|\bar{G}_{yw}(j\Omega_k)\right|^2 - \Gamma_k^2/\Omega_k^4 \\ \phi_1 + \angle\bar{G}_{yw}(j\Omega_1) - \Psi_1 \\ \phi_2 + \angle\bar{G}_{yw}(j\Omega_2) - \Psi_2 \\ \vdots \\ \phi_k + \angle\bar{G}_{yw}(j\Omega_k) - \Psi_k \end{bmatrix} \tag{6.18}$$

The unknown variables, v, are partitioned as $v = \left[\bar{B}_{w_1}\ \bar{B}_{w_2} \cdots \bar{B}_{w_n}\ \bar{D}_w\ \phi_1\ \phi_2 \cdots \phi_k\right]$. It is essential in any nonlinear optimization problem to have accurate, and preferably computationally efficient, expressions for the gradient of the objective function. Denoting the $2k \times (n+k+1)$ jacobian matrix of $F(v)$ as $J(v)$, and the gradient vector of $f(v)$ as $G(v)$, we have

$$G(v) = 2J^T(v)F(v) \tag{6.19}$$

Considering the structure of $F(v)$ from Equation 6.18 and the partitioning of v, the jacobian matrix takes the following form:

$$J(v) = \begin{bmatrix} \frac{\partial F_1}{\partial v_1} & \cdots & \frac{\partial F_1}{\partial v_{n+1}} & 0 & \cdots & \cdots & 0 \\ \frac{\partial F_2}{\partial v_1} & \cdots & \frac{\partial F_2}{\partial v_{n+1}} & 0 & \cdots & \cdots & 0 \\ \vdots & \cdots & \cdots & 0 & \cdots & \cdots & 0 \\ \frac{\partial F_k}{\partial v_1} & \cdots & \frac{\partial F_k}{\partial v_{n+1}} & 0 & \cdots & \cdots & 0 \\ \frac{\partial F_{k+1}}{\partial v_1} & \cdots & \frac{\partial F_{k+1}}{\partial v_{n+1}} & 1 & 0 & \cdots & 0 \\ \frac{\partial F_{k+2}}{\partial v_1} & \cdots & \frac{\partial F_{k+2}}{\partial v_{n+1}} & 0 & 1 & 0 & 0 \\ \vdots & \cdots & \cdots & \vdots & \cdots & \cdots & \vdots \\ \frac{\partial F_{2k}}{\partial v_1} & \cdots & \frac{\partial F_{2k}}{\partial v_{n+1}} & 0 & 0 & \cdots & 1 \end{bmatrix} = \begin{bmatrix} J_{11} & J_{12} \\ J_{21} & J_{22} \end{bmatrix} \tag{6.20}$$

From 6.20 we see that the $2k \times k$ partition containing blocks J_{12} and J_{22} requires no further discussion. The remaining blocks, J_{11} and J_{21}, may be obtained analytically as well. To explore this further, consider the expression for the transfer function

$$\bar{G}_{yw}(s) = \begin{bmatrix} C(sI - A_2)^{-1} & 1 \end{bmatrix} \begin{bmatrix} \bar{B}_w \\ \bar{D}_w \end{bmatrix} = N(s) \begin{bmatrix} \bar{B}_w \\ \bar{D}_w \end{bmatrix} \tag{6.21}$$

The magnitude squared is therefore

$$\left|\bar{G}_{yw}(s)\right|^2 = \bar{G}_{yw}^H(s)\bar{G}_{yw}(s) = \begin{bmatrix} \bar{B}_w^T & \bar{D}_w^T \end{bmatrix} N^H(s)N(s) \begin{bmatrix} \bar{B}_w \\ \bar{D}_w \end{bmatrix} \tag{6.22}$$

The elements of the J_{11} block are derivatives of the magnitude squared with respect to the i^{th} design variable for $i \leq n+1$. Direct differentiation of Equation 6.22 gives

$$\frac{\partial\left|\bar{G}_{yw}(s)\right|^2}{\partial v_i} = \begin{bmatrix}\bar{B}_w^T & \bar{D}_w^T\end{bmatrix} N^H(s)N(s)\frac{\partial v}{\partial v_i} + \frac{\partial v^T}{\partial v_i} N^H(s)N(s)\begin{bmatrix}\bar{B}_w \\ \bar{D}_w\end{bmatrix} \tag{6.23}$$

Equation 6.23 can be further simplified as follows

$$\frac{\partial\left|\bar{G}_{yw}(s)\right|^2}{\partial v_i} = \begin{bmatrix}\bar{B}_w^T & \bar{D}_w^T\end{bmatrix} N^H(s)N(s)\frac{\partial v}{\partial v_i} + \left(\begin{bmatrix}\bar{B}_w^T & \bar{D}_w^T\end{bmatrix} N^H(s)N(s)\frac{\partial v}{\partial v_i}\right)^H \tag{6.24}$$

$$\frac{\partial\left|\bar{G}_{yw}(s)\right|^2}{\partial v_i} = 2Re\left(\begin{bmatrix}\bar{B}_w^T & \bar{D}_w^T\end{bmatrix} N^H(s)N(s)\frac{\partial v}{\partial v_i}\right)$$

From Equation 6.24 we see that the m^{th} row of the J_{11} block of the jacobian is

$$\frac{\partial\left|\bar{G}_{yw}(j\Omega_m)\right|^2}{\partial v} = 2Re\left(\begin{bmatrix}\bar{B}_w^T & \bar{D}_w^T\end{bmatrix} N^H(j\Omega_m)N(j\Omega_m)\right) \tag{6.25}$$

Equation 6.25 is an exact expression for the derivative of the magnitude squared. Furthermore, by comparing it to Equation 6.22 we see that it can be efficiently formed requiring few additional computations.

Proceeding in a similar manner, analytic expressions for the J_{21} block may also be obtained. The phase of the transfer function is

$$\angle\bar{G}_{yw}(s) = \text{atan}\left(\frac{Im(\bar{G}_{yw}(s))}{Re(\bar{G}_{yw}(s))}\right) \tag{6.26}$$

The elements of the J_{21} block are derivatives of the phase of the transfer with respect to the i^{th} design variable for $i \le n+1$. Direct differentiation of Equation 6.26 gives

$$\frac{\partial}{\partial v}\angle\bar{G}_{yw}(s) = \frac{\frac{\partial}{\partial v}Im(\bar{G}_{yw}(s))Re(\bar{G}_{yw}(s)) - Im(\bar{G}_{yw}(s))\frac{\partial}{\partial v}Re(\bar{G}_{yw}(s))}{Re(\bar{G}_{yw}(s))^2 + Im(\bar{G}_{yw}(s))^2} \tag{6.27}$$

Equation 6.27 can be simplified by using the following identities:

$$Im(\bar{G}_{yw}(s)) = \frac{\bar{G}_{yw}(s) - \bar{G}_{yw}(-s)}{2j} \tag{6.28}$$

$$Re(\bar{G}_{yw}(s)) = \frac{\bar{G}_{yw}(s) + \bar{G}_{yw}(-s)}{2} \tag{6.29}$$

Using Equations 6.28 and 6.29 in Equation 6.27 and the notation introduced in 6.21 gives the following expression for the m^{th} row of the J_{21} block of the jacobian:

$$\frac{\partial}{\partial v}\angle\bar{G}_{yw}(j\Omega_m) = \frac{-Im\left(\left[\bar{B}_w^T \; \bar{D}_w^T\right] N^H(j\Omega_m) N(j\Omega_m)\right)}{\left|\bar{G}_{yw}(j\Omega_m)\right|^2} \tag{6.30}$$

Notice the similarities in the required computations between Equations 6.25 and 6.30. In fact, once Equations 6.22 and 6.25 have been computed, computing Equation 6.30 is trivial.

The disturbance and plant identification methodology developed above has been applied to a simulation model of the flexible beam test article. The disturbance is modeled as closely as possible to the known imbalance on the test article's reaction wheel, i.e., $Me = 2.290e-4 \;\; KgM$. Wheel profiles, similar to those presented in Figure 6.1, are used. Equation 3.4 gives the tip lateral disturbance force input. The validation procedure was as follows:

1. Excite the system with $w(t) = Me(\omega^2(t)\sin(\theta(t)) - \dot{\omega}(t)\cos(\theta(t)))$ where $\theta(t)$, $\omega(t)$, and $\dot{\omega}(t)$ are defined by Equations 6.5, 6.6, and 6.7.

2. Record the steady state response data using an arbitrary time index as discussed above.

3. Corrupt the steady state simulation data with broadband noise of the form $y(t) = noise \times randn(size(y)) \times max(y_{ss}) + y(t)$, where y_{ss} is the steady state response, and *noise* was set to *0.20*.

4. Fit the terms Γ and Ψ from Equation 6.4 using a least squares technique on the noise corrupted steady state response data.

5. Solve the nonlinear least squares optimization problem, i.e., Equation 6.17, using a normally distributed random initial guess for the unknown variables $\left[\bar{B}_{w_1}\ \bar{B}_{w_2}\ \ldots\ \bar{B}_{w_n}\ \bar{D}_w\ \phi_1\ \phi_2\ \ldots\ \phi_k\right]$.

6. Compare the disturbance to output transfer functions of the true and identified plants.

7. Use the computed disturbance phase angles, $\left[\phi_1\ \phi_2\ \ldots\ \phi_k\right]$, along with a simulated encoder signal, to identify the true location of the static imbalance.

The robustness of the identification methodology was demonstrated by using both noise corrupted data and a simulation versus identification model order size mismatch. Simulation data was generated using a model that contained the first eight modes (sixteen states) of the flexible system. This simulation model was truncated without static correction to the first six modes (twelve states) and used in the identification process. Thirteen different steady state data sets were simulated. For each of these data sets a different and arbitrary (random) time index was used. A representative disturbance and the steady state response are shown in Figure 6.3. A comparison of the disturbance to output magnitude and phase plots of the true and identified plant using the methodology developed in this section are shown in Figure 6.4. In this figure, the full-order (sixteen state) model and the identified model (twelve states) are plotted together. The magnitude plots of the true and identified models match very well, with only minor deviations at high frequencies and excellent agreement in the low frequency region, despite the lack of frequency points below 1 *Hz*. The phase plots also agree very well up until the high frequency region. The asterisks on the plot indicate the frequencies that were selected for use in the solution process. An attempt was made to avoid using frequencies at points where the transfer function had

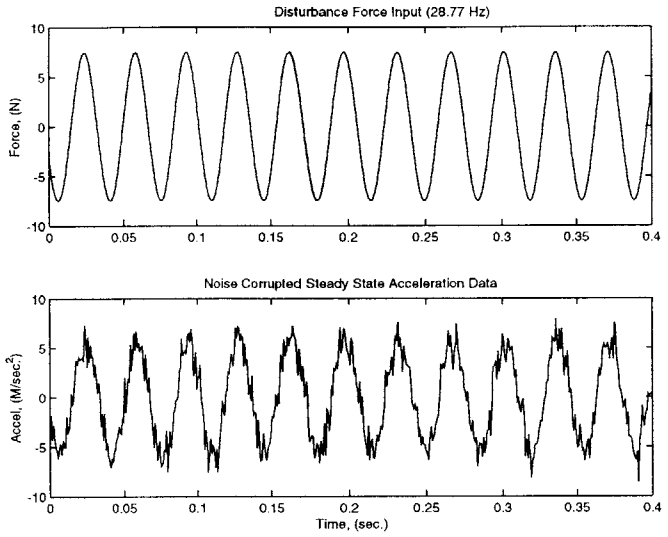

Figure 6.3 Tip force input and acceleration output.

extreme values, i.e., directly at poles or zeros. This was done simply to avoid exploiting too much a priori knowledge of the system. Table 6.1 contains the actual frequency points used in the identification process. Experience with this methodology has shown that, in

TABLE 6.1 System Identification Test Points

Test Points	
ω_1=1.00 Hz	ω_2=1.75 Hz
ω_3=3.07 Hz	ω_4=5.37 Hz
ω_5=5.79 Hz	ω_6=9.40 Hz
ω_7=16.45 Hz	ω_8=16.74 Hz
ω_9=28.77 Hz	ω_{10}=33.06 Hz
ω_{11}=50.33 Hz	ω_{12}=70.71 Hz
ω_{13}=101.13 Hz	

general, the more frequency points used the better the match; however, relatively few points can produce acceptable results.

The computed disturbance phase angles, $\left[\phi_1 \ \phi_2 \ \ldots \ \phi_k\right]$, along with an encoder signal, can be used to identify the true location of the static imbalance. In the simulation, an encoder signal was shifted from the imbalance by 18 degrees. Each of the computed disturbance phase angles provides a direct measure of this encoder-imbalance offset. For this example, the mean value of the encoder shift was computed to be 16.99 degrees, just slightly more than a 1-degree error from its true value. Tighter optimization convergence tolerances and more frequency data points generally improve this estimate, as well as estimates in the transfer function. In fact, simply doubling the number of frequency data points to 26 improves the encoder-imbalance offset estimate to 18.172 degrees. Nonetheless, a 1-degree error in phase will pose virtually no performance degradation in the optimal feed-forward control.

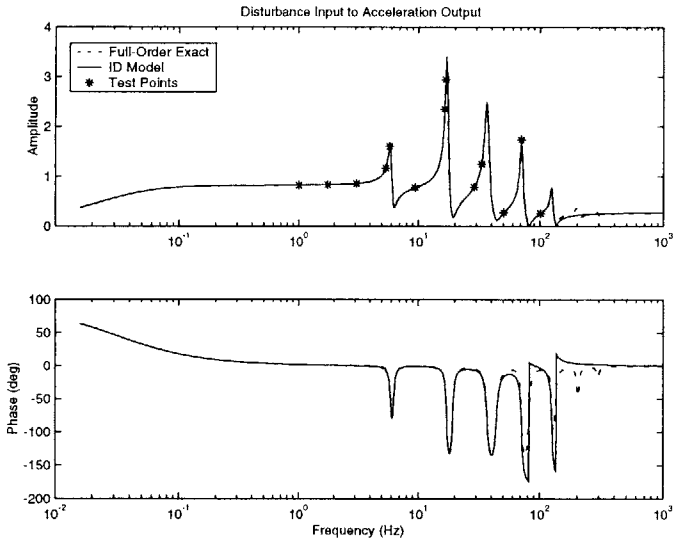

Figure 6.4 Disturbance parameter identification results.

Steady state reaction wheel data collected from the flexible beam test article will now be used to experimentally validate this methodology. Six frequency points will be used to identify the unknown disturbance influence matrices B_w, D_w of a reduced order plant model. The plant model was reduced to six states: one rigid-body mode and the first two

flexible modes. The tip accelerometer was selected as the output sensor to be used in the identification. The data was recorded at a *250 Hz* sample rate and the response of the first harmonic was extracted from the data at each wheel speed and used in the identification process. A representative sample of this data is shown in Figure 6.5. Notice the presence of the additional harmonics and that the data is relatively noise free.

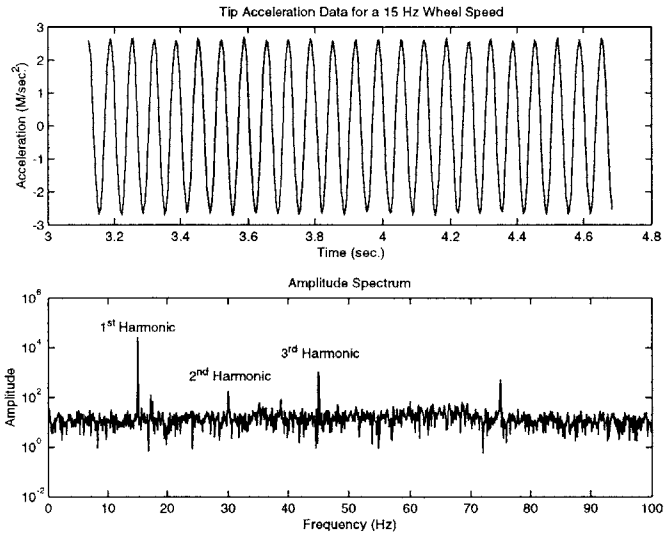

Figure 6.5 Experimentally obtained tip acceleration response.

Recall, that Γ_i and Ψ_i from Equation 6.4 must be computed for each wheel speed. In this work, first a spectral analysis was performed on the data to identify the predominant harmonics, then using the frequency locations obtained from this analysis, a linear least squares problem was solved to give the magnitude and phase information. Table 6.2 summarizes the magnitude and phase data corresponding to the first harmonic for the six wheel speeds. The nonlinear least squares problem, i.e., Equation 6.17, was solved using normally distributed random initial values for the unknown plant and phase parameters. The results are presented in Figure 6.6. Considering that only six frequency points were used, the results show reasonably good agreement. It should be mentioned that for plotting purposes to permit comparison with the finite element model, the disturbance influence

matrices used to generate the disturbance to acceleration transfer function in Figure 6.6 were scaled by the known imbalance magnitude. Furthermore, the data used in this experiment did not contain an encoder signal and therefore could not be used to identify the imbalance location.

TABLE 6.2 Magnitude and output phase data used in identification.

	3 *Hz*	5 *Hz*	10 *Hz*	12 *Hz*	15 *Hz*	20 *Hz*
Γ	0.0727	0.2094	0.7247	1.1772	2.6813	0.9684
Ψ	-2.297	2.423	-2.545	-0.6745	2.7985	-3.002

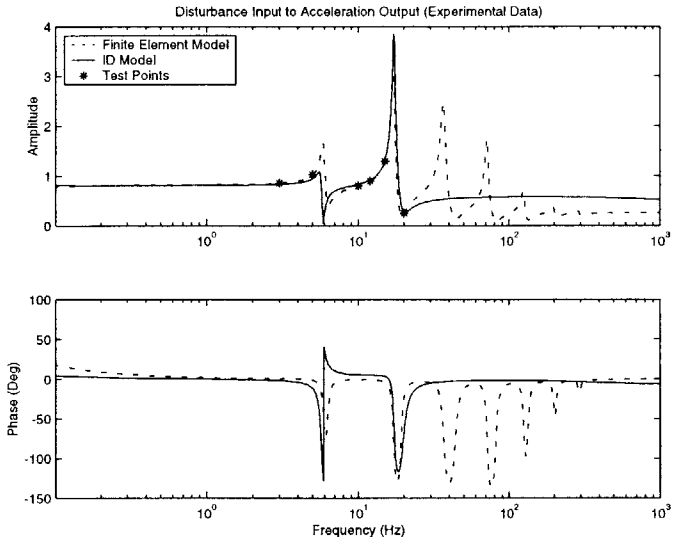

Figure 6.6 Experimentally identified $G_{yw}(s)$ transfer function.

In this section we presented a methodology for determining unknown scaled disturbance influence matrices $\bar{B}_w$, $\bar{D}_w$ and the disturbance phase information, ϕ_i, using steady state response data. The methodology was applied to both simulation and experimentally obtained data of the flexible beam test article and was shown to produce excellent agreement to known system parameters.

6.2 Identification with known Disturbance Influence Matrices

This section will present the development of a methodology to identify unknown disturbance forces (and moments) from measured system outputs by using a known MIMO system. In contrast to Section 6.1, here it is assumed that plant matrices, A_2, B_w, C, D_w, are completely known and that only the disturbance parameters are unknown. The plant parameters may be obtained from a finite element model of the system or through system identification. If system identification is used the system must be capable of producing known inputs at the disturbance location with sufficiently rich spectral content to accurately identify the plant, A_2, B_w, C, D_w, or at a minimum the disturbance influence matrices B_w, D_w.

A finite-difference model in the discrete-time domain can describe the input-output relationship of a system. For a general system with m control inputs and q measurement outputs, the one-step ahead model is

$$\begin{aligned} &y(k) + \alpha_1 y(k-1) + \alpha_2 y(k-2) + \ldots + \alpha_p y(k-p) \\ &= \Gamma_0 u(k) + \Gamma_1 u(k-1) + \Gamma_2 u(k-2) + \ldots + \Gamma_p u(k-p) + \eta(k) \end{aligned} \tag{6.31}$$

where $\eta(k)$ represents the effect of disturbances on the system outputs. The model in Equation 6.31 is commonly known as an ARX model (AutoRegressive with eXogenous input). The disturbance term $\eta(k)$ may also be represented as

$$\eta(k) = \beta_0 w(k) + \beta_1 w(k-1) + \beta_2 w(k-2) + \ldots + \beta_p w(k-p) \tag{6.32}$$

In the absence of a control signal, Equation 6.31 takes the form

$$\begin{aligned} &y(k) + \alpha_1 y(k-1) + \alpha_2 y(k-2) + \ldots + \alpha_p y(k-p) \\ &= \beta_0 w(k) + \beta_1 w(k-1) + \beta_2 w(k-2) + \ldots + \beta_p w(k-p) \end{aligned} \tag{6.33}$$

where the coefficients, α_i, β_i, may be easily obtained from the known plant model. Equation 6.33 can be rewritten in block matrix form as

$$\begin{bmatrix} I & \alpha_1 & \alpha_2 & \cdots & \alpha_p \end{bmatrix} \begin{bmatrix} y(k) \\ y(k-1) \\ \vdots \\ y(k-p) \end{bmatrix} = \begin{bmatrix} \beta_0 & \beta_1 & \cdots & \beta_p \end{bmatrix} \begin{bmatrix} w(k) \\ w(k-1) \\ \vdots \\ w(k-p) \end{bmatrix} \tag{6.34}$$

Equation 6.34 is valid at any timestep and may be applied *l-times* to give the following system of equations:

$$\begin{bmatrix} A & 0 & 0 & 0 \\ \vdots & \ddots & \cdots & \vdots \\ 0 & 0 & A & 0 \\ 0 & 0 & 0 & A \end{bmatrix} \begin{bmatrix} Y(k+l) \\ \vdots \\ Y(k+1) \\ Y(k) \end{bmatrix} = \begin{bmatrix} B & 0 & 0 & 0 \\ \vdots & \ddots & \cdots & \vdots \\ 0 & 0 & B & 0 \\ 0 & 0 & 0 & B \end{bmatrix} \begin{bmatrix} W(k+l) \\ \vdots \\ W(k+1) \\ W(k) \end{bmatrix} \tag{6.35}$$

where A, B, $Y(k)$, and $W(k)$ are defined as

$$A = \begin{bmatrix} I & \alpha_1 & \alpha_2 & \cdots & \alpha_p \end{bmatrix}, \quad B = \begin{bmatrix} \beta_0 & \beta_1 & \cdots & \beta_p \end{bmatrix} \tag{6.36}$$

and

$$Y(k) = \begin{bmatrix} y(k) \\ y(k-1) \\ \vdots \\ y(k-p) \end{bmatrix}, \quad \mathrm{W}(k) = \begin{bmatrix} w(k) \\ w(k-1) \\ \vdots \\ w(k-p) \end{bmatrix} \tag{6.37}$$

The dimensions of A and B in Equation 6.36 are $q \times q(p+1)$ and $q \times m(p+1)$, respectively. Recall, the objective is to determine the unknown disturbances, $W(k)$, from the measured system outputs, $Y(k)$. To this end, we will seek a solution to Equation 6.35 for the unknown disturbances using the known ARX model together with experimentally obtained steady-state response data. The disturbance identification process is repeated for a variety of fixed wheel speeds in an attempt to obtain a disturbance model parameterized in terms of wheel speed. A minimum norm (or least-squares) solution to Equation 6.35 can be obtained using singular value decomposition (SVD). First, to simplify the notation further, write Equation 6.35 as

$$\bar{A}\bar{Y} = \bar{B}\bar{W} \tag{6.38}$$

The dimensions of $\bar{A}$ and $\bar{B}$ in Equation 6.38 are $lq \times q(p+l)$ and $lq \times m(p+l)$, respectively. Performing an SVD on $\bar{B}$ gives

$$\bar{B} = U\Sigma V^T = \begin{bmatrix} U_1 & U_2 \end{bmatrix} \begin{bmatrix} \Sigma_1 & 0 \\ 0 & 0 \end{bmatrix} \begin{bmatrix} V_1^T \\ V_2^T \end{bmatrix} \tag{6.39}$$

where U and V are unitary matrices and Σ is diagonal. Using Equation 6.39 in Equation 6.38 gives

$$\bar{W} = V_1 \Sigma_1^{-1} U_1^T \bar{A}\bar{Y} \tag{6.40}$$

The disturbance identification methodology developed above has been applied to a simulation model of the flexible beam test article. In this example, a force input at the tip and a torque input at the hub were used as the excitation for the simulation. Steady state data was collected from the tip accelerometer and the hub tachometer. The hub and tip disturbance frequencies were *10 Hz* and *20 Hz*, respectively. Unity magnitude was chosen for both disturbance inputs. A *20* percent broadband noise, similar to that used in the simulation example in Section 6.1, was added to both of the output signals. It should be clear from Equation 6.40 that noise on the output signal will be propagated through to the estimate of the disturbance signal. Eliminating the noise from the disturbance estimate is accomplished by fitting sinusoids of known frequency to the noise corrupted disturbance estimates using a linear least squares procedure. The results of the simulation study are shown in Figure 6.7. This figure has four subplots: two subplots for each disturbance signal. The signals labeled as "Identified W" are the solution to Equation 6.40, and those labeled as "Curve Fit W" are those obtained by fitting sinusoids of *10 Hz* and *20 Hz* to the identified signals. Despite the noisy appearance of the identified signals, the fitted sinusoidal signals match the true disturbance signals extremely well, as indicated by the legends on the "Curve Fit W" plots.

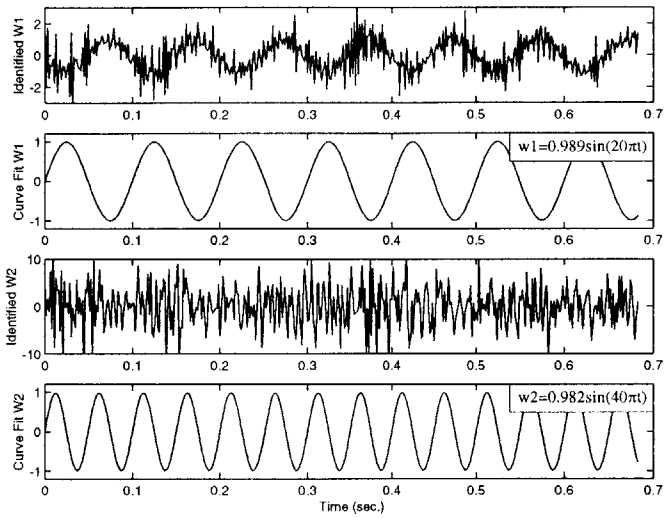

Figure 6.7 MIMO disturbance identification.

Steady state reaction wheel data collected on the flexible beam test article (see Section 6.1) will now be used to experimentally validate the methodology presented in this section. The validation uses an eight-mode finite element model to identify the static imbalance using steady state tip acceleration data. It should be noted that no model updating has been preformed on the disturbance to output transfer functions. The acceleration data was recorded at a *250 Hz* sample rate and no signal processing to identify individual harmonics was preformed. All results were generated using an ARX model order of $p = 16$. Results are presented in Table 6.3 and Figures 6.8 and 6.9. Table 6.3 contains the

TABLE 6.3 Identified imbalance (true value, *Me=2.290e-4 KgM*)

	3 *Hz*	5 *Hz*	10 *Hz*	12 *Hz*	15 *Hz*	20 *Hz*
Me	2.4701e-4	2.0046e-4	2.2962e-4	2.3101e-4	2.2842e-4	2.3091e-4

identified value of the imbalance computed for the six different wheel speeds. The mean value of the data presented in Table 6.3 is $Me = 2.2791e-4 \quad KgM$, which represents a

0.48 percent difference from the true value. Figure 6.8 is a plot of the six identified values for $Me\omega^2$ together with the assumed form of the parameterized imbalance model.

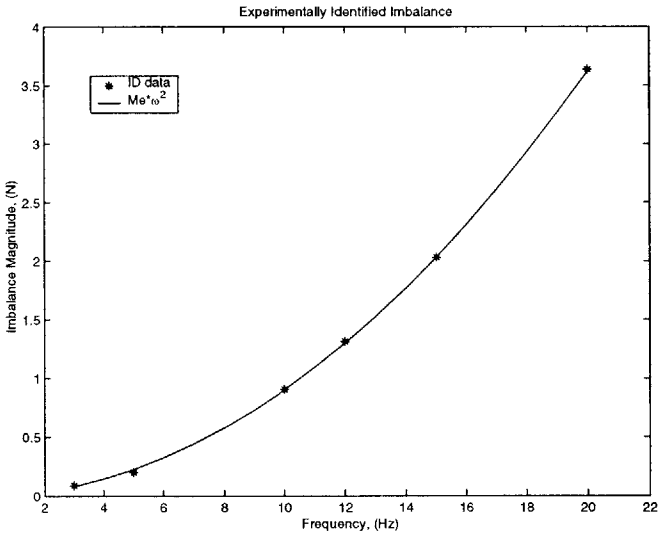

Figure 6.8 Experimentally identified static imbalance.

Figure 6.9 presents the identification data corresponding to the *10 Hz* wheel speed case. The top-most subplot in Figure 6.9 contains the raw data from the solution of Equation 6.40, while the middle subplot is a *10 Hz* sinusoid fitted to the raw identified disturbance. The bottom subplot in Figure 6.9 is a magnitude spectrum of the raw identified disturbance. Notice the presence of the higher harmonics in the identified disturbance. It should be mentioned that no attempt has been made to parameterize the higher harmonics.

This section has presented a methodology for identifying tonal imbalance disturbances from steady state response data. The method uses known plant matrices to form a MIMO ARX model followed by a singular value decomposition to compute a multi-tonal time domain representation of the unknown disturbances. The time domain data can be post-processed to extract the individual harmonics. The method has been applied to both simulation and experimental data and has been shown to produce excellent results.

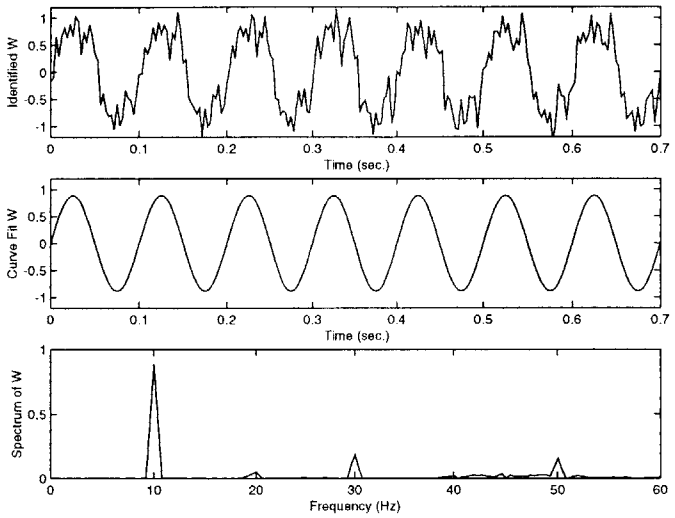

Figure 6.9 Identified disturbance for a *10 Hz* wheel speed

6.3 Summary

This chapter has developed two methods for characterizing plant disturbance influence properties and disturbance imbalance parameters from steady-state measurement data. The first method is applicable to SISO or SIMO systems with unknown disturbance influence matrices, B_w, D_w, and unknown disturbance magnitude and phase characteristics. The second method is applicable to MIMO systems with known disturbance influence matrices. Both methods are capable of identifying multi-tonal sinusoidal disturbance magnitude and phase parameters.

The case when both the disturbance influence matrices and disturbance imbalance parameters are unknown has been formulated as a nonlinear optimization problem. Numerically efficient and analytically exact expressions for the Jacobian have been developed. Results of the optimization are scaled disturbance influence matrices $\bar{B}_w, \bar{D}_w$ and disturbance phase information. The methodology was applied to both simulation and experimentally obtained data from the flexible beam test article and was shown to produce excellent agreement with known system parameters.

A MIMO ARX model together with a minimum norm solution using singular value decomposition forms the basis of a time domain disturbance identification methodology. This approach has been developed for the case with unknown disturbance magnitude and phase parameters, but with known plant disturbance influence matrices. It was shown that the solution, a time domain representation of the disturbance, could be post-processed to extract individual harmonics from noise-corrupted data. The method has been applied in simulation using a two-input disturbance and experimentally using data generated by the flexible beam test article and has been shown to produce excellent results.

Chapter 7

CONTROL DESIGN WITH EXPERIMENTAL VALIDATION

Using the general feed-forward control methodology developed in Chapter 3, optimal disturbance rejection controllers can be synthesized for a wide range of dynamic systems. As the example in Chapter 3 has shown, the feed-forward control derived using this approach is very effective in mitigating the effect of disturbances on performance outputs for linear systems. However, in order to fully demonstrate the effectiveness of this methodology, implementation on hardware is required. This chapter will present the results and many of the implementation details of an experimental validation of the optimal feed-forward control methodology applied to the flexible beam test article described in Chapter 5

7.1 Controller Limitations

It is well known that designing stable feedback control for highly compliant systems with non-collocated sensors and actuators such as the flexible beam test article can pose a challenge. For an excellent treatment of the limitations of control on highly compliant systems, see [Masters, 1997]. To demonstrate these limitations, consider the root locus plot in Figure 7.1 of a constant gain controller with a loop that is closed from the hub motor to the tip accelerometer. The system becomes unstable at very small values of gain. In fact, the 2^{nd} and 4^{th} flexible modes become unstable at gain values of *0.4584* and *0.2937*, respectively. Tip velocity and position loops produce similar results. Obviously, dynamic compensation can improve the situation, but the presence of the non-minimum phase zeros

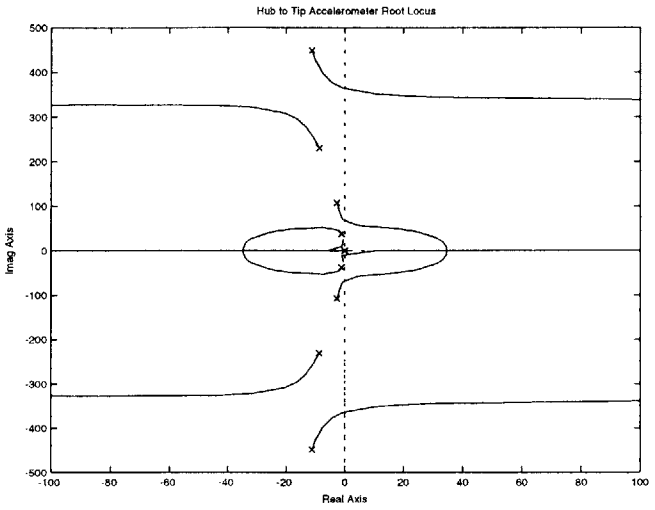

Figure 7.1 Hub torque to tip accelerometer root locus.

will always severely limit the system bandwidth. This bandwidth limitation holds for controllers designed using optimal control methods as well. The SISO closed-loop poles of an optimal controller can be graphically visualized using the root-square locus. A root-square locus shows the location of the optimal closed-loop poles as a function of control penalty. For the cheap controls case, the closed-loop poles go to the stable zeros as well as to the mirror image (with respect to the imaginary axis) of the unstable zeros. For expensive controls, the closed-loop poles go to the stable open-loop poles and to the mirror image of the unstable open-loop poles. Therefore, the bandwidth of systems with low-frequency, non-minimum phase zeros, such as the flexible beam test article, is fundamentally limited. The practical limits on bandwidth are reduced even further when state estimation is required. This is one of the benefits of feed-forward control. Since pure feed-forward control does not affect the stability of the system, the overall disturbance rejection properties of the system are improved without compromising stability margins.

Throughout this work the assumption has been made that the full state was available for feedback. Of course this assumption, although commonly used in theoretical development, is almost never true for real-world applications, particularly for large-order flexible sys-

tems. In the next two sections, we will present the details for implementing a state estimator design and discus the fundamental differences and limitations of disturbance estimation versus pure feed-forward control.

7.2 State Estimation with Feed-Forward Control (Case 1)

First, consider the case of state estimation with pure feed-forward control, i.e., the disturbance states are completely known. This case is true when disturbance identification similar to that presented in Chapter 6 has been preformed. The control associated with this case is given by

$$u(t) = \begin{bmatrix} -K_1 & -K_2 \end{bmatrix} \begin{bmatrix} x_1(t) \\ \bar{x}_2(t) \end{bmatrix} \tag{7.1}$$

where the "overbar" indicates an estimated quantity. The control is therefore a combination of an estimated term and a known term. The estimated term is the nominal plant dynamics and the known term is the disturbance dynamics. The state dynamics and measurement equations are

$$\dot{x}_2(t) = A_2 x_2(t) + B_u u(t) + B_w w(t) \tag{7.2}$$

$$y(t) = C x_2(t) + D_u u(t) + D_w w(t) \tag{7.3}$$

The estimator dynamics are therefore given as

$$\dot{\bar{x}}_2(t) = A_2 \bar{x}_2(t) + B_u u(t) + B_w w(t) + L(y - C\bar{x}_2(t) - D_u u(t) - D_w w(t)) \tag{7.4}$$

Using Equations and 3.12 the closed-loop estimator dynamics are

$$\begin{aligned} \dot{\bar{x}}_2(t) = {} & (A_2 - B_u K_2 - L(C + D_u K_2))\bar{x}_2(t) + \\ & (LD_u K_1 - B_u K_1)x_1(t) + (B_w - LD_w)w(t) + Ly(t) \end{aligned} \tag{7.5}$$

If we define the feed-forward component of control as $U_{ff}(t) = -K_1 x_1(t)$, Equations 7.3 and 7.5 become

$$y(t) = Cx_2(t) - D_u K_2 \bar{x}_2(t) + D_w w(t) + D_u U_{ff}(t) \tag{7.6}$$

$$\dot{\bar{x}}_2(t) = (A_2 - B_u K_2 - L(C + D_u K_2))\bar{x}_2(t) + (B_u - LD_u)U_{ff}(t) + (B_w - LD_w)w(t) + Ly(t) \tag{7.7}$$

Combining Equations 7.2, 7.6, and 7.7 gives

$$\begin{bmatrix} \dot{x}_2(t) \\ \dot{\bar{x}}_2(t) \end{bmatrix} = \begin{bmatrix} A_2 & -B_u K_2 \\ LC & (A_2 - B_u K_2 - LC) \end{bmatrix} \begin{bmatrix} x_2(t) \\ \bar{x}_2(t) \end{bmatrix} + \begin{bmatrix} B_w \\ B_w \end{bmatrix} w(t) + \begin{bmatrix} B_u \\ B_u \end{bmatrix} U_{ff}(t) \tag{7.8}$$

Notice that in Equation 7.8 the feed-forward signal appears as an external input to the system. In the next section we will see that when the disturbance states are included as part of the estimator, the feed-forward portion is no longer present and instead a purely feedback system results.

7.3 Plant and Disturbance Estimation (Case 2)

The second case of state estimation is when both the plant and disturbance states are estimated together. The control associated with this case is given by

$$u(t) = \begin{bmatrix} -K_1 & -K_2 \end{bmatrix} \begin{bmatrix} \bar{x}_1(t) \\ \bar{x}_2(t) \end{bmatrix} \tag{7.9}$$

The estimator dynamics are therefore given as

$$\dot{\bar{x}}_1(t) = A_1 \bar{x}_1(t) + L_1(y - C\bar{x}_2(t) - D_u u(t) - D_w \bar{w}(t)) \tag{7.10}$$

$$\dot{\bar{x}}_2(t) = A_2 \bar{x}_2(t) + B_u u(t) + B_w \bar{w}(t) + L_2(y - C\bar{x}_2(t) - D_u u(t) - D_w \bar{w}(t)) \tag{7.11}$$

where $\bar{w}(t) = C_1\bar{x}_1(t)$. Combining Equations 7.10 and 7.11 gives

$$\begin{bmatrix}\dot{\bar{x}}_1(t)\\ \dot{\bar{x}}_2(t)\end{bmatrix} = \begin{bmatrix}A_1 - L_1D_wC_1 & -L_1C\\ (B_w - L_2D_w)C_1 & A_2 - L_2C\end{bmatrix}\begin{bmatrix}\bar{x}_1(t)\\ \bar{x}_2(t)\end{bmatrix} + \begin{bmatrix}L_1\\ L_2\end{bmatrix}y(t) + \begin{bmatrix}-L_1D_u\\ B_u - L_2D_u\end{bmatrix}u(t) \tag{7.12}$$

Incorporating the control law into Equation 7.12 gives

$$\begin{bmatrix}\dot{\bar{x}}_1(t)\\ \dot{\bar{x}}_2(t)\end{bmatrix} = \begin{bmatrix}A_{11} & A_{12}\\ A_{21} & A_{22}\end{bmatrix}\begin{bmatrix}\bar{x}_1(t)\\ \bar{x}_2(t)\end{bmatrix} + \begin{bmatrix}L_1\\ L_2\end{bmatrix}y(t) \tag{7.13}$$

where the block partitions are defined as

$$\begin{aligned}A_{11} &= A_1 + L_1(D_uK_1 - D_wC_1)\\ A_{12} &= L_1(D_uK_2 - C)\\ A_{21} &= (L_2D_u - B_u)K_1 + (B_w - L_2D_w)C_1\\ A_{22} &= A_2 - B_uK_2 - L_2(C - D_uK_2)\end{aligned} \tag{7.14}$$

The plant dynamics and measurement equations are

$$\dot{x}_2(t) = A_2x_2(t) - B_uK_1\bar{x}_1(t) - B_uK_2\bar{x}_2(t) + B_ww(t) \tag{7.15}$$

$$y(t) = Cx_2(t) - D_uK_1\bar{x}_1(t) - D_uK_2\bar{x}_2(t) + D_ww(t) \tag{7.16}$$

Combing Equations 7.13, 7.15, and 7.16 gives the following closed-loop system:

$$\begin{bmatrix}\dot{x}_2(t)\\ \dot{\bar{x}}_1(t)\\ \dot{\bar{x}}_2(t)\end{bmatrix} = \begin{bmatrix}A_2 & -B_uK_1 & -B_uK_2\\ L_1C & A_1 - L_1D_wC_1 & -L_1C\\ L_2C & (B_w - L_2D_w)C_1 - B_uK_1 & A_2 - B_uK_2 - L_2C\end{bmatrix}\begin{bmatrix}x_2(t)\\ \bar{x}_1(t)\\ \bar{x}_2(t)\end{bmatrix} + \begin{bmatrix}B_w\\ L_1D_w\\ L_2D_w\end{bmatrix}w(t) \tag{7.17}$$

7.3.1 Decoupled Estimator Gains

In general, the estimator gains L_1 and L_2 are partitions of the optimal estimator gain designed for the disturbance-augmented plant, as defined in Equation 3.21. It's very important to notice that the matrix Riccati equation used to solve for the optimal estimator gains L_1 and L_2 does not decouple in the same way as when computing the control gains K_1 and K_2 (see Equations 3.27, 3.28, and 3.29). However, it is still possible to obtain a sub-optimal decoupled solution. To this end, assume an estimator has been designed for a system without consideration of the disturbances. In this case, the estimator dynamics are

$$\dot{\underline{x}}_2(t) = A_2\underline{x}_2(t) + B_u u(t) + L(y - C\underline{x}_2(t) - D_u u(t)) \tag{7.18}$$

where the "underbar" indicates an estimated quantity in the disturbance-free system. Also define estimate residual as

$$\underline{r}(t) = L(y - C\underline{x}_2(t) - D_u u(t)) \tag{7.19}$$

Further, assume that the estimated states and the disturbance-free states are related as follows:

$$\bar{x}_2(t) = \underline{x}_2(t) + V\bar{x}_1(t) \tag{7.20}$$

Using Equations 7.10, 7.11, and 7.20 gives

$$\dot{\bar{x}}_2(t) = A_2\underline{x}_2(t) + B_u u(t) + (L + VL_1)\underline{r}(t) + V(A_1 - L_1(D_w C_1 + CV))\bar{x}_1(t) \tag{7.21}$$

Using Equation 7.20 in Equation 7.11 gives

$$\dot{\bar{x}}_2(t) = A_2\underline{x}_2(t) + B_u u(t) + L_2\underline{r}(t) + (A_2 V + B_w C_1 - L_2(D_w C_1 + CV))\bar{x}_1(t) \tag{7.22}$$

The following must be true if both Equations 7.21 and 7.22 hold for all residuals and all estimates of $\bar{x}_1(t)$:

$$(L + VL_1) = L_2 \tag{7.23}$$

$$V(A_1 - L_1(D_w C_1 + CV)) = (A_2 V + B_w C_1 - L_2(D_w C_1 + CV)) \tag{7.24}$$

Simplifying gives

$$VA_1 - (A_2 - LC)V = (B_w - LD_w)C_1 \tag{7.25}$$

Equation 7.25 is a matrix Lyapunov equation and, assuming conditions given in Equation 3.33 hold, can be readily solved for any given disturbance model defined by A_1. In fact, Equation 7.25 is similar in form to Equation 3.39, which was solved to yield parameterized control gains. Using a similar approach, Equation 7.25 could be solved to yield parameterized solutions for V. The design procedure would be as follows:

1. Design an estimator, L, for the disturbance-free plant.
2. Solve Equation 7.25 to obtain a parameterized solution for V.
3. Design a parameterized L_1 estimator gain for the disturbance states.
4. Use Equation 7.23 to define the parameterized L_2 estimator gain.

The estimator eigenvalues can be obtained by considering the following transformation:

$$\begin{bmatrix} \bar{x}_1(t) \\ \bar{x}_2(t) \end{bmatrix} = \begin{bmatrix} I & 0 \\ V & I \end{bmatrix} \begin{bmatrix} \bar{x}_1(t) \\ x_2(t) \end{bmatrix} \tag{7.26}$$

Using the above transformation in Equation 7.12 together with Equation 7.25 gives

$$\begin{bmatrix} \dot{\bar{x}}_1(t) \\ \dot{\bar{x}}_2(t) \end{bmatrix} = \begin{bmatrix} A_1 - L_1(D_w C_1 + CV) & -L_1 C \\ 0 & A_2 - LC \end{bmatrix} \begin{bmatrix} \bar{x}_1(t) \\ x_2(t) \end{bmatrix} + \begin{bmatrix} L_1 \\ L \end{bmatrix} y(t) + \begin{bmatrix} -L_1 D_u \\ B_u - LD_u \end{bmatrix} u(t) \tag{7.27}$$

The estimator eigenvalues are clearly the eigenvalues of the disturbance-free estimator $A_2 - LC$ plus the eigenvalues of $A_1 - L_1(D_w C_1 + CV)$.

Despite the ability to compute decoupled estimator gains L_1 and L_2 as outlined above, these gains are different than those obtained from optimal estimator theory using the disturbance-augmented plant. To demonstrate this, estimator gains for the flexible beam test article were designed using the two different methods. One method uses optimal estimator theory on the disturbance-augmented plant the other uses the decoupled method outlined above. The output sensors are tip acceleration and hub angle. Figure 7.2 presents a few selected gains for the accelerometer channel as a function of wheel speed. Most gains show some variation in the very low frequency region with a substantial variation observed near *4 Hz* and a general convergence at high frequency.

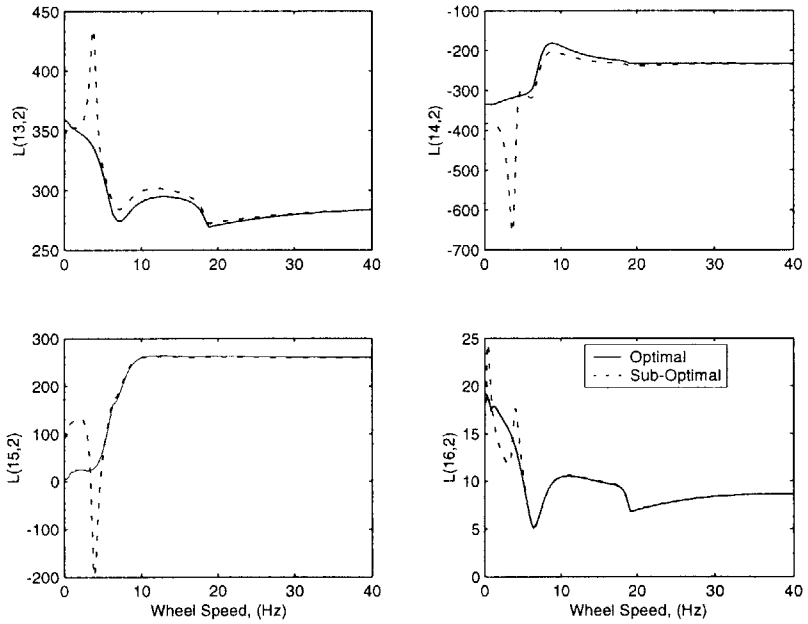

Figure 7.2 Optimal and sub-optimal gains as a function of wheel speed.

7.4 Controller Design and Performance Comparison

This section will present simulation results obtained using a model of the flexible beam test article. The control/disturbance topology used in this section is representative of case 3 as defined in Chapter 3, that is, performance sensor and disturbance nearly collocated

with a non-collocated control actuator. The control gains were designed using a performance index that consisted of a weighted combination of tip displacement, $y_p(t)$, plus tip velocity, $y_v(t)$. Specifically, the output index was $y_{perf} = \alpha(10y_p(t) + y_v(t))$, where alpha was chosen as *0.04*. The hub actuator was the only control actuator used in this study and the control penalty was chosen to be $\rho = 1/350000$. A control design model was chosen to include the first eight modes (sixteen states) of the flexible system. The feedback control gains resulting from these parameters are given in Table 7.1.

TABLE 7.1 Feedback control gains

K(1,1)	K(1,2)	K(1,3)	K(1,4)	K(1,5)	K(1,6)	K(1,7)	K(1,8)
406.96	-0.0083	0.0019	-0.0286	0.0054	-0.1186	0.0303	0.4785
K(1,9)	K(1,10)	K(1,11)	K(1,12)	K(1,13)	K(1,14)	K(1,15)	K(1,16)
-0.1761	0.7888	-0.4429	0.8335	-0.2416	0.2886	0.0516	383.91

The closed-loop eigenvalues, natural frequencies, and damping ratios are given in Table 7.2.

TABLE 7.2 Closed-loop eigenvalues, natural frequencies and damping ratios

Eigenvalues	Frequency (Hz)	Damping
$-7.48 \pm 5.18i$	1.44	0.822
$-5.96 \pm 34.66i$	5.60	0.169
$-22.84 \pm 107.52i$	17.49	0.208
$-22.34 \pm 232.47i$	37.17	0.096
$-16.02 \pm 449.36i$	71.56	0.036
$-20.50 \pm 789.34i$	125.67	0.026
$-31.53 \pm 1255.71i$	199.92	0.025
$-46.13 \pm 1843.17i$	293.44	0.025

The feed-forward gains, K_{1_1} and ωK_{1_2}, computed assuming a single tone disturbance model, are presented in Figure 7.3

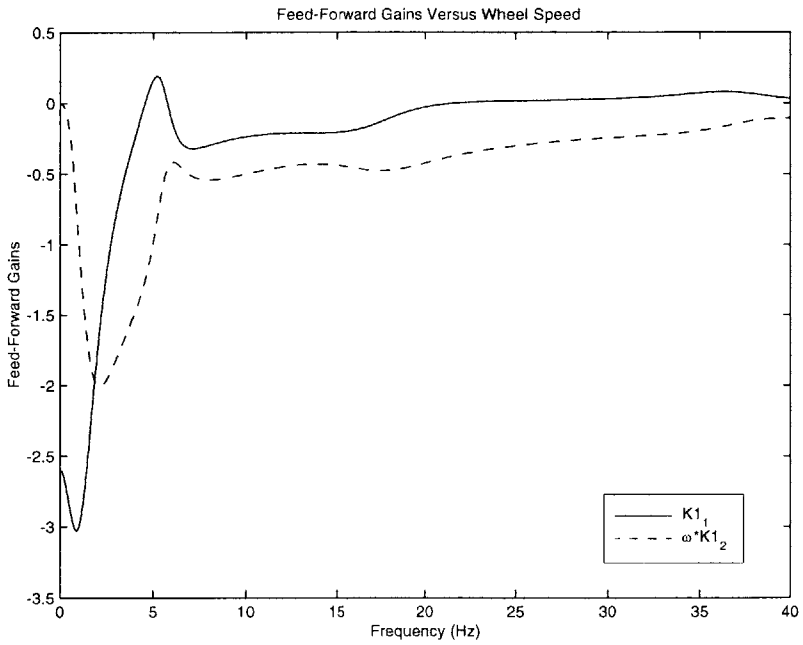

Figure 7.3 Feed-forward gains versus wheel speed.

The measurement sensors (tip acceleration and hub angle) used to generate the estimator presented in Figure 7.2 are the same as those used here. The estimator's closed-loop eigenvalues, natural frequencies, and damping ratios from Equation 7.12 are given in Table 7.3 (for $\omega = 10\ Hz$). Figure 7.4 contains plots of the L_1 estimator gains obtained using optimal estimator theory.

The steady state performance of both case 1 and case 2 state estimation as defined in Sections 7.2 and 7.3, respectively, is defined by the frequency domain response of Equations 7.16 and 7.17. It should be noted that their steady state performance is identical; however, their transient performance is not. These equations may also be used to evaluate the performance of the system without disturbance estimation or feed-forward by simply setting K_1 to zero. Figure 7.5 presents this performance comparison both with and without K_1 as applied to the flexible beam test article. Notice that with the exception of a small region

TABLE 7.3 Estimator eigenvalues, natural frequencies and damping ratios

Eigenvalues	Frequency (Hz)	Damping
$-1.566 \pm 1.955i$	0.398	0.625
$-3.237 \pm 24.025i$	3.858	0.134
$-1.932 \pm 62.769i$	9.995	0.031
$-111.46 \pm 23.371i$	18.126	0.979
$-280.02 \pm 200.08i$	54.775	0.814
$-331.27 \pm 379.36i$	80.157	0.658
$-442.62 \pm 865.00i$	154.645	0.456
$-432.79 \pm 1186.4i$	200.995	0.343
$-709.09 \pm 2142.1i$	359.123	0.314

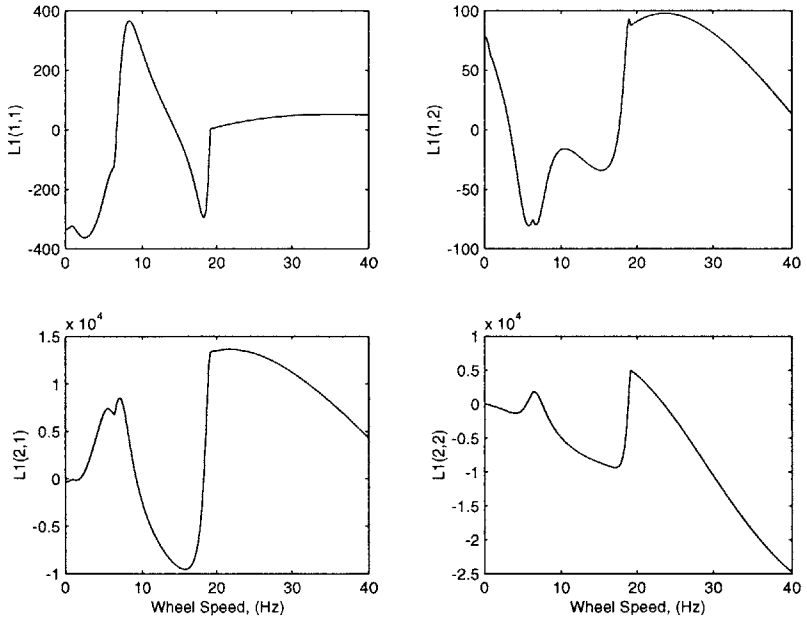

Figure 7.4 L_1 optimal estimator gains as a function of wheel speed.

near *4 Hz*, the performance of the system with K_I shows substantial improvement over that obtained using conventional LQG control, i.e., $K_I=0$.

The transient behavior must be considered to fully evaluate the performance of the system. As noted previously, the implementation of case 2 for a non-steady wheel speed scenario

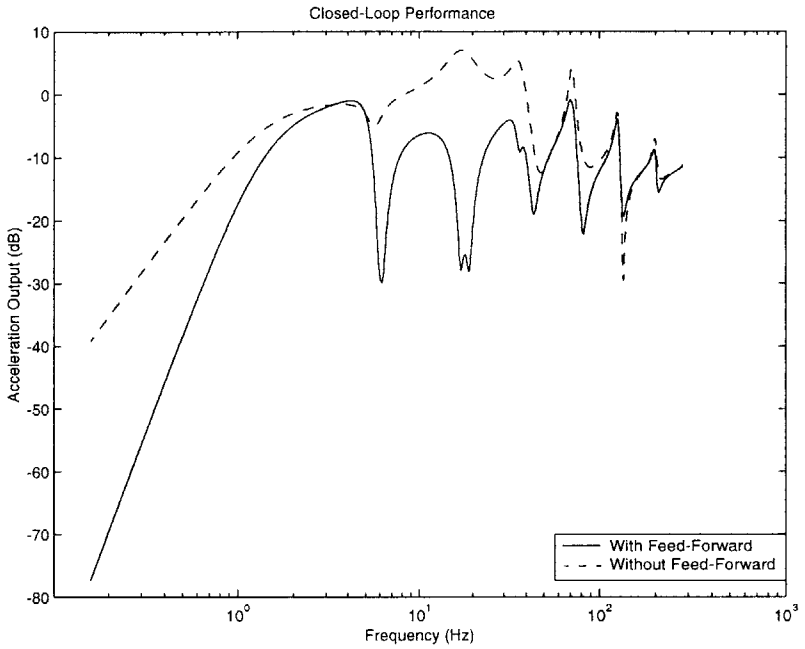

Figure 7.5 Steady state closed-loop performance.

requires gain scheduling the L_1 and L_2 estimator gains. In addition, the scheduling of K_1 is required for both case 1 and case 2. In this demonstration, the L_1 and L_2 estimator gains were obtained using optimal estimator theory instead of the decoupled solution presented in Section 7.3.1. A block diagram of the system used to generate the simulation results is shown in Figure 7.6. The signals labeled y_1 and y_2 correspond to tip acceleration for cases 1 and 2, respectively. The following is a description of the various blocks in Figure 7.6

1. Ref Signal: Generates the wheel speed profile.
2. Feed-Forward and Disturbance: Outputs the feed-forward control signal, $U_{ff}(t) = -K_1 x_1(t)$, using the scheduled K_1 gain and outputs the disturbance, $w(t)$.
3. Frequency Dependent Estimator: Outputs the scheduled L_1 and L_2 estimator gains.
4. Frequency Dependent O-L plant: Outputs the disturbance augmented open-loop plant.
5. Compensator: Implements the compensator defined by Equation 7.8 and control defined by Equation 7.1.

6. Full-State Compensator: Implements the compensator defined by Equation 7.13 and control defined by Equation 7.9.
7. Plant: Nominal open-loop plant without disturbance dynamics.

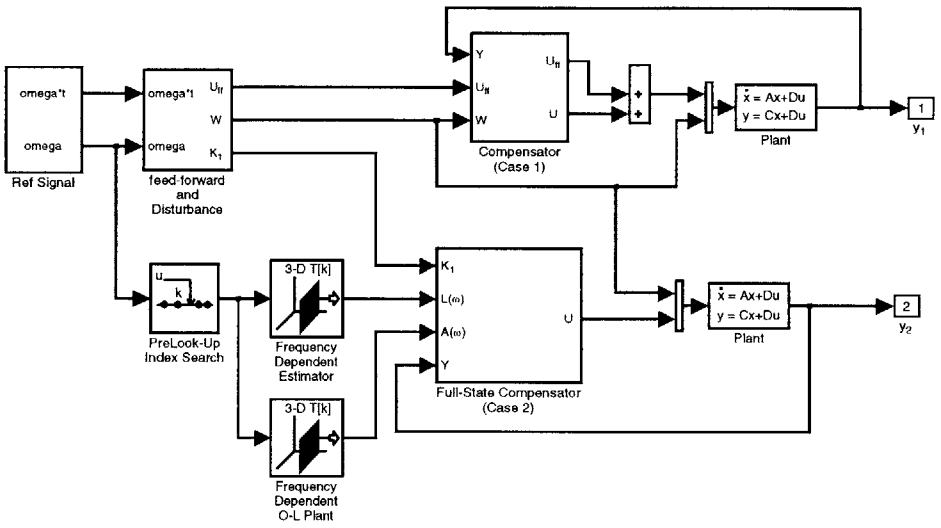

Figure 7.6 Block diagram of the simulation for cases 1 and 2.

To investigate the transient behavior of the two cases, the response to a wheel speed change was simulated. The wheel speed profile used for the simulation is shown in Figure 7.7. The wheel speed started with an initial spin rate of *10 Hz* and was held constant for five seconds. It was then accelerated using a constant rate of acceleration to *11 Hz* during the next five seconds, then held constant for the remainder of the simulation. The results of the simulation are shown in Figure 7.8. Notice that the initial transient of case 2 quickly decays and in steady state matches the response of case 1. However, during the wheel speed change portion of the simulation, the performance of the two methods differs rather dramatically. The fact is that the $\overline{x}_1(t)$ states are part of a dynamic system driven by the system output error and therefore cannot respond instantly to changes in the disturbance. For case 1, the $x_1(t)$ states are computed from the measured wheel speed, and in

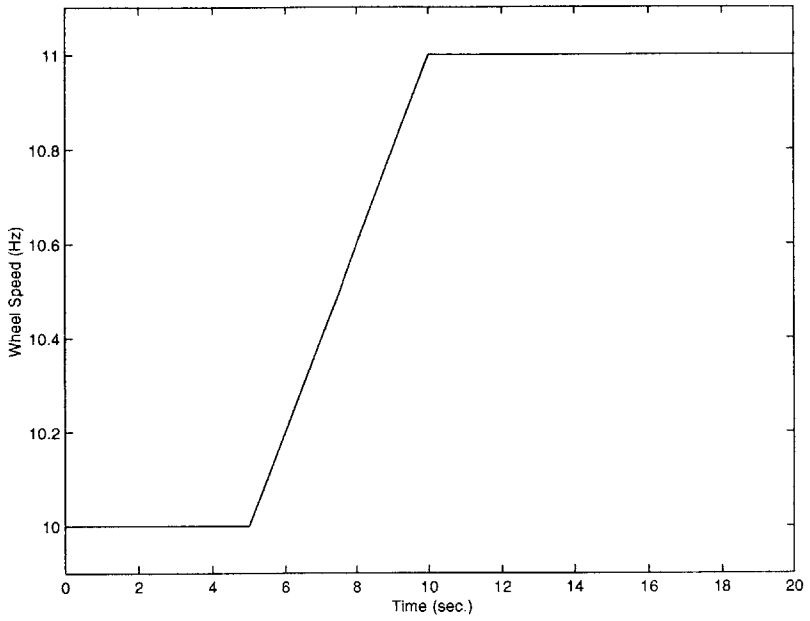

Figure 7.7 Wheel speed profile.

this sense, the feed-forward control signal responds instantaneously to changes in the disturbance. Control implementations based upon case 1 are highly recommended for situations where the disturbance profile's spectral content is nonstationary. Beyond its improved transient performance, case 1 has many other advantages over case 2. For example, case 1 has fewer real-time implementation complexities, a simpler estimator design, it scales well with disturbance dynamics, and is incapable of destabilizing the system. The primary advantage of case 2 is that it does not require rigorous disturbance modeling as required by case 1. In fact, the $\bar{x}_1(t)$ states in case 2 are real-time estimates of the disturbance dynamics and in steady state converge to the true disturbance states. This leads to the recommendation of a hybrid approach. The hybrid approach would be fundamentally based upon the methods defining case 1 for feed-forward control, but would use case 2 to provide real-time disturbance identification and calibration information as required by case 1. Recall from Section 6.1 that a start-up disturbance phase calibration was required for those systems without a wheel angular position sensor. The disturbance phase information would be readily available using a hybrid scheme employing the methods of case 2

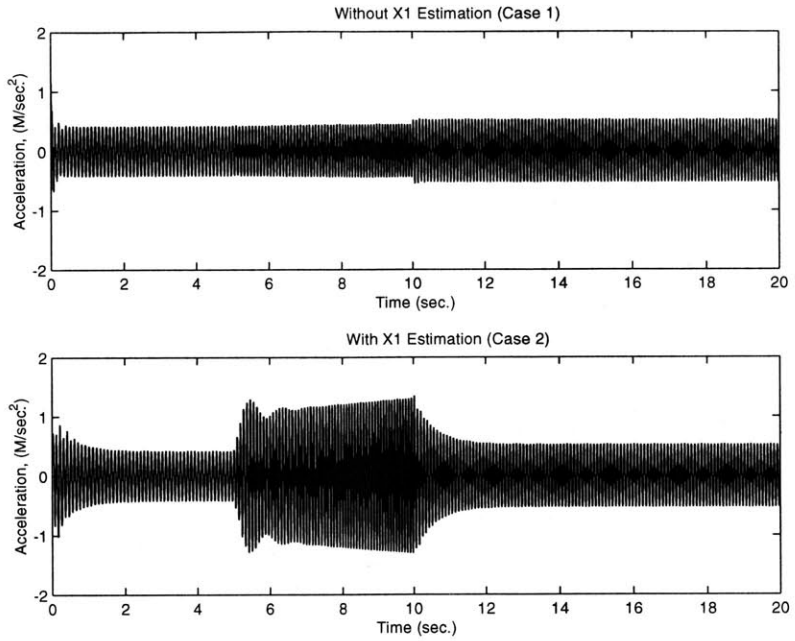

Figure 7.8 Simulation results for case 1 and case 2.

for disturbance identification. Notice that both cases require knowledge of the disturbance influence matrices B_w and D_w. The methods developed in Section 6.1 may be applied in situations when these matrices are not readily available. The next section will present the real-time experimental results of the above case 1 design applied to the flexible beam test article.

7.5 Experimental Results

This section will present the results of an experimental implementation of the optimal feed-forward control developed in this work as applied to the flexible beam test article. The control and estimator designs used in this implementation are identical to those presented in Section 7.4. In this validation, the control methodology uses the approach presented in Section 7.2, i.e., case 1, with disturbance identification based upon methods given in Section 6.2. Figure 7.9 presents a simplified block diagram of the real-time environment. The primary differences between the system in Figure 7.9 and that used for sim-

ulation, as shown in Figure 7.6, are the inclusion of the digital encoder inputs and the reaction wheel control loop. The reaction wheel controller uses proportional plus integral control using a measure of wheel speed to produce control currents to the motor. An

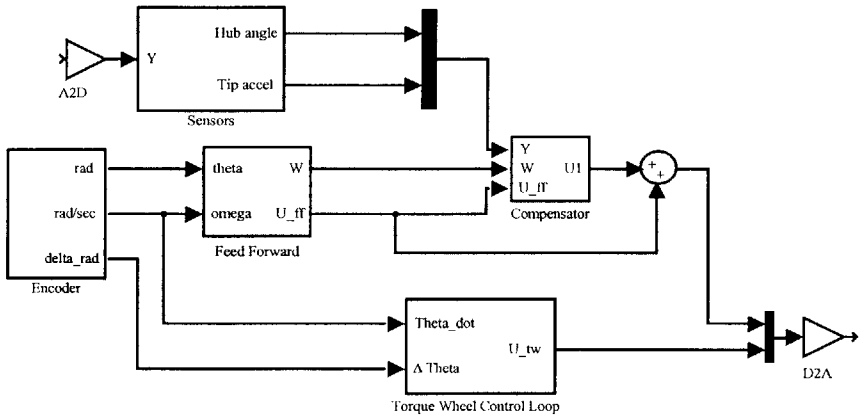

Figure 7.9 Block diagram of the optimal feed-forward control.

expanded view of the feed-forward block is given in Figure 7.10. Notice that single harmonic control is implemented in this demonstration. The outputs of the feed-forward block are two of the inputs required by Equation 7.7. The block labeled as compensator in Figure 7.9 directly implements Equation 7.7 together with the control $U(t) = -K_2\bar{x}_2(t)$.

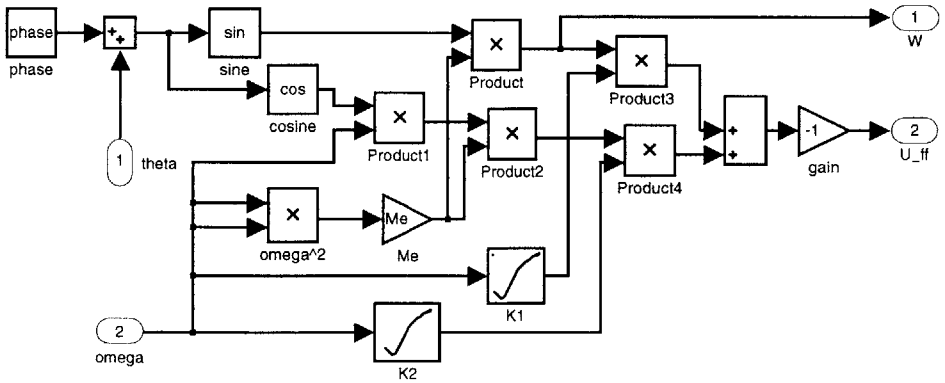

Figure 7.10 Expanded view of the feed-forward block.

As mentioned previously, the dSPACE product called ControlDesk is used to monitor and interact with the experiment in real-time. A screen shot of the ControlDesk interface is given in Figure 7.11. The interface permits the user to set a variety of parameters used in control, for example, wheel speed, proportional and integral gains on reaction wheel speed loop, disturbance phase angle, to monitor real-time process turn-around time and system performance, and to toggle on/off feed-forward and feedback control. Notice that the sample rate used in the experiment was *1000 Hz*.

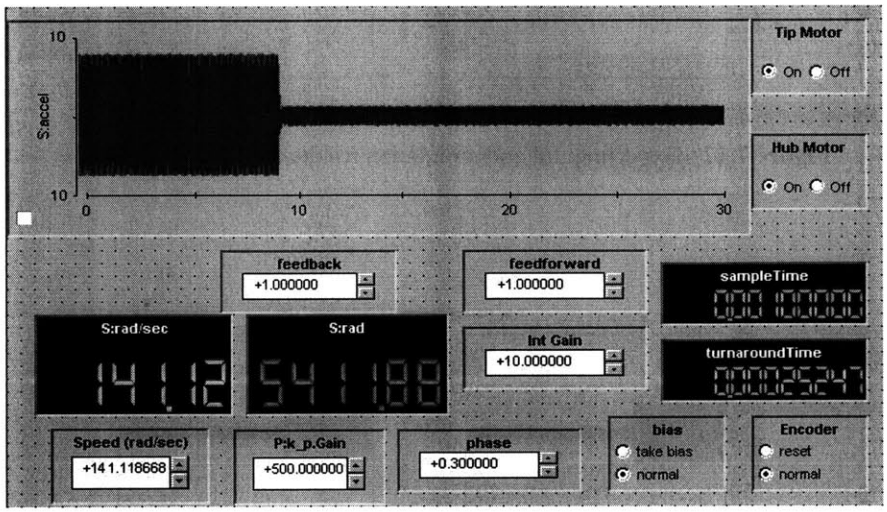

Figure 7.11 ControlDesk interface.

The performance of the system was evaluated at fifteen different steady state wheel speeds. In all cases, the system was first allowed to reach steady state using feedback control before the feed-forward control was turned on. Real-time tip accelerometer data was recorded for each wheel speed case and are presented in Figures 7.12 through 7.19. In each of these figures, the experimental response is plotted alongside the corresponding simulated response that was generated using the finite element model. In all cases, the experimental response matches reasonably well with the simulated data.

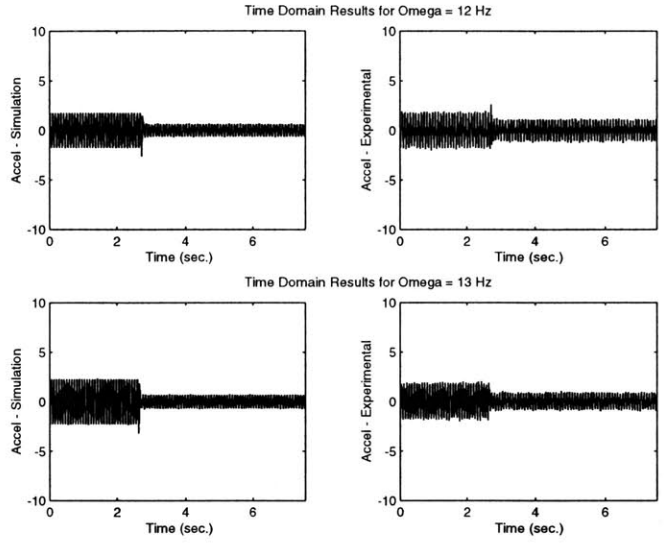

Figure 7.12 Experimental and simulation results for 12 and 13 Hz.

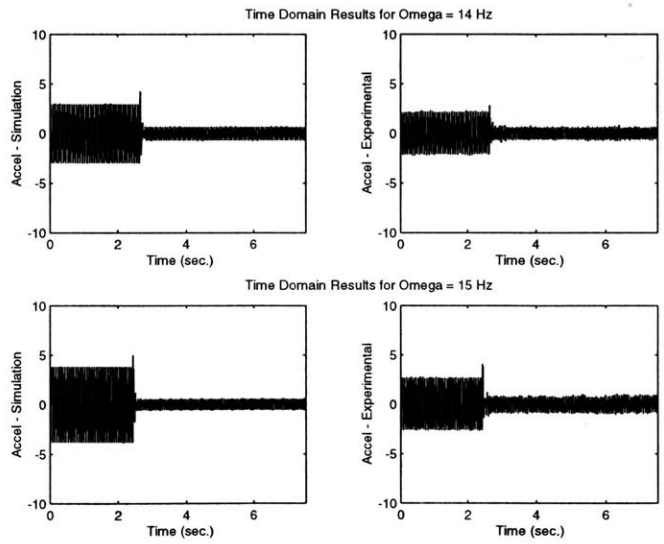

Figure 7.13 Experimental and simulation results for 14 and 15 Hz.

A frequency domain experimental performance plot, similar to the theoretical performance plot given in Figure 7.5, has also been generated from this data. This plot, see Figure 7.20, is simply the amplitude spectrum of the data computed for with and without

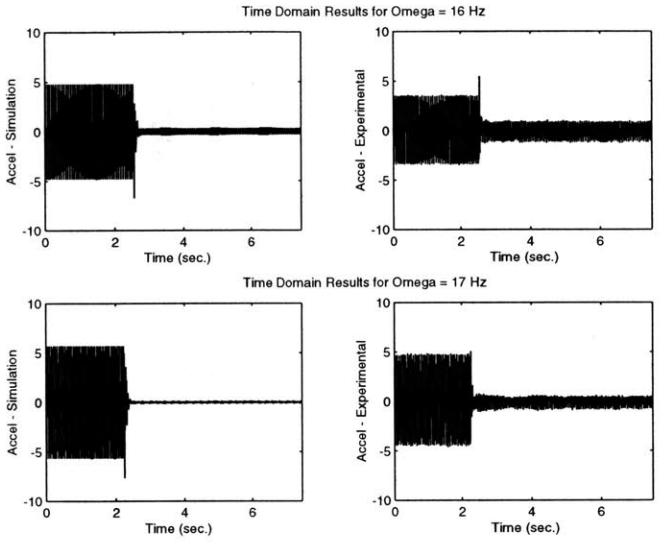

Figure 7.14 Experimental and simulation results for 16 and 17 Hz.

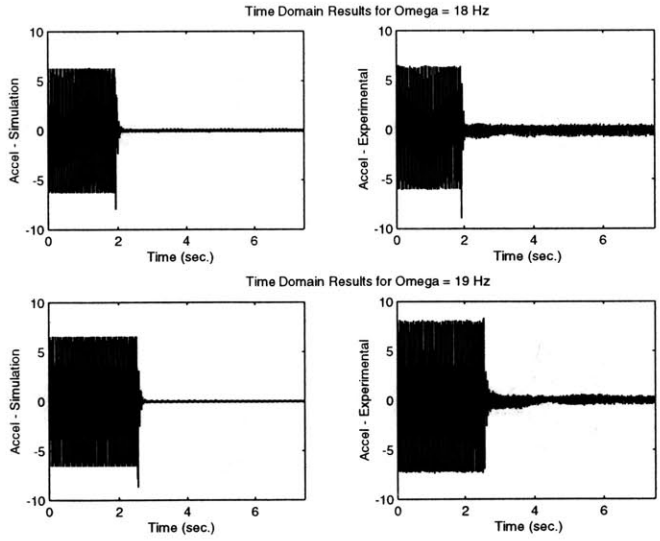

Figure 7.15 Experimental and simulation results for 18 and 19 Hz.

feed-forward. The experimental performance is in excellent agreement with the predicted theoretical performance.

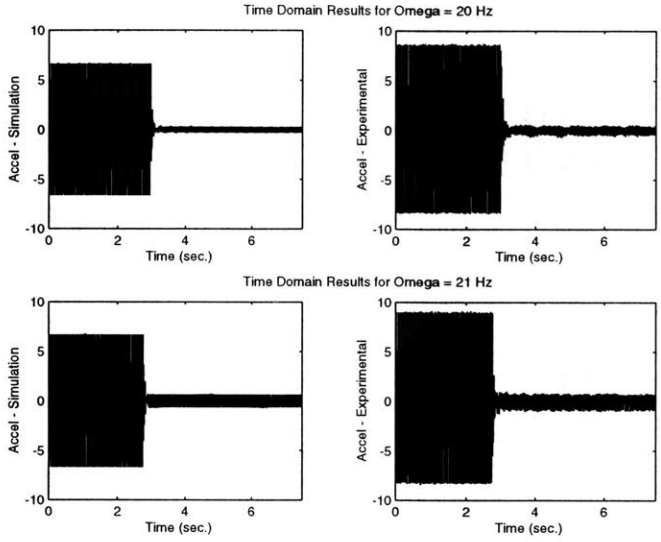

Figure 7.16 Experimental and simulation results for 20 and 21 Hz.

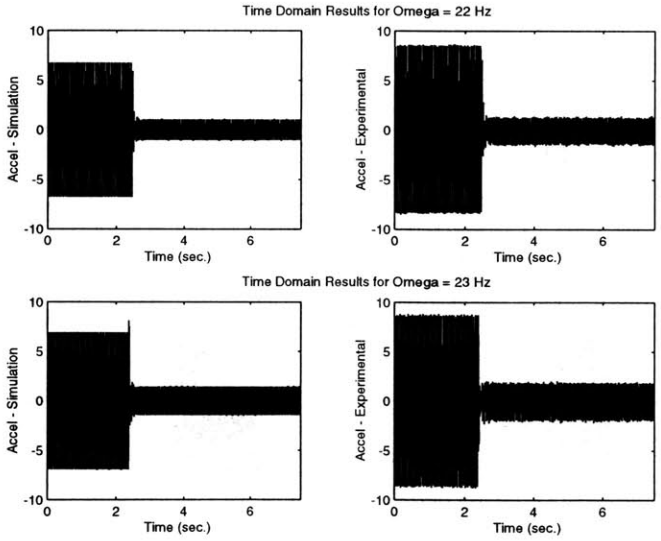

Figure 7.17 Experimental and simulation results for 22 and 23 Hz.

A non-stationary wheel speed test was also conducted. In this experiment, the reference wheel speed was prescribed to be $\omega(t) = 15 + 6.75\sin(2\pi t/10)$ *Hz*, which equates to a frequency modulation index, β/α=*67.5*. The experiment was run for a total of sixty sec-

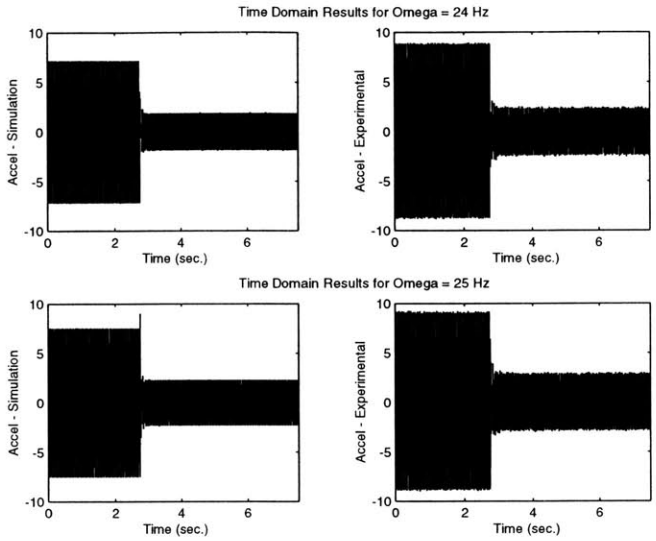

Figure 7.18 Experimental and simulation results for 24 and 25 Hz.

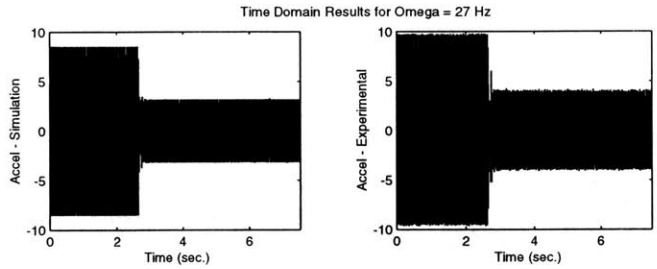

Figure 7.19 Experimental and simulation results for 27 Hz.

onds. During the first thirty seconds, only feedback control was used. At $t = 30$ the feed-forward control was engaged and remained on for the duration of the experiment. The results are shown in Figure 7.21. It should be noted that the feed-forward control was based upon a disturbance model that did not account for the acceleration of the wheel. The results show no signs of adverse transient response and yield significant improvement over conventional LQG control.

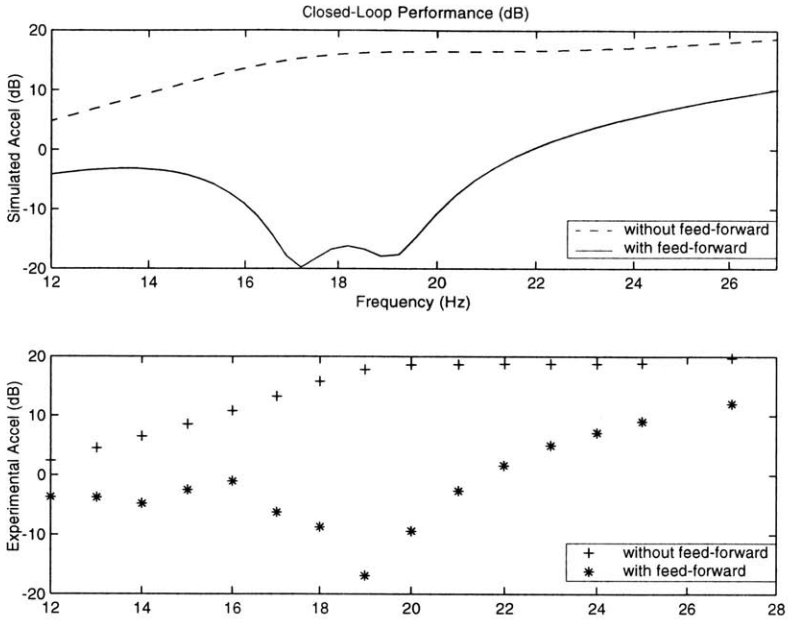

Figure 7.20 Frequency domain performance comparison.

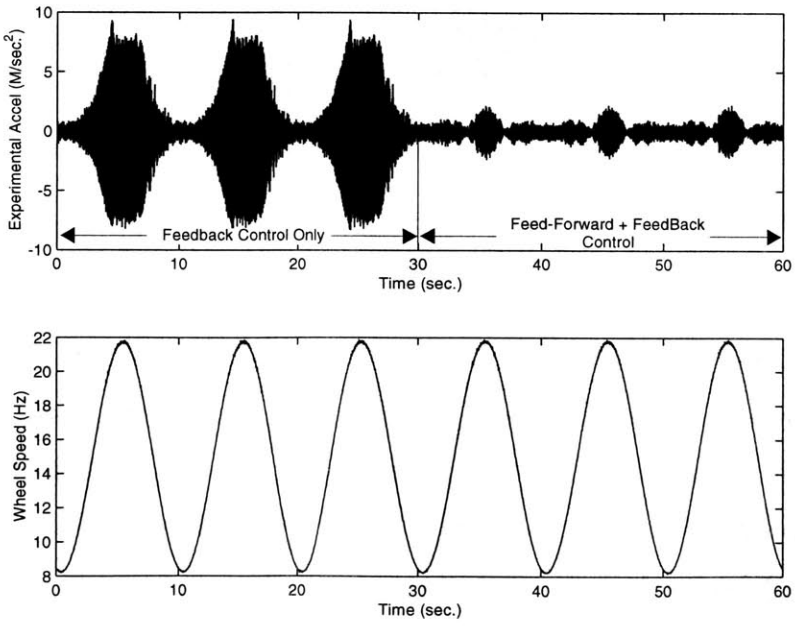

Figure 7.21 Nonstationary wheel speed experiment.

7.6 Summary

This chapter has experimentally demonstrated the effectiveness of the optimal feed-forward control methodology applied to a highly compliant system with a non-collocated sensor/actuator pair. Experimental results show excellent performance across a broad range of frequencies, with peak performance yielding nearly 40 dB improvement over conventional LQG control.

Two forms of state estimation have been presented. The first, which retains the purely feed-forward nature of the system, employs state estimation for the plant states only and uses a known disturbance model to compute the disturbance states necessary to implement the feed-forward control. The second form, which results in a feedback-only system, employs estimation for both the plant and disturbance states. A technique to decouple the disturbance and plant state estimator gains was presented and the duality between it and feed-forward gain computations was introduced. The recommendations were given to employ the first form of estimation because of its improved transient performance, fewer real-time implementation complexities, scalability with disturbance dynamics, and inability to destabilize the system. A hybrid technique was discussed that included feed-forward control, but with real-time disturbance identification, or simply phase calibration, coming from a combined disturbance plus plant state estimator.

Optimal feed-forward performance was evaluated using fifteen different steady state wheel speed experiments. The experiments used wheel speeds ranging from *12* to *27 Hz*. For each case, the corresponding simulation results were presented and comparisons with conventional LQG control were given. In all cases, the simulation and experimental results showed good agreement, while demonstrating superior performance over LQG-only control.

Chapter 8

CONCLUSIONS, CONTRIBUTIONS AND RECOMMENDATIONS

This chapter will provide a general overview of the developments leading to the creation of a nonstationary narrowband optimal disturbance rejection methodology for flexible systems. Unique contributions to the disturbance rejection field are given, followed by recommendations for future work.

8.1 Thesis Summary

Narrowband disturbances are present in a broad class of engineering systems. The primary systems of interest in this work are spaceborne telescopes whose attitude is maintained using reaction wheels. It is expected that most future telescope missions will utilize reaction wheels as the primary control effector while operating in the science data-collecting mode. The dominant disturbances source while operating in this mode are expected to be the wheel speed dependent forces and moments resulting from residual static and dynamic imbalances or other well-documented effects. This work develops an optimal feed-forward control methodology aimed at rejecting these speed dependent forces and moments. The basic premise here is that these speed dependent forces and moments can be modeled parametrically and then used in an optimal control problem to give feed-forward control gains defined analytically in terms of these parametric disturbance models. This thesis develops a methodology for solving this nonstationary disturbance rejection problem and experimentally validates it using a highly compliant test article.

Chapter 1 provided an introduction and a review of previous work. Chapter 2 presented an overview of the fundamental concepts of optimal control. A review of optimal control for a fixed final time with free final states for the general nonlinear time-varying plant has been given. Simplifications based upon the assumption of linearity are made and the classic solution for quadratic cost functionals is presented. The continuous-time algebraic Riccati equation is introduced and solutions to the finite-horizon and stochastic linear optimal control problems are given. Finally, the concept of loop shaping is presented in the discussion on frequency-weighted cost functionals.

Chapter 3 presented the parameterized feed-forward control design methodology for disturbances that possess stationary or slowly varying narrow-band spectral distributions. The feed-forward control is directly parameterized in terms of the eigenvalues and eigenvectors of the disturbance model. For the class of disturbances of interest in this study, the disturbance model's eigensystem may be expressed analytically in terms of the individual harmonics of the disturbance, thereby permitting an arbitrarily large number of harmonics to be considered. A demonstration of this feed-forward control methodology was given using a low-order spring-mass system. Feed-forward control results were compared to conventional LQR designs and were shown to yield significantly improved performance over conventional LQR control alone - upwards of *40 dB* in selected frequency regions. A control design combining frequency weighting together with feed-forward was also demonstrated.

An optimal feed-forward control solution to reaction wheel imbalances with nonstationary spectral distributions was presented in Chapter 4. The formulation involved expanding the wheel angular states in terms of a general series representation. This series was further expanded using Bessel functions of the first kind to arrive at an expression for the time-varying imbalance disturbances characterized by an infinite set of discrete frequencies. The properties of Bessel functions were employed to permit the practical truncation of the infinite series to a finite set of frequencies. It was shown that the frequency modulation index played an essential role in this truncation process, and hence in defining the band-

width of the feed-forward control. Once the finite-set series representation had been obtained, the methods of Chapter 3 were used to generate the sub-optimal feed-forward control signal. A simplified wheel speed parameter identification technique was developed and used to demonstrate the feasibility of the proposed sub-optimal implementation.

Chapter 5 introduced the flexible beam test article. This system was designed for the purpose of validating the optimal feed-forward control methodology. The system consists of a long, thin, very flexible aluminum blade that is controlled using a direct current motor located at the root of the beam. A torque wheel actuator located at the tip of the beam was designed as a disturbance generator to provide a harmonic imbalance source. A partially updated finite element model was presented and shown to match the experimentally obtained transfer functions.

Chapter 6 presented two methods for identifying reaction wheel imbalances from steady-state measurement data. The first method is applicable to single-input, single-output or single-input, multiple-output systems with unknown disturbance influence matrices and unknown disturbance magnitude and phase characteristics. The second method is applicable to multiple-input, multiple-output systems with known disturbance influence matrices and is capable of identifying multi-tonal sinusoidal disturbance magnitude and phase parameters. Both approaches were validated using simulation and experimentally obtained data from the flexible beam test article and were shown to produce excellent agreement with known system parameters.

An experimental demonstration of the effectiveness of the optimal feed-forward control methodology as applied to the flexible beam test article, was presented in Chapter 7. Experimental results show excellent performance across a broad range of frequencies, with peak performance yielding nearly 40 dB improvement over conventional LQG control. The practical issue of state estimation was also considered in this chapter. Two forms of state estimation were presented. The first form employs state estimation for the plant states only and uses a known disturbance model to compute the disturbance states neces-

sary to implement feed-forward control. It was shown that this form retains the purely feed-forward nature of the system. The second form employs estimation for both the plant and disturbance states and results in a purely feedback system. In this second form of estimation, the optimal disturbance and plant estimator gains are coupled. A technique to decouple the disturbance and plant estimator gains was presented and a duality between disturbance state estimator and feed-forward control gains was introduced. A conclusion was reached to employ the first form of estimation because of its improved transient performance, fewer real-time implementation complexities, scalability with disturbance dynamics, and an inability to destabilize the system.

8.2 Contributions

- A closed-form symbolically parameterized optimal feed-forward disturbance rejection methodology for flexible systems has been developed. The methodology combines disturbance modeling for a class of narrowband disturbances with optimal control to yield a parameterized feed-forward control system. In the case of the reaction wheel disturbance rejection problem, the symbolic optimal control gains are parameterized in terms of wheel spin rate, enabling continuous and analytically exact gain adjustments as a function of the measurable scheduling parameter. The methodology was shown to be compatible with loop-shaping control design methods, such as frequency-weighted optimal control. Expressions for the asymptotic properties of the parameterized feed-forward gains as a function of control cost were given.

- Development of a sub-optimal feed-forward control methodology for the rejection of nonstationary reaction wheel imbalances. The formulation involved expanding the wheel's angular states in terms of a general series representation. Bessel functions and their properties were employed to define an equivalent stationary multi-harmonic disturbance signal. Once the

equivalent stationary disturbance was determined, feed-forward control methods that were developed in Chapter 3 were used. In support of this development, a technique for real-time sinusoidal parameter estimation was developed and validated in simulation.

- Steady state multi-tonal reaction wheel imbalance identification procedures have been developed. Two forms of the reaction wheel imbalance identification problem were considered. The first was developed for systems with both unknown disturbance influence matrices and unknown disturbance magnitude and phase characteristics and is applicable for SISO or SIMO systems. The second method, applicable to MIMO systems with known disturbance influence matrices, is capable of identifying sinusoidal disturbance magnitude and phase parameters.

- Experimental demonstrations of optimal feed-forward control applied to a highly compliant system with a non-collocated sensor/actuator pair have been provided. Optimal feed-forward performance was evaluated on the flexible beam test article using a variety of steady state wheel speeds. In all cases, the optimal feed-forward control demonstrated superior performance over LQG-only control, with peak performance providing approximately 40 dB improvement over LQG.

- Experimental verification of the SIMO and MIMO reaction wheel imbalance disturbance identification methodologies has been provided.

- Specilized software tools for: parameterized feed-forward control design, real-time control implementation, and reaction wheel imbalance disturbance identification have been developed.

8.3 Recommendations

- Although this research has addressed a critical issue in the fine pointing of scientific and military spacecraft controlled by reaction wheels, further experimental validation on more dynamically complex systems employing multiple reaction wheels is recommended.

- The impact of plant model uncertainty on feed-forward gains and the effectiveness of optimal feed-forward control for uncertain systems needs to be evaluated.

- Discrete-time representations of the parameterized optimal feed-forward gains should be considered.

- Multiple-input, multiple-output reaction wheel imbalance identification methodology for cases with unknown disturbance influence matrices should be developed.

- A robust sinusoidal parameter identification technique capable of handling multiple frequency modulation indices with minimal phase delay should be developed.

REFERENCES

[Abhyankar, 1993] Abhyankar, N. S., "A Brief Description of ASTREX," Phillips Lab, Edwards AFB, Report number ASTREX-93-01, April 1993.

[Anderson, 1971] Anderson, B. D. O. and J. B. Moore, *Linear Optimal Control*, Prentice-Hall, NJ, 1971

[Annaswamy, 2000] Annaswamy, A. M., N. Ho, C. Cao, and A. Kojic, "A Convergent Frequency Estimator," *Proceedings of the 2000 American Control Conference*, June 2000.

[Athans, 1966] Athans, M., and P. L Falb, *Optimal Control*, New York: McGraw-Hill, 1966.

[Bellman, 1960] Bellman, R., *Introduction to Matrix Analysis*, New York: McGraw-Hill, 1960.

[Bialke, 1997] Bialke, B., "A Compilation of Reaction Wheel Induced Spacecraft Disturbances," *20th Annual American Astronautical Society Guidance and Control Conference*, February 1997. AAS paper 97-038

[Bialke, 1998] Bialke, B., "High Fidelity Mathematical Modeling of Reaction Wheel Performance," *21st Annual American Astronautical Society Guidance and Control Conference*, February 1998. AAS paper 98-063

[Burgess, 1981] Burgess, J. C., "Active Adaptive Sound Control in a Duct: A Computer Simulation," *Journal of the Acoustical Society of America*, Vol. 70, pp. 715-726, 1981.

[Cao, 2002] Cao, C., and A. M. Annaswamy, "Parameter Convergence in Systems with a General Nonlinear Parameterization Using a Hierarchical Algorithm," *To appear in the Proceedings of the 2002 American Control Conference*, May 2002.

[Couch, 1993] Couch, L. W., *Digital and Analog Communication Systems,* Macmillan Publishing Co., 1993

[Cuccia, 1952] Cuccia, C. L., *Harmonics, Sidebands, and Transients in Communication Engineering*, McGraw-Hill, 1952.

[Davis, 1997] Davis, L. D., and D. C. Hyland, "Adaptive Neural Control for the ASTREX Testbed," *Proceeding of the American Control Conference*, June 1997.

[Davison, 1975] Davison, E., "The Numerical Solution of $\dot{X} = A_1X + XA_2 + D, X(0) = C$,"

IEEE Transactions on Automatic Control, August 1975, Vol. AC-20, No. 4, pp. 566-567.

[Elias, 2001] Elias, L. M., *A Structurally Coupled Disturbance Analysis Method Using Dynamic Mass Measurement Techniques, with Application to Spacecraft-Reaction Wheel Systems*, Master's thesis, Massachusetts Institute of Technology, March 2001. SERC Report # 9-01.

[Elliott, et al., 1987] Elliott, S. J., I. M. Stothers, and P. A. Nelson, "Multiple error LMS Algorithm and its Application to the Active Control of Sound and Vibration," *IEEE Trans. Acoust., Speach, Signal Processing, Vol. 35, No. 10, Oct. 1987*

[Friedland, 1986] Friedland, B., *Control System Design, An Introduction to State-Space Methods*, McGraw-Hill, 1986.

[Giacoletto, 1947] Giacoletto, L. J. "Generalized Theory of Multitone Amplitude and Frequency Modulation," *Proceeding of the Institute of Radio Engineers Conference*, Vol. 35, July, 1947.

[Goodzeit, 2000] Goodzeit, N. E., and M. Q. Phan, "System and Disturbance Identification for Feedforward and Feedback Control Applications," *Journal of Guidance and Control*, Vol. 23, No. 2, March-April 2000.

[Gupta, 1980] Gupta, N. K., "Frequency-Shaped Cost Functionals: Extension of Linear-Quadratic-Gaussian Design Methods," *Journal of Guidance and Control*, Dec. 1980, Vol. 3, No. 6, pp. 529-535.

[Hall, 1989] Hall, S. R., "Linear Control Issues in the Higher Harmonic Control of Helicopter Vibrations," *Proceeding of the 45th Annual Forum of the American Helicopter Society*, May 1989

[Hyland, 1996] Hyland, D. C., and L. D. Davis, "A Multiple-Input, Multiple-Output Neural Architecture for the Suppression of a Multi-Tone Disturbance," *Proceeding of the 19th Annual AAS Guidance and Control Conference,* Feb. 1996.

[Johnson, 1971] johnson, C. D., "Accomodation of External Disturbances in Linear Regulator and Servomechanism Problems," *IEEE Transactions on Automatic Control*, Vol. AC-16, No. 6, Dec. 1971.

[Juang, 1985] Juang, J. N., and R. S. Pappa, "An Eigensystem Realization Algorithm for Modal Parameter Identification and Model Reduction," *Journal of Guidance, Control and Dynamics,* 1985, Vol. 8, No. 5, pp. 620-627

[Juang, 1998] Juang, J., and K. W. Eure, "Predictive Feedback and Feedforward Control for Systems with Unknown Disturbance," NASA TM-1998-208744

[Junkins, 1986] Junkins, J., and J. Turner, *Optimal Spacecraft Rotational Maneuvers, Vol. 3, Elsevier, 1986*

[Kalman, 1960] Kalman, R. E., "Contributions to the Theory of Optimal Control," *Bol. Soc. Mat. Mexicana.,* Vol. 5, pp. 102-119, 1960

[Kay, 1993] Kay, S. M. *Fundamentals of Statistical Signal Processing: Estimation Theory,* New Jersey: Prentice-Hall, 1993

[Kirk, 1970] Kirk, D. E., *Optimal Control Theory,* New Jersey: Prentice-Hall, 1970.

[Kwakernaak and Sivan, 1972] Kwakernaak, H., and R. Sivan, *Linear Optimal Control Systems*, John Wiley & Sons, Inc., 1972

[Laub, 1979] Laub, A. J., "A Schur Method for Solving Algebraic Riccati Equations," *IEEE Transactions on Automatic Control*, December 1979, Vol. AC-24, No. 6, pp. 913-921.

[Li, 1992] Li, T-H., and B. Kedem, *Estimation of Multiple Sinusoids by Parametric Filtering*, Technical Research Report, University of Maryland, Report # TR 92-51, January 1992.

[MacMartin, 1994] MacMartin D. G., "A Feedback Perspective on the LMS Disturbance Feedforward Algorithm," *Proceeding of the American Control Conference*, June 1994

[Mallory, 2000] Mallory, G. J. W., *Development and Experimental Validation of Direct Controller Tuning for Spaceborne Telescopes*, Ph.D. thesis, Massachusetts Institute of Technology, April 2000. SERC Report # 1-2000.

[Masters, 1997] Masters, B., *Evolutionary Design of Controlled Structures*, Ph.D. thesis, Massachusetts Institute of Technology, April 1997. SERC Report # 1-97.

[Masterson, et al., 1999] Masterson, R., D. W. Miller, and R. Grogan, "Development of Empirical and Analytical Reaction Wheel Disturbance Models," *AIAA/ASME/ ASCE/AHS/ASC Structures, Structural Dynamics and Materials Conference*, April 1999.

[Miller et al., 1996] Miller D. W., E. F. Crawley, J. P. How, K. Liu, M. E. Campbell, S. C. O. Grocott, R. M. Glaese, T. D. Tuttle, G. Stover, J. A. Woods-Vedeler, J. deLuis, E. Bokhour, R. Grimes, K. Scholle, C. Krebs, and R. Renshaw, "The Middeck Active Control Experiment (MACE): Summary Report," June 1996, SERC Report #7-96.

[Nixon et al., 1997] Nixon, M. W., Kvaternik, R. G., and Settle, T. B., "Tiltrotor Vibration Reduction Through Higher Harmonic Control," *Presented at the American Heli-*

copter Society 53rd Annual Forum, April 1997.

[Ogata, 1970] Ogata, K., *Modern Control Engineering*, Prentice-Hall, 1970.

[Phan, 1997] Phan, M. Q., N. E. Goodzeit and J. Juang, "Identification of System and Periodic Disturbances," *Proceedings of DETC'97, 1997 ASME Design Engineering Technical Conference*, Sept. 1997.

[Pontryagin, et al., 1962] Pontryagin, L. S., V. G. Boltyanskii, R. V. Gamkrelidze, and E. F. Mishchenko, *The Mathematical Theory of Optimal Processes*, John Wiley & Sons, Inc., 1962

[Potter, 1966] Potter, J. E., "Matrix Quadratic Solutions," *SIAM Journal of Applied Mathematics*, Vol. 14, pp. 496-501, 1966.

[Quinn, 1991] Quinn, B. G. and J. M. Fernandes, "A Fast Efficient Technique for the Estimation of Frequency," *Biometrika*, Vol. 78, No. 3, pp. 489-497, 1991.

[Rahman, 1987] Rahman, Md. A., and K. Yu, "Total Least Squares Approach for Frequency Estimation Using Linear Prediction", *IEEE Trans. Acoust., Speach, Signal Processing,* Vol. 35, No. 10, pp. 1440-1454, Oct. 1987.

[Scribner, 1993] Scribner, K. B., L. A. Sievers and A. H. von Flotow, "Active Narrowband Vibration Isolation of Machinery Noise from Resonant Substructures," *Journal of Sound and Vibration*, Vol. 167, No. 1, pp. 17-40, 1993.

[Shaw, 1980] Shaw, J., *Higher Harmonic Blade Pitch Control: A System for Helicopter Vibration Reduction*, Ph.D. thesis, Massachusetts Institute of Technology, 1980.

[Shaw, 1981] Shaw, J., and N. Albion, "Active Control of the Helicopter Rotor for Vibration Reduction," *Journal of the American Helicopter Society*, Vol. 26, No. 3, 1981.

[Shaw, 1989] Shaw, J., N. Albion, E. Hanker, Jr., and R. Teal, "Higher harmonic control: Wind tunnel demonstration of fully effective vibratory hub force suppression," *Journal of the American Helicopter Society*, Vol. 34, No. 1, 1989.

[Sievers, 1989] Sievers, L. A., and A. H. von Flotow, "Comparison of Two LQG-Based Methods for Disturbance Rejection," *Proceeding of the 28th Conference on Decision and Control*, Dec. 1989.

[Sievers, 1991] Sievers, L. A., G. H. Blackwood, M. Mercadal, and A. H. von Flotow, "MIMO Narrowband Disturbance Rejection Using Frequency Shaping of Cost Functionals," *Proceeding of the American Control Conference*, June 1991.

[Sievers, 1992] Sievers, L. A., and A. H. von Flotow, "Comparison and Extensions of Control Methods for Narrow-Band Disturbance Rejection," *IEEE Trans on Sig-*

nal Processing, Vol. 40, No. 10, pp. 2377-2391, Oct. 1992

[Sima, 1999] Sima, V., and S. Van Huffel, "High-performance Algorithms and Software for Systems and Control Computations," *Proceeding of the IEEE International Symposium on Computer Aided Control System Design,* August 1999.

[Suhardjo, 1989] Suhardjo, J., B. F. Spencer, Jr., and M. K. Sain, "Feedback-Feedforward Control of Structures Under Seismic Excitation," *Euromech 250 Colloquium on Nonlinear Structural Systems under Random Conditions*, June 1989.

[Stengel, 1986] Stengel, R. F., *Stochastic Optimal Control Theory and Application,* John Wiley & Sons, Inc., 1986

[Stoica, et al., 1989] Stoica, P., R. L. Moses, B. Friedlander, and T. Soderstrom, "Maximum Likelihood Estimation of the Parameters of Multiple Sinusoids from Noisy Measurements," *IEEE Trans. Acoust., Speach, Signal Processing*, Vol. 37, No. 3, pp 378-392, 1989.

[Widrow, et al, 1985] Adaptive Signal Processing, Prentice-Hall, 1985